UNIVERSITEIT VAN PRETORIA
UNIVERSITY OF PRETORIA
YUNIBESITHI YA PRETORIA

Identification and standardisation of parameters to improve the understanding of mechanical properties of FFF/FDM/MEX parts

S Crous

CVD 800

2023-03-19

© University of Pretoria

UNIVERSITEIT VAN PRETORIA
UNIVERSITY OF PRETORIA
YUNIBESITHI YA PRETORIA

Identification and standardisation of parameters to improve the understanding of mechanical properties of FFF/FDM/MEX parts

S Crous

Department of Chemical Engineering
University of Pretoria

CVD 800

2023-03-19

© University of Pretoria

Identification and standardisation of parameters to improve the understanding of mechanical properties of FFF/FDM/MEX parts

Abstract

Fused Deposition Modelling (FDM)/Fused Filament Fabrication (FFF)/Material Extrusion (MEX) is a well-known Additive Manufacturing (AM) process used in various fields of production. The extrusion/printing speed, nozzle temperature and build plate/bed temperature were determined through literature screening to be the printing parameters that have the greatest effect on the tensile strength of a printed specimen. These were used in a two-level fractional factorial design to obtain the Design of Experiments (DOE). The DOE was used during the development of a material evaluation guideline for the printing of polylactic acid (PLA) on open-source printers. All printers used Cura® as slicing software. Various filaments were used on different printer models. CRON PLA yielded the highest average Ultimate Tensile Strength (UTS), while Zortrax PLA resulted in the best repeatability between samples within one experiment. The Creality Ender-6 delivered consistent results irrespective of the type of filament used. The effect of printing- and bed temperature on the UTS were significant for Wanhao PLA/Creality Ender-6. Printing temperature was significant for Buildvolume PLA/Creality Ender-6. Bed temperature, printing speed and the interaction between these parameters were significant for Flashforge PLA/Creality Ender-6 and Wanhao PLA/Creality Ender-3 Max. Printing temperature, bed temperature and printing speed had a significant effect on the UTS for Zortrax PLA/Creality Ender-6. There were no statistically significant effects for CRON PLA/Creality Ender-6, Wanhao PLA/Creality Ender-5 Plus and Wanhao PLA/Wanhao Duplicator 9 300. Printing speed was statistically significant for Wanhao PLA/Creality Ender-5. The effect of bed temperature and printing speed were significant on UTS for CRON PLA/Wanhao Duplicator 9 I3.

Keywords: Additive Manufacturing (AM); Cura; Design of Experiments (DOE); Material Evaluation Guideline; Polylactic Acid (PLA); Tensile Testing

© University of Pretoria

Declaration

ANNEXURE B – Declaration of originality

DECLARATION OF ORIGINALITY

UNIVERSITY OF PRETORIA

The Department of Chemical Engineering places great emphasis upon integrity and ethical conduct in the preparation of all written work submitted for academic evaluation.

Academics teach you about referencing techniques and how to avoid plagiarism; it is your responsibility to act on this knowledge. If you are at any stage uncertain as to what is required, you should speak to your lecturer before any written work is submitted.

You are guilty of plagiarism if you copy something from another author's work (e.g. a book, an article or a website) without acknowledging the source and pass it off as your own. In effect you are stealing something that belongs to someone else. This is not only the case when you copy work word-for-word (verbatim) but also when you submit someone else's work in a slightly altered form (paraphrase) or use a line of argument without acknowledging it.

Students who commit plagiarism will not be given any credit for plagiarised work. The matter may also be referred to the Disciplinary Committee (Students) for a ruling. Plagiarism is regarded as a serious contravention of the University's rules and can lead to expulsion from the University.

The declaration which follows must accompany all written work submitted while you are a student of the Department of Chemical Engineering No written work will be accepted unless the declaration has been completed and submitted.

Full names and surname of student: Stephani Crous

Student number: 17014663

Topic of work: Identification and standardisation of parameters to improve the understanding of mechanical properties of FFF/FDM parts

Declaration

1. I understand what plagiarism is and am aware of the University's policy in this regard.

2. I declare that this dissertation (e.g. essay, report, project, assignment, dissertation, thesis, etc) is my own original work. Where other people's work has been used (either from a printed source, Internet or any other source) this has been properly acknowledged and referenced in accordance with departmental requirements.

Scrous
SIGNATURE

29/11/2022
DATE

© University of Pretoria

Acknowledgements

I, Stephani Crous, a postgraduate student in Chemical Engineering at the University of Pretoria, would like to thank the following individuals who helped and guided me to complete my dissertation. The individuals include:

- Professor FJWJ Labuschagne
- Professor R Coetzer
- C van der Steenhoven

I would lastly like to thank my family and partner for their insights, guidance and support during the duration of the project.

© University of Pretoria

Contents

Abstract ii

Nomenclature xiv

1 Introduction 1

2 Additive Manufacturing (AM) 2

2.1 AM processes . . . 3

2.1.1 Stereolithography (SLA)/Vat Photopolymerisation (VPP) and Liquid Thermal Polymerisation (LTP) . . . 3

2.1.2 Fused Deposition Modelling (FDM)/Material Extrusion (MEX) . 5

2.1.3 Ballistic Particle Manufacturing (BPM)/Material Jetting (MJT) . 6

2.1.4 Binder Jet Printing (BJP) . . . 7

2.1.5 Laser-Engineering Net-Shaping (LENS)/Direct Energy Deposition (DED) . . . 8

2.1.6 Selective Laser Melting (SLM)/Powder Bed Fusion (PBF) . . . 9

2.2 Existing standards . . . 10

2.2.1 Standards for AM . . . 11

2.2.2 Standards for Powder Bed Fusion (PBF) . . . 17

3 Fused Deposition Modelling (FDM) 18

3.1 Advantages . . . 21

3.2 Disadvantages . . . 21

3.3 Industrial application . . . 22

3.4 Parameters . . . 23

© University of Pretoria

3.5 Design considerations and troubleshooting 31
3.5.1 Shrinkage and warp 31
3.5.2 Holes 31
3.5.3 Pins and columns 32
3.5.4 Wall thickness and thin sections 32
3.5.5 Threads 32
3.5.6 Undercuts, draft angles and fillets 33
3.5.7 Size and build orientation 33
3.5.8 Assemblies and sectioning parts 34
3.5.9 Living hinges and text 34
3.5.10 Text size 34
3.5.11 Bosses, ribs and gussets 34
3.5.12 Finishing of parts 35
3.6 Printers 35
3.6.1 Prusa3D 36
3.6.2 Creality 36
3.6.3 Ultimaker BV 37
3.6.4 Flashforge 38
3.6.5 Printrbot 38

4 Materials **40**

5 Previous studies **45**

© University of Pretoria

6 Experimental **54**

6.1 Overview 55

6.2 Design of Experiments (DOE) 58

6.2.1 Printing parameters 60

6.2.2 Materials 61

6.2.3 Apparatus 62

6.2.4 Samples printed and printer settings 64

6.3 Tensile testing 66

6.3.1 ASTM D638 66

6.3.2 Tensile machine 67

7 Results and Discussion **69**

7.1 Visual inspection on printed samples 69

7.2 Visual inspection on broken samples 73

7.3 Tensile data 77

7.3.1 Wanhao PLA on the Creality Ender-6 84

7.3.2 Buildvolume PLA on the Creality Ender-6 85

7.3.3 Flashforge PLA on the Creality Ender-6 86

7.3.4 Zortrax PLA on the Creality Ender-6 87

7.3.5 CRON PLA on the Creality Ender-6 89

7.3.6 Wanhao PLA on the Creality Ender-3 Max 90

7.3.7 Wanhao PLA on the Creality Ender-5 91

7.3.8 Wanhao PLA on the Creality Ender-5 Plus 92

7.3.9 CRON PLA on the Wanhao Duplicator 9 I3 93

© University of Pretoria

7.3.10 Wanhao PLA on the Wanhao Duplicator 9 300 95

7.4 Material evaluation guideline 99

8 Conclusion and Recommendations 100

© University of Pretoria

List of Figures

1 An illustration of SLA adapted from Manjaiah *et al* (2019). 4

2 A schematic illustration of LTP adapted from Pham & Dimov (2001). . . 5

3 A schematic illustration of FDM adapted from Lim (2016). 6

4 An illustration of BPM adapted from Zhang & Jung (2018). 7

5 An illustration of the BJP setup adapted from Mirzababaei & Pasebani (2019). 8

6 An illustration of the LENS setup adapted from Aliakbari (2012). 9

7 The SLM setup adapted from Manjaiah *et al* (2019). 10

8 The benefits of AM standards adapted from Tilton, Dobner & Holdownsky (2017). 11

9 The standardisation roadmap for AM as adapted from ASTM (2017). . . 14

10 A framework of ISO/ASTM 52910 as adapted from ISO & ASTM (2018). 15

11 Process-specific design guidelines as developed for PBF. 17

12 Steps in production of a 3D printed part adapted from Buswell *et al* (2016). 19

13 FDM parameters as adapted from Mwema & Akinlabi (2020). 23

14 The seven primary infill patterns Dezaki & Ariffin (2020). 27

15 The six primary build orientations adapted from ISO & ASTM (2019). . 27

16 An illustration of layer thickness. 28

17 A cause-and-effect diagram for FDM adapted from Villalpando, Eiliat & Urbanic (2015). 30

18 AM materials adapted from Medellín-Castillo & Zaragoza-Siqueiros (2019). 40

19 Materials used in FDM. 42

20 The cause-and-effect diagram developed after parameter elimination. . . 57

© University of Pretoria

21 The fractional factorial method excluding the lack-of-fit point (Montgomery, 2013). 59

22 (a) Ender-3 Max, (b), Ender-5, (c), Ender-5 Plus, (d) Ender-6, (e) Duplicator 9 I3 and (f) Duplicator 9 300 (Wanhao, 2021; Creality, 2021). . . . 63

23 A standard ASTM D638 Type I tensile bar (ASTM, 2015). 66

24 (a) A Mitutoyo micrometer and (b) a vernier calliper. 67

25 The tensile machine used during testing. 68

26 (a) The placement of the extensometer on a specimen and (b) the extensometer. 68

27 Stress-strain behaviour of Group A. 77

28 Stress-strain behaviour of Group B. 78

29 Stress-strain behaviour of Group C. 78

30 Stress-strain behaviour of Group D. 79

31 Sample comparison for Wanhao PLA on the Creality Ender-6. 84

32 Sample comparison for Buildvolume PLA on the Creality Ender-6. 85

33 Sample comparison for Flashforge PLA on the Creality Ender-6. 87

34 Sample comparison for Zortrax PLA on the Creality Ender-6. 88

35 Comparison of Experiment 4 samples for Zortrax PLA on the Creality Ender-6. 89

36 Sample comparison for CRON PLA on the Creality Ender-6. 90

37 Sample comparison for Wanhao PLA on the Creality Ender-3 Max. . . . 91

38 Sample comparison for Wanhao PLA on the Creality Ender 5. 92

39 Sample comparison for Wanhao PLA on the Creality Ender-5 Plus. . . . 93

40 Sample comparison for CRON PLA on the Wanhao Duplicator 9 I3. . . . 94

41 CRON PLA comparison between different printers. 95

© University of Pretoria

42 Sample comparison for Wanhao PLA on the Wanhao Duplicator 9 300. . . 95

43 Creality Ender-6 comparison between different filaments. 97

44 Wanhao PLA comparison between different printers. 98

45 Cost comparison between filaments printed on the Creality Ender-6. . . . 98

© University of Pretoria

List of Tables

1 The existing standards for AM adapted from Wang *et al* (2020). 16

2 A summary of the descriptions of various printing/machine parameters. . 24

3 FDM parameter categorisation (Wang *et al*, 2020; Sola *et al*, 2022) 25

4 Recommended wall thicknesses as adapted from Stratasys (2021). 32

5 Recommended text sizes as adapted from Stratasys (2021). 34

6 A summary of several polymers used in FDM (Daminabo *et al*, 2020). . . 44

7 A summary of various studies performed in the past with respect to FDM. 45

8 Low, medium and high levels of the parameters used in the DOE. 56

9 The coordinates of the points used in the three-level fractional factorial design. 59

10 The parameters that were kept constant during the execution of the experiments. 60

11 The DOE constructed based on the two-level fractional factorial design. . 61

12 Filament brands and its corresponding manufacturer. 61

13 The printer models used to produce the various prints. 62

14 Printing sets completed based on the DOE. 64

15 The printing parameters that were set in Cura for each experiment. . . . 65

16 A summary of the visual inspection performed on the printed samples. . 70

17 A summary of the visual inspection performed on the broken samples. . . 74

18 Mechanical properties for various filament on different types of printers. . 80

19 The ANOVA obtained for Wanhao PLA/Creality Ender-6. 85

20 The ANOVA obtained for Buildvolume PLA/Creality Ender-6. 86

21 The ANOVA obtained for Flashforge PLA/Creality Ender-6. 87

© University of Pretoria

22 A summary of similar experiments printed on different printers and filament rolls. 88

23 The ANOVA obtained for Zortrax PLA/Creality Ender-6. 89

24 The ANOVA obtained for CRON PLA/Creality Ender-6. 90

25 The ANOVA obtained for Wanhao PLA/Creality Ender-3 Max. 91

26 The ANOVA obtained for Wanhao PLA/Creality Ender-5. 92

27 The ANOVA obtained for Wanhao PLA/Creality Ender-5 Plus. 93

28 The ANOVA obtained for CRON PLA/Wanhao Duplicator 9 I3. 94

29 The ANOVA obtained for Wanhao PLA/Wanhao Duplicator 9 300. . . . 96

30 The material evaluation guideline for PLA filament. 99

© University of Pretoria

Nomenclature

A	Layer thickness	mm
B	Air gap	–
C	Raster angle	°
D	Build orientation	°
E	Road with	mm
F	Number of contours	contours
R_i	Inner radius	mm
R_o	Outer radius	mm
t	Wall thickness	mm

© University of Pretoria

1 Introduction

The manufacturing and fabrication of parts in an economical manner are fundamental in several sectors. The optimisation of the production of high-quality parts has become a major concern as the majority of parts have pre-determined design outcomes. The production of these parts should be manufactured in a reasonable time frame and material costs should be minimised. Additive Manufacturing (AM) made both affordable and fast manufacturing possible. AM had an initial growth spurt between the years 1990 and 2000. Metal-based AM processes (*e.g.* Selective Laser Melting (SLM)) were developed during the late 2000s. Raw material/feedstock is used to produce parts through layer-by-layer-, line-by-line-, surface-by-surface- or plane-by-plane deposition. The AM technology fabricates the part by making use of projection patterns and/or tool paths. Post-processing techniques can be utilised to improve the quality of a printed part. (Thompson *et al*, 2016)

This document focuses on one AM process in particular, namely Fused Deposition Modelling (FDM)/Fused Filament Fabrication (FFF)/Material Extrusion (MEX). Several mechanical-, geometric-, printing- and material parameters affect the mechanical properties of a printed part. The inter-connectivity and statistical significance of these parameters are undefined. No material evaluation guideline has been developed for FDM that can be used as guideline for material- and part development.

The purpose of this project was to identify the parameters that have the greatest affect on the mechanical properties of a printed part. These parameters were used to specify a generic statistical Design of Experiments (DOE), which could have been used irrespective of brand of filament and/or type of printer model. The latter accompanied by the settings selected in the Cura® slicing software were used for the development of a material evaluation guideline for PLA filament on open-source printers.

Extrusion/printing speed, nozzle temperature and build plate/bed temperature were the three parameters identified and used during the two-level fractional factorial design utilisation to obtain a generic DOE. The final DOE design resulted in six experiments. Ten specimens were printed during each experiment to evaluate the statistical significance of each parameter. A material evaluation guideline was developed based on the results obtained from the DOE and Cura settings.

© University of Pretoria

2 Additive Manufacturing (AM)

The field is expanding quite rapidly as there is a continuous need to improve product development cycles, personalisation of products, sustainability and business models. Over the years the market has shifted from model- and prototype development to the fabrication of parts and products. AM technology and patent development originated as early as the 1960s. The roots of photopolymerisation date back to the 1960s, those of powder fusion to 1972 and those of sheet lamination to 1979. Hand-in-hand to the process development was the development of software (*e.g.* CAD systems in the 1960s) and control machine tools (*e.g.* computer monitors in the 1970s). Academic publications and further process development (*e.g.* laser beam melting) increased between the 1980s and 1990s. Academic fields and the AM hobby community started to show an interest, which resulted in the growth of market supply and demand (Thompson *et al*, 2016). AM forms an important part of the fourth industrial revolution (Valerga *et al*, 2018).

There are few geometric constraints when developing an AM part. The technology allows for the designing of complex internal features which enhances part performance and functionality. Reduced part counts, reduction in waste generation and an acceleration in the production timeline are achieved by utilising AM (Ferrell, Arndt & TerMaath, 2021). The parts can be produced by utilising various materials (Davies *et al*, 2021). Macrostructure topology optimised objects can be created by using AM. When considering the above, it can be noted that AM is an advantageous method compared to technologies such as Direct Metal Laser Sintering (DMLS) (Thompson *et al*, 2016). The versatile nature of the processes leads to the application of AM technology in various fields. Some of the fields where AM technology is used include the automotive-, aerospace-, medical-, construction-, jewelry-, turbomachinery-, dental-, shipping-, optometric-, sport-, clothing- and electronic fields (Oleff *et al*, 2021).

AM has several disadvantages associated with it. These disadvantages include the limitations associated with the designing of complete and comprehensive digital models, the part quality is inconsistent, the boundaries between various parts are seldomly seamless, mechanical properties are sometimes jeopardised to decrease the cost of production and inconsistent properties of feedstock. These constraints should be considered when the manufacturer stands at the crossroad between the cost-effectiveness of production of the existing product or the redesigning of a new product. AM is not always the most economical choice of manufacturing as the constraints are undesirable but perpetual. Methods of troubleshooting for constraints associated with FDM are discussed in more detail in Section 3.5. (Thompson *et al*, 2016)

© University of Pretoria

2.1 AM processes

AM is divided into seven processes. The primary difference between these processes is the deposition technique exploited. The processes are fabricated similarly thermally, mechanically and chemically and include Liquid Thermal Polymerisation (LTP), Fused Deposition Modelling (FDM), Stereolithography (SLA), Ballistic Particle Manufacturing (BPM), Binder Jet Printing (BJP), Laser-Engineering Net-Shaping (LENS) and Selective Laser Melting (SLM) (Zhang & Jung, 2018). The principles of each process are discussed separately and in more detail in this section. These should be considered when determining the fabrication method utilised to produce parts with desired properties. According to ISO & ASTM (2021), the process categories used for AM are BJP, Direct Energy Deposition (DED), Material Extrusion (MEX), Material Jetting (MJT), Powder Bed Fusion (PBF), Sheet Lamination (SHL) and Vat Photopolymerisation (VPP).

2.1.1 Stereolithography (SLA)/Vat Photopolymerisation (VPP) and Liquid Thermal Polymerisation (LTP)

SLA and Liquid Thermal Polymerisation (LTP) are similar, as both use liquid feedstock. SLA uses photo-curable materials/photopolymers, while LTP uses thermoset materials /thermosetting (Bikas, Stavropoulos & Chryssolouris, 2016). SLA was first developed by Dr Hidoe Kodama in 1981 and the first commercial SLA printer was patented by Charles W Hull in 1987 (Schmidleithner & Kalaskar, 2018).

SLA is one of the oldest and most used AM processes. It is a vat polymerisation method. The curing step of SLA is when the feedstock selectively solidifies after being exposed to ultraviolet (UV) laser light. The chemical polymerisation reaction is locally activated after a photoinitiator (PI) molecule is irradiated. The layers are consecutively deposited and solidified (Gardan, 2015; Manjaiah *et al*, 2019). The light source determines whether the printing is either laser scanning based or mask projection based. Parts of high precision, high shaping accuracy, low equipment cost and high flexibility are produced (Wu *et al*, 2023). Post-processing is required after the fabrication of some parts. Figure 1 is a schematic illustration of the SLA setup.

© University of Pretoria

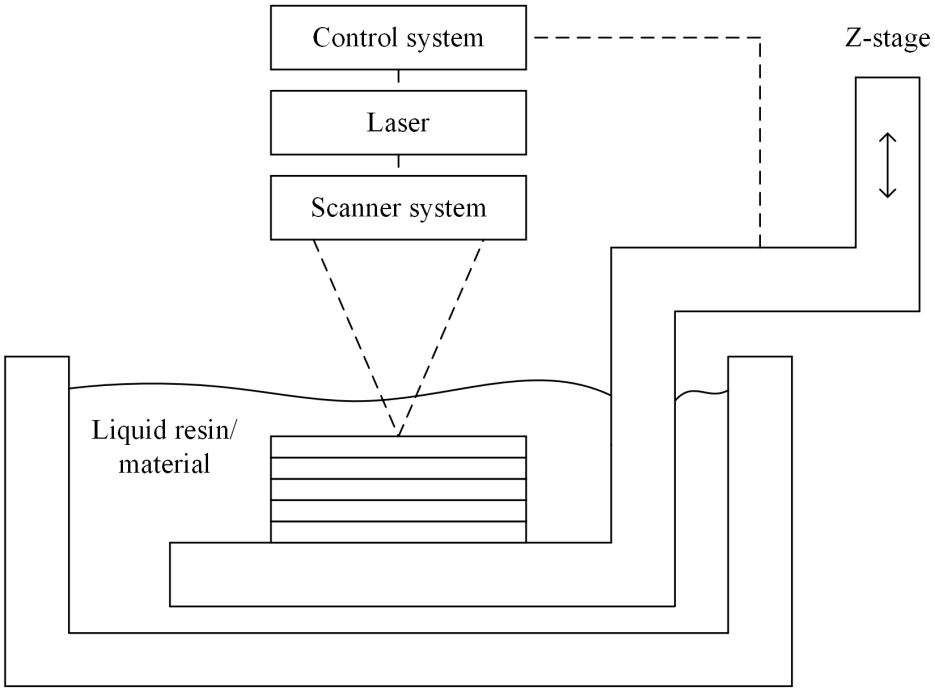

Figure 1: An illustration of SLA adapted from Manjaiah *et al* (2019).

In LTP the feedstock is deposited by jetting heads on the building platform. The location of the droplet deposition is monitored by means of computer control. Simultaneously another jetting head deposits adhesion material to the already jetted droplets. The layers solidify after the application of heat. This dissipation of heat ensures that the layers are of a desired composition (Pham & Dimov, 2001).

A downside of the process is not uniform layer thickness throughout the printed part–droplet geometry is strenuous to control. The latter may be resolved by using a milling machine after the deposition of each layer of material (Pham & Dimov, 2001). LTP has adequate production throughputs, but the parts fabricated are less accurate when compared to those fabricated by SLA (Bikas, Stavropoulos & Chryssolouris, 2016). Figure 2 is a schematic illustration of the LTP setup.

© University of Pretoria

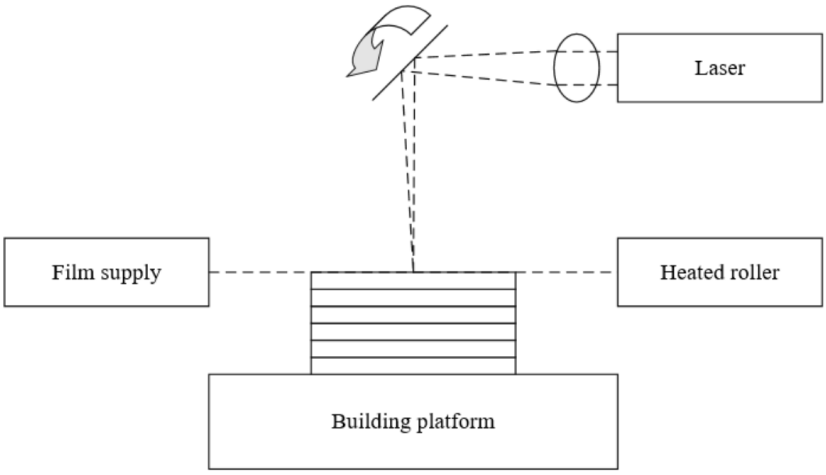

Figure 2: A schematic illustration of LTP adapted from Pham & Dimov (2001).

2.1.2 Fused Deposition Modelling (FDM)/Material Extrusion (MEX)

According to Ferrell, Arndt & TerMaath (2021), Fused Filament Fabrication (FFF)/Fused Deposition Modelling (FDM) is the most readily used technique in industry. It is also known as Material Extrusion (MEX). FDM is an AM process that uses thermoplastic material as feedstock. After the extrusion process, the material rapidly cools and holds the design shape/geometry (Ferrell, Clement & TerMaath, 2021). The sub-categories grouped under MEX vary in kinematic design, type of extruder and form of feedstock (Oleff *et al*, 2021).

Molten material is deposited in beads onto the build surface layer-by-layer in a specific pattern, by utilising a fine computer-controlled nozzle (Oleff *et al*, 2021). The control mechanism allows the nozzle to move in an X-Y direction. The latter is only applicable to certain control mechanisms as some use radial control. All control mechanisms use Z-access control. (Medellín-Castillo & Torres, 2009)

The 3D printer setup primarily consists of one nozzle, but a second nozzle can be installed if the deposition of secondary material (*e.g.* for the construction of support) is required. The filament first enters an extrusion chamber where it is heated to a temperature above the polymeric materials melting temperature. The material must solidify after extrusion and deposition (Bikas, Stavropoulos & Chryssolouris, 2016). The process is advantageous as no or few post-processing methods have to be used (Manjaiah *et al*, 2019). Other advantages include the reduction in cost, increased productivity, decreased material waste and the applicability of part production in various fields (Ferrell, Clement & TerMaath, 2021). This process will be discussed in more detail in Section 3. Figure 3 is a schematic illustration of the FDM setup.

© University of Pretoria

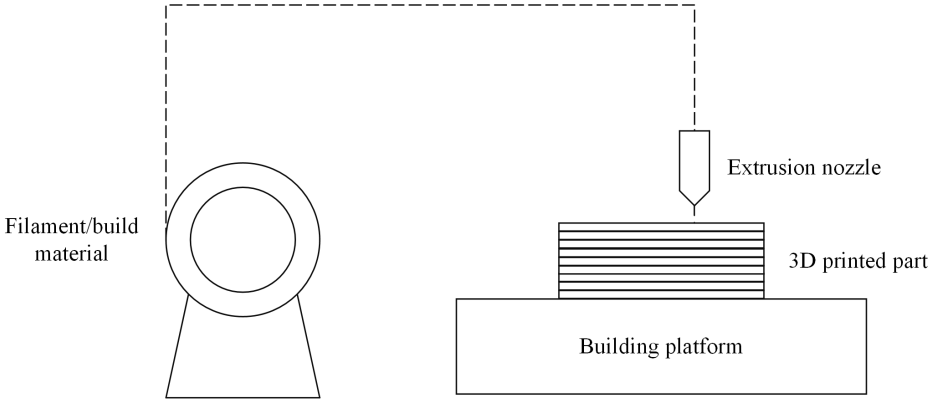

Figure 3: A schematic illustration of FDM adapted from Lim (2016).

2.1.3 Ballistic Particle Manufacturing (BPM)/Material Jetting (MJT)

Ballistic Particle Manufacturing (BPM) is an AM process where the molten droplets are deposited on the substrate employing piezoelectric inkjet printing nozzles (Bikas, Stavropoulos & Chryssolouris, 2016). It is also known as Material Jetting (MJT). This technology enables the production of high resolution parts with complex structures (Segura *et al*, 2023). This method ensures that a continuous stream of molten material is ejected from the nozzle. The adhesion between the layers is promoted once the material comes into contact with the cold substrate–the form of the material changes from semisolid to solid (Zhang & Jung, 2018).

The droplets are guided utilising an electrical field. The guidance of flow ensures correct deposition and utilisation of material to form the desired geometries. BPM can be used for the fabrication of high quality and accurate parts for which no post-processing operations are required (Zhang & Jung, 2018). Figure 4 is a schematic illustration of the BPM setup. It can be noted that the extrusion head has multi-axis control.

© University of Pretoria

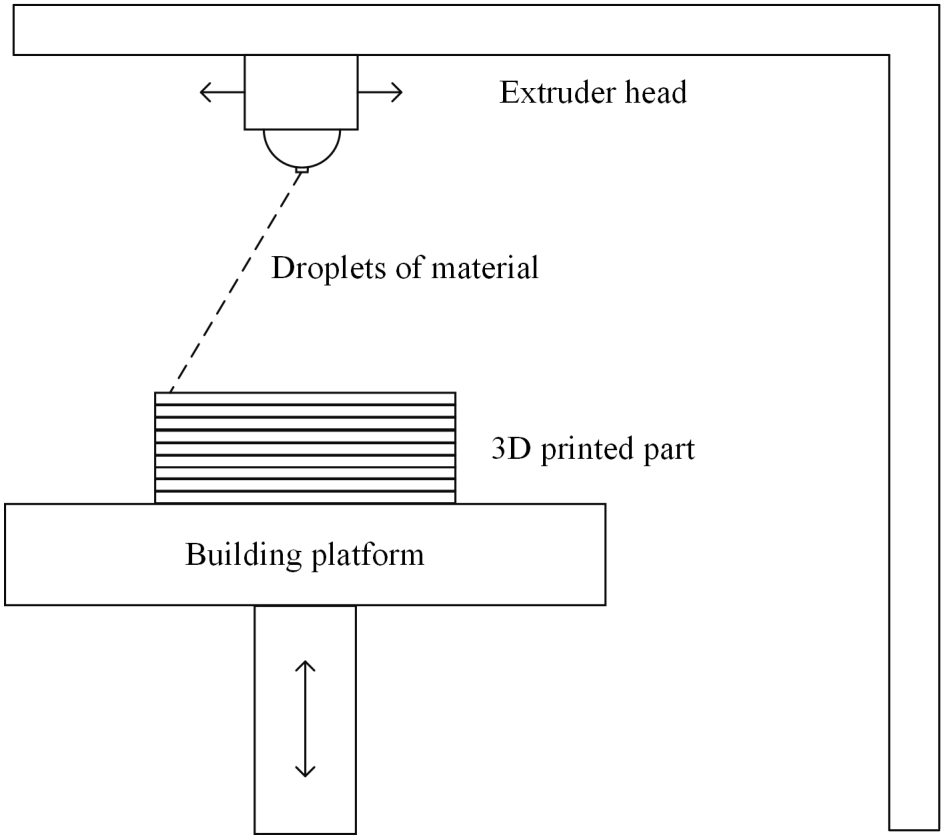

Figure 4: An illustration of BPM adapted from Zhang & Jung (2018).

2.1.4 Binder Jet Printing (BJP)

Binder Jet Printing (BJP) is a process that is used primarily for the production of metal parts. It has been reported that not only metallic but also ceramic and polymeric materials can be utilised (Manjaiah *et al*, 2019). The process uses a computer-controlled nozzle. The liquid binder droplets are deposited onto a powder layer, forming a cross-section of the part. A roller is used to ensure uniform thickness throughout the part. A new powder layer is spread and the droplet deposition is repeated (Fuchs *et al*, 2022). The slicing of the 3D CAD file monitors the amount of adhesive applied to the deposited material layer. Adhesion between the layers is ensured by the use of an adhesive injector head. The latter is different for Material Jetting (MJT) as no binder material is required (Fuchs *et al*, 2022).

BJP fabricated parts require post-processing to increase the mechanical strength, unlike the parts of Selective Laser Melting (SLM) or FDM (Fuchs *et al*, 2022). Post-processing improves surface roughness and reduces fluctuations in flatness. The parts need to be cured in a furnace at a specific curing temperature, which is determined by the adhesive and deposited materials used. Post-processing processes (*e.g.* high-temperature firing)

© University of Pretoria

ensure that the part obtains the desired properties. According to Manjaiah *et al* (2019), the particles will be well bonded and intact. Figure 5 is a schematic illustration of the BJP setup.

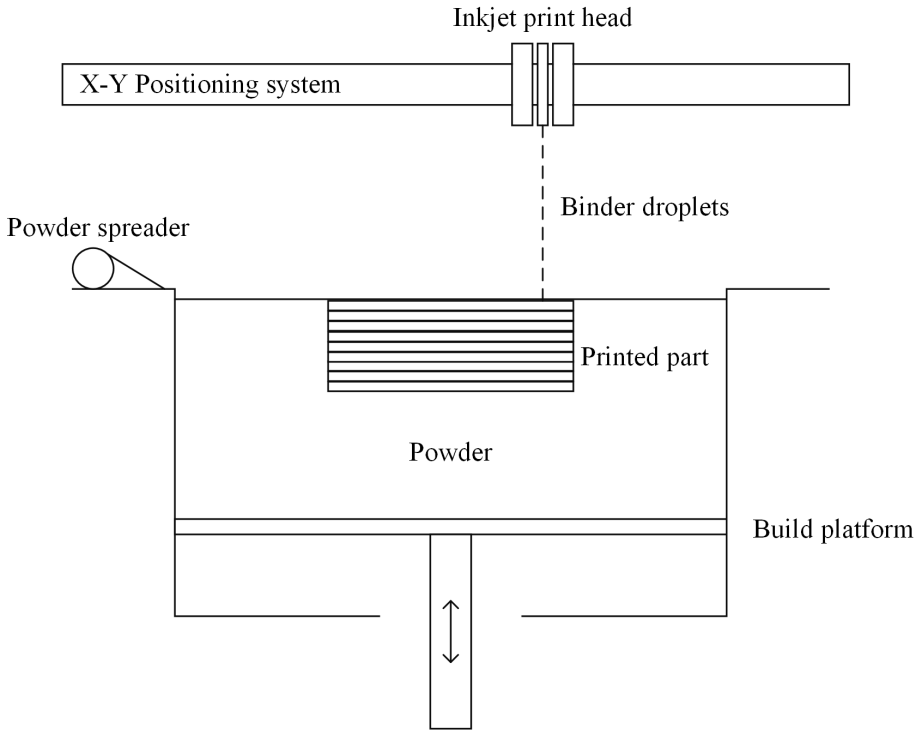

Figure 5: An illustration of the BJP setup adapted from Mirzababaei & Pasebani (2019).

2.1.5 Laser-Engineering Net-Shaping (LENS)/Direct Energy Deposition (DED)

The production and fabrication of metallic parts are not only done by using BJP, but also Laser-Engineering Net-Shaping (LENS). LENS is also known as Direct Energy Deposition (DED). It is a powder-based AM process, which melts a continuous stream of feedstock (wire or powder) by utilising lasers (Bikas, Stavropoulos & Chryssolouris, 2016; Fuchs *et al*, 2022). A stream of powder particles is created by one of more nozzles. This stream is focused at the laser interaction zone. The three-dimensional relative motion between the deposition head and substrate defines the shape of the final part (Fuchs *et al*, 2022).

There are several similarities between LENS and SLM. One such similarity is the use of a computer-controlled nozzle. The nozzles are in a coaxial position to the laser head. The feedstock material is fed in powder form. A pressured carrier gas *(e.g.* an inert gas or air) is the driving force that moves the feedstock to the tip of the laser. An additional laser beam, with adjustable energy densities, is used for the melting of the feedstock powder after being deposited onto the surface (Gardan, 2015; Manjaiah *et al*, 2019).

© University of Pretoria

Another similarity between SLM and LENS is the relative density of the fabricated parts. The integrity and density of the part are enhanced due to the flowing feedstock used. The form of the feedstock may vary (*i.e.* particles, wires and rods). The process materials used range from soft metals such as copper and aluminium to stainless steel. In each of the AM processes, several parameters are affecting the mechanical properties of the printed part. This statement is discussed in more detail in Section 3.4. It is an ideal technique to utilise when repairing or refurbishing damaged parts/components as well as for the production of parts with complex geometries (Manjaiah *et al*, 2019). Figure 6 is a schematic illustration of the LENS setup.

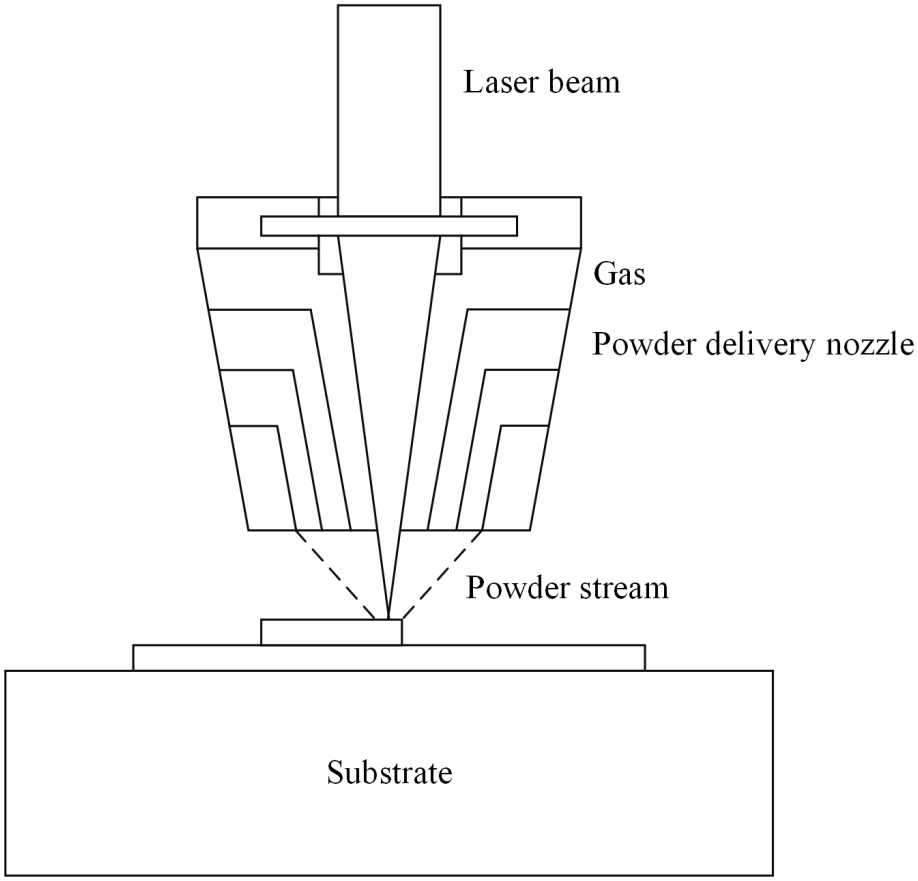

Figure 6: An illustration of the LENS setup adapted from Aliakbari (2012).

2.1.6 Selective Laser Melting (SLM)/Powder Bed Fusion (PBF)

Selective Laser Melting (SLM) is an AM process for metals. It is also known as Powder Bed Fusion (PBF). It has a more complex control system in comparison with the methods used for the processing of polymers. Thin layers of metal powder are fused and melted to create a layer-by-layer formation. Capillary forces, surface tension, wetting and temperature dependence are the driving forces of the process (Fuchs *et al*, 2022).

© University of Pretoria

According to Bikas, Stavropoulos & Chryssolouris (2016), the laser beam power generally used is 400 W. The chamber is filled by a material powder, where after it is transported by means of a roller/coater into the location of fabrication. The powder that has been in contact with the laser melts due to the thermal effect of the beam, while the other powder remains intact. Usually, the intact powder is recycled and reused in future runs. The process is carried out under constant vacuum pressure (at atmosphere) or constant inert gas pressure (at air pressure). Figure 7 is a schematic illustration of the SLM setup.

Some of the advantages for using SLM include parts have good mechanical properties, parts have high accuracy and density, parts can be fabricated at relatively high process speeds, intricate-shaped geometries can be created and there is a vast range of metallic materials and their alloys that can be utilised (Manjaiah *et al*, 2019).

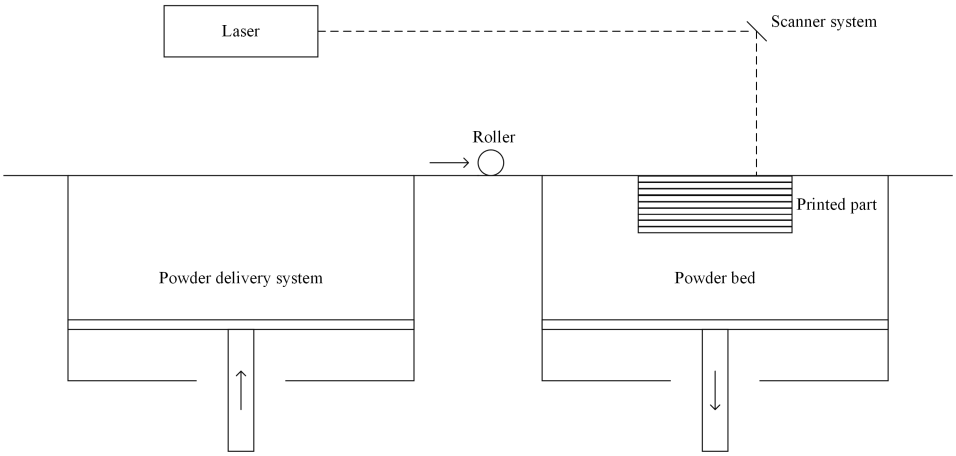

Figure 7: The SLM setup adapted from Manjaiah *et al* (2019).

2.2 Existing standards

Standards are defined as characteristics, rules and guidelines stipulated in a document format for either an activity or its results. Concerning AM, the standards focus on technical systems and the analysing of the products produced through these systems. Processes, definitions, technical methods and specifications are referred to as "AM standards". The development and implementation of standards are fundamental as it define best practices, benchmarks and rules. The standards act as a framework to develop a safe working environment and to ensure that all aspects of the process, from raw materials to sold products, are of a desirable quality and consistency. Figure 8 illustrates the benefits of AM standard. (Tilton, Dobner & Holdownsky, 2017)

© University of Pretoria

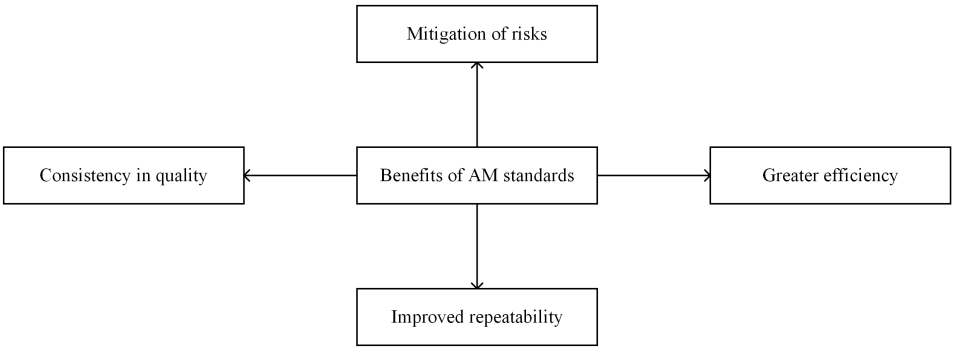

Figure 8: The benefits of AM standards adapted from Tilton, Dobner & Holdownsky (2017).

Standards Development Organisations (SDOs) are responsible for the developed of technical standards and focusses on several specialisations in the industry. The National Standards Body (NSB) in the United States of America is the American National Standards Institute (ANSI). One of the main objectives is to develop standards that have an international impact. The International Organisation for Standardisation (ISO) and the American Society of Testing and Materials (ASTM) are leading developers of international standards. (Tilton, Dobner & Holdownsky, 2017)

In the past, several standards were developed by ASTM (*e.g.* ASTM D638) and ISO (*e.g.* ISO 527-2) separately. Confusion occurred due to small differences between similar standards developed by both organisations and therefore it was decided to develop conjoined standards (*e.g.* ISO/ASTM 52900). The standards assist in the determination of mechanical properties of printed parts. The Additive Manufacturing Standardisation Collaboration (AMCS) is responsible for the acceleration and coordination of the development of AM standards. The AMCS developed a Standardisation Roadmap for AM. Several gaps were identified in the AM market and were summarised in this roadmap. AMCS defined a gap as a topic for which no published specifications and standards exist.

A total of 89 gaps were identified and categorised in low-, medium- and high priority. Tilton, Dobner & Holdownsky (2017) suggested that companies developed their own standards for the pre-determined gaps. To achieve the latter the company should identify the need, determine the variables, determine the best route for success, plan data collection, perform experiments and draw conclusions based on the observations made during the experimental analysis.

2.2.1 Standards for AM

Standards are developed for the production of repeatable and consistent parts. Tilton, Dobner & Holdownsky (2017) divided the AM standards into three groups, namely part

© University of Pretoria

design, data, materials and production. The AMCS developed an extensive categorising chart as illustrated in Figure 9. The Digital Thread for Additive Manufacturing (DTAM) consists of several steps. The steps with their corresponding standards are (Tilton, Dobner & Holdownsky, 2017):

- Scan/design and analyse (ISO STEP AP 242 and ISO STEP AP 203).
- Build and monitor (ISO/ASTM CD 52903-2 and ASTM F3187-16).
- Test and validate (ISO/ASTM 52900: 2021, ISO/ASTM 52921: 2013 and ASTM E1316-16a).
- Deliver and manage.

Terminology used in AM standards as well as basic principles for ceramic, metallic and plastic AM fabricated parts are standardised (*e.g.* ISO/ASTM 52900: 2021). The required file format is explained in ISO/ASTM 52915:2020. ISO/ASTM 52910: 2018 discussed recommendations, requirements and guidelines for designing AM parts. The framework of the standard is illustrated in Figure 10. In this document there are references to various standards for the evaluation of the mechanical properties of an AM part.

Some standards replace others depending on the application and material availability. Designation D1708-18 replaced ASTM D638 when material availability was limited. The latter explained the testing conditions and equipment required for specimens with a thickness up to and less than 3.2 mm. Another aspect to consider is the required material properties for engineering designs. Designation D5592-94 described the material properties required for structural designs including snap-fits, press-fits, beams and plates. The test method used for the determination of the mechanical properties (*e.g.* tensile properties) of plastic AM parts as stipulated in Designation D638-14. Several types of samples can be prepared and the testing conditions (*e.g.* speed of testing) depend on the type of sample. Standards have been developed not only for plastic AM parts, but also for metal AM parts (*e.g.* Designation F3122-14). Table 1 summarise the existing standards for AM as developed by ISO and/or ASTM.

Process-specific design guidelines were developed for Powder Bed Fusion (PBF). It was noted that these guidelines were developed by ISO or ASTM and are currently the only guidelines for AM processes. Figure 11 is an illustration of the framework of ASTM/ISO JG57 (*i.e.* exposition of the PBF guidelines). ASTM/ISO JG57 comprises of two parts namely, ASTM/ISO 52911-1: 2019 and ASTM/ISO 52911-2: 2019. Phillips, Kortschot & Azhari (2022) mentioned that peer-reviewed articles drove the development of standards

© University of Pretoria

for powder-based AM processes and that the development of MEX/FDM standardisation will be driven by similar comprehensive reviews. The standard developed for PBF can be used as a basis for the development of process-specific design guidelines for FDM as there is currently none.

Valerga *et al* (2018) mentioned that the standardisation of procedures and materials in FDM are lacking. The FDM design space and all its elements (specimen preparation and mechanical testing) are not accounted for in the current available standards (Davies *et al*, 2021). According to Ferrell, Clement & TerMaath (2021), there was two important factors that should be incorporated in a detailed classification standard. The first was repeatability during testing and the second was consistency when reporting the mechanical properties.

Phillips, Kortschot & Azhari (2022) mentioned that the standards for MEX/FDM do not indicate the influence of slicing software and factors impacting void formation. The effect of direct fabrication in comparison to machining the geometry are unclear. It was also noted that visual inspections are impractical for MEX/FDM. It was advised to incorporate guidelines on dimensions of specimens, raster and build orientation, toolpath optimisation, slicing parameters, material and printer specifications, when compiling a standard for MEX/FDM (Phillips, Kortschot & Azhari, 2022). The latter was confirmed by Sola *et al* (2022).

© University of Pretoria

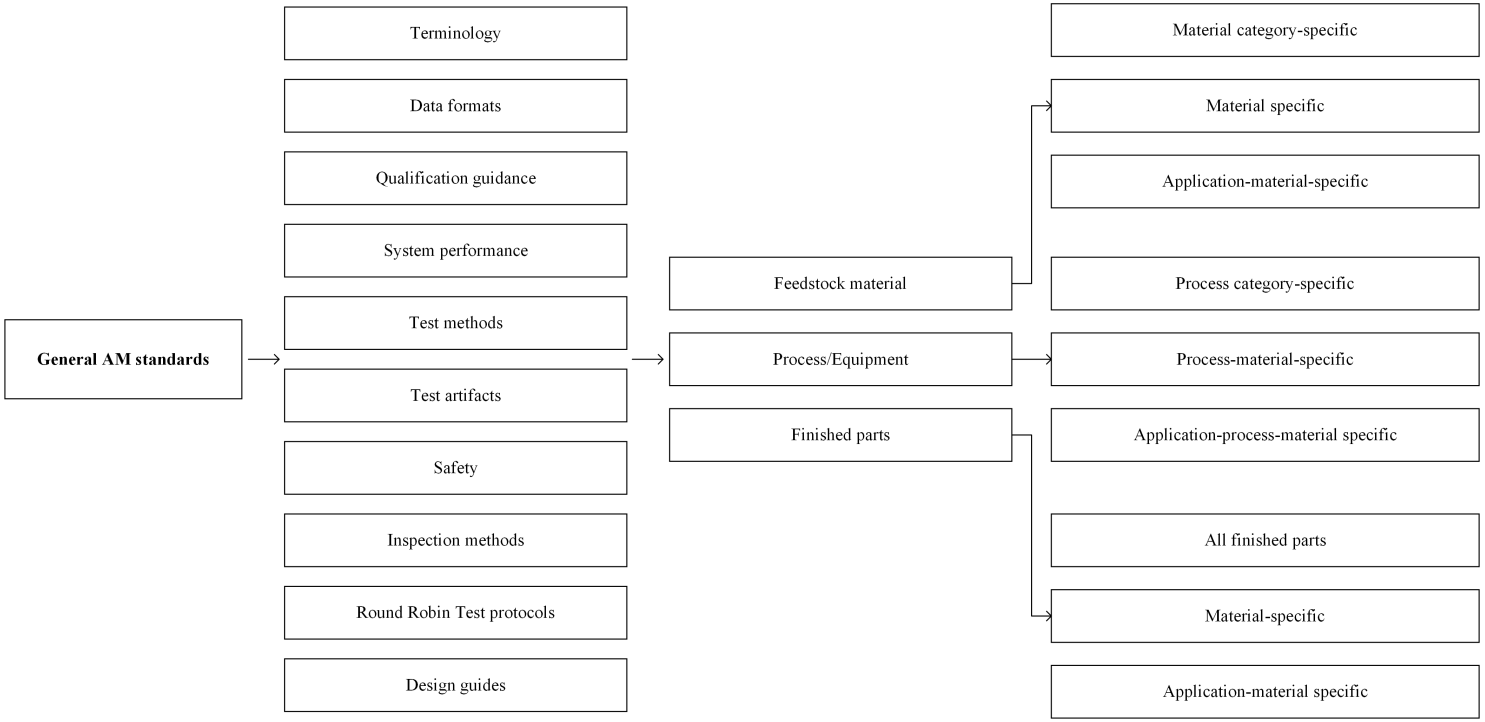

Figure 9: The standardisation roadmap for AM as adapted from ASTM (2017).

© University of Pretoria

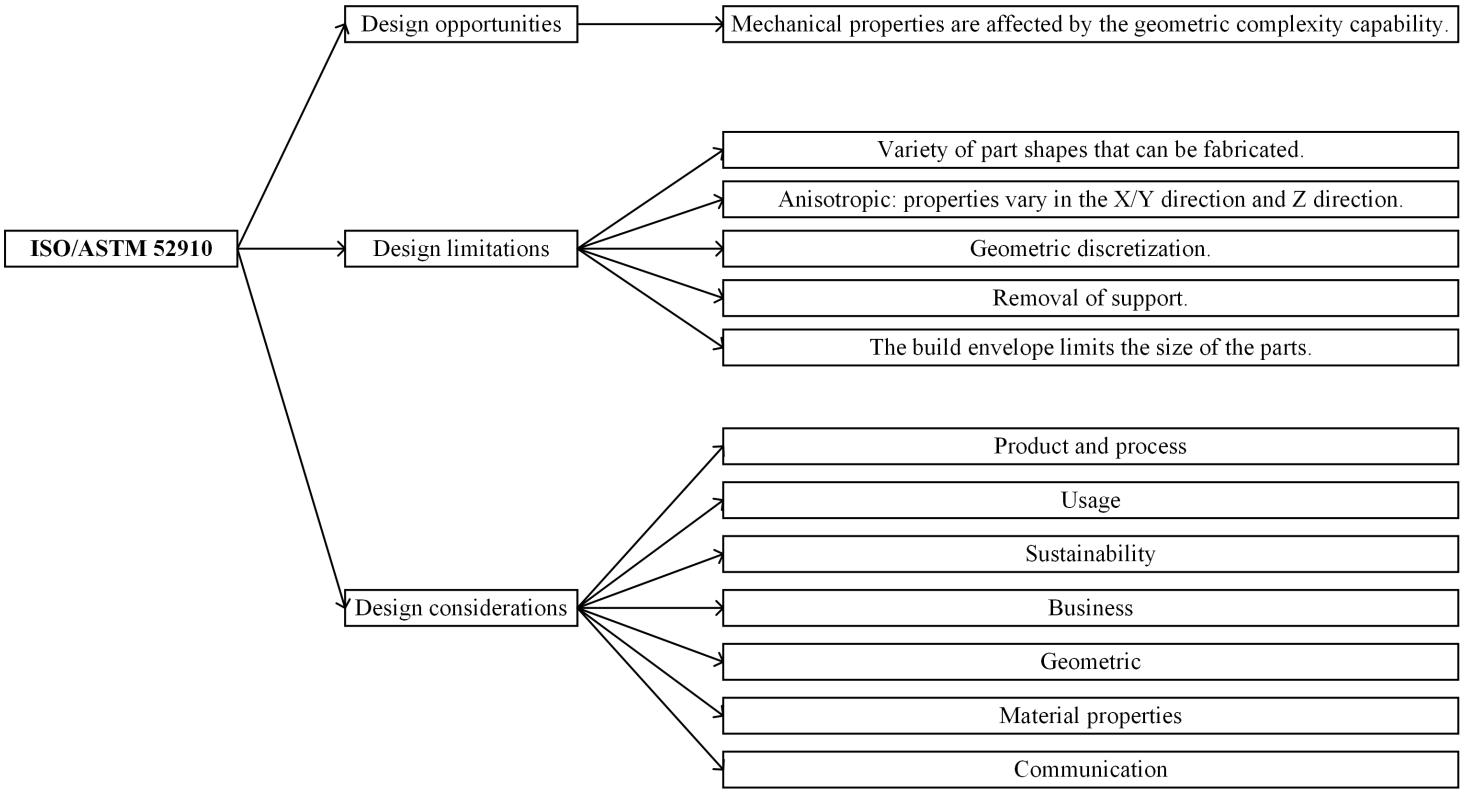

Figure 10: A framework of ISO/ASTM 52910 as adapted from ISO & ASTM (2018).

© University of Pretoria

Table 1: The existing standards for AM adapted from Wang *et al* (2020).

Standards
ISO/ASTM 52900:2021–AM General principles–Fundamentals and vocabulary
ASTM F2924-14 Standard specification for AM Ti-6 Al-4 V with PBF
ISO/ASTM 52901:2017–AM General principles–Requirement for purchased AM parts
ASTM F2971-13–Standard practice for reporting data for test specimens
ISO/ASTM 52902:2019–AM–Test artifacts
ASTM F30001-14–Standard specification for AM Ti-6 Al-4 V ELI with PBF
ISO/ASTM 52904:2019–AM–Process characteristics and performance
ASTM F3049-14–Standard guide for characterising properties for metal powders
ISO/ASTM 52907:2019–AM–Feedstock materials
ASTM F3055-14a–Standard specification for AM Nickel alloy with PBF
ISO/ASTM 52910:2018–AM–Design–Requirements, guidelines and recommendations
ASTM F3056-14el–Standard specification for AM Nickel alloy with PBF
ISO/ASTM 52911-1:2019–AM–Design–Part 1: Laser-based PBF of metals
ASTM F3091/F3091M-14–Standard specification for PBF of plastic materials
ISO/ASTM 52911-2:2019–AM–Design–Part 2: Laser-based PBF of polymers
ASTM F3122-14–Standard guide for evaluating mechanical properties of metal materials
ISO/ASTM 52915:2016–Specification for AM file format (AMF) Version 1.2
ASTM F3184-16–Standard specification for AM stainless steel alloy with PBF
ISO/ASTM 52921:2013–Standard terminology for AM–Coordinate systems
ASTM F3187-16–Standard guide for directed energy deposition of metals
ISO 17296-2:2015–General principles–Overview of process categories and feedstock
ASTM F3213-17–Standard specification for Co-28 Cr-6 Mo via PBF
ISO 17296-3:2014–Main characteristics and corresponding test methods
ASTM F3301-18a–Standard specification for thermal post-processing metal parts
ISO 17296-4:2014–Overview of data processing
ASTM F3302-18–Standard specification for Ti alloys via PBF
ISO 27547-1:2010–General principles and laser sintering of test specimens
ASTM F3318-18–Specifications for AlSi10Mg with PBF–Laser beam

© University of Pretoria

2.2.2 Standards for Powder Bed Fusion (PBF)

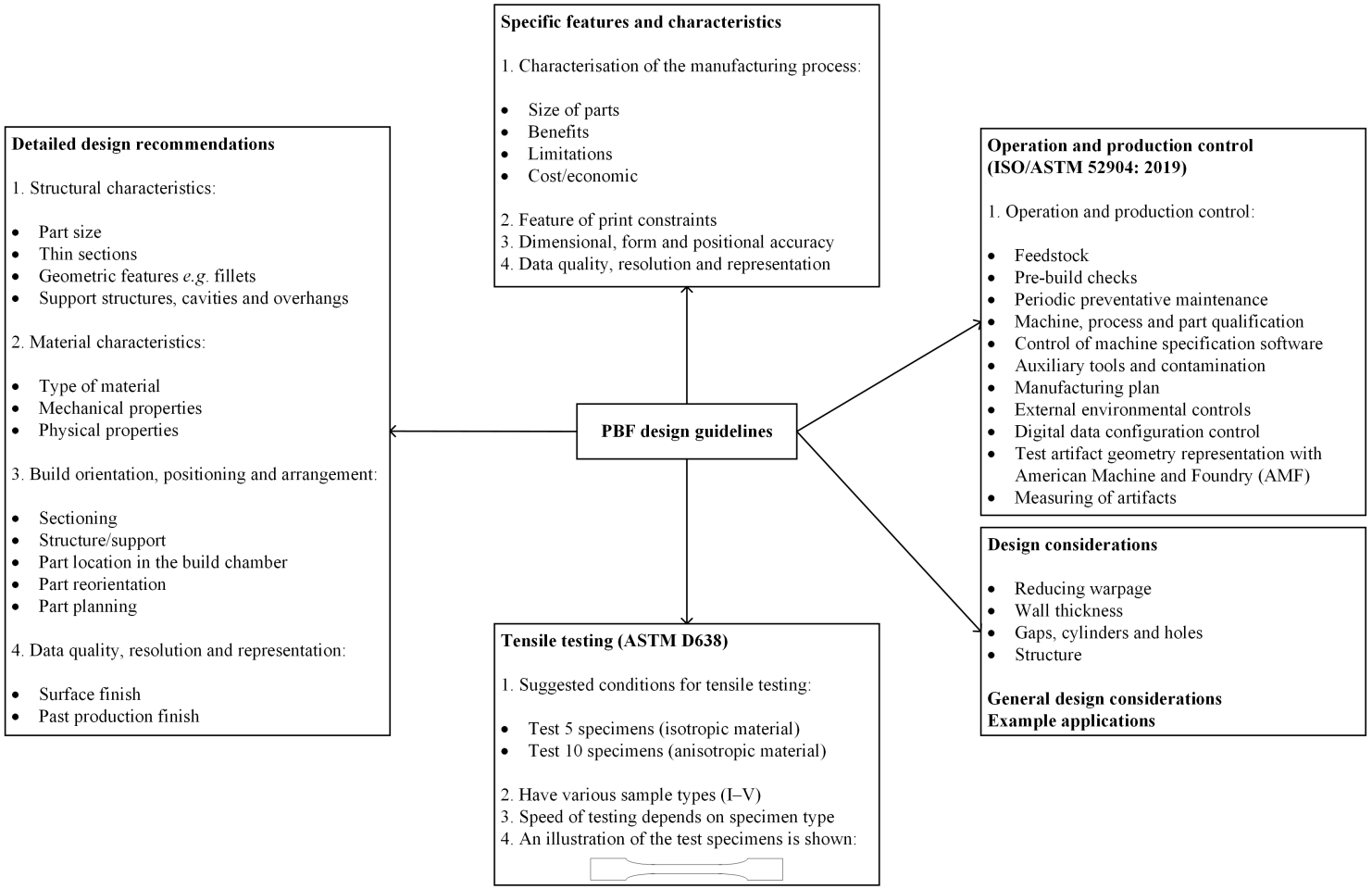

Figure 11: Process-specific design guidelines as developed for PBF.

© University of Pretoria

3 Fused Deposition Modelling (FDM)

Stratasys Ltd trademarked the term FDM, while the un-trademarked term used in industry is Fused Filament Fabrication (FFF). The technology is referred to as Material Extrusion (MEX) in ISO & ASTM (2021). FDM is more readily used than FFF and therefore is referred to in this document. The field of AM is broad and therefore for this research only FDM will be discussed in detail. FDM is a Rapid Prototyping (RP) technology, but more specifically a dispensing process. Medellín-Castillo & Torres (2009) described a dispensing process as a process where a filament or droplet are deposited after the material has been melted or vaporised. The layer-by-layer deposition causes anisotropic effects, because the elastic properties are depended on the orientation (Onwubolu & Rayegani, 2014).

FDM possesses seven characteristics associated with an extrusion process. The characteristics are loading of feedstock, material liquefication, transport of material due to applied pressure, extrusion mechanism, material extrusion on a predetermined path, adhesion between material and/or a secondary material and the application of support structures. The parts produced should meet several geometric, cost and mechanical requirements. The process was developed to increase the flexibility of new parts and to optimise the designing and production time (Medellín-Castillo & Zaragoza-Siqueiros, 2019). According to Xometry (2021), the parts produced by FDM are partially rigid as rigidity is dependent on feedstock. The physical printing process is discussed and a schematic illustration of FDM is summarised in Section 2.1.2.

Prior to printing, the part is designed using CAD software (*e.g.* SolidWorks, Inventor™, CATIA™, Fusion360 and AutoCAD), where after the CAD design is converted into a shell (Buswell *et al*, 2016). Slicing software (*e.g.* Cura) is used to slice the CAD shell into layers. The printing parameters are set and adjusted in the slicing software. The software converts the data of each slice/layer into G-code. The printer uses this code as a coordinate system to determine the tool path that has to be followed by the printer to obtain the desired part Xometry (2021). Buswell *et al* (2016) mentioned that there were several limitations associated with the CAD- and STL software. These include the problems associated with the resolution, file size, robustness and the potential to develop sufficient CAD models. The software is beneficial as it allows for system integration and design freedom. It is important to note that errors occur during all stages (*e.g.* errors in the tessellation algorithms of the STL file). These errors will result in open loops and cannot be interpreted by the machine code generation algorithms. Raster (*i.e.* individual dots) or vectors are used to control the printing operations (Buswell *et al*, 2016). The steps required during production are illustrated in Figure 12.

© University of Pretoria

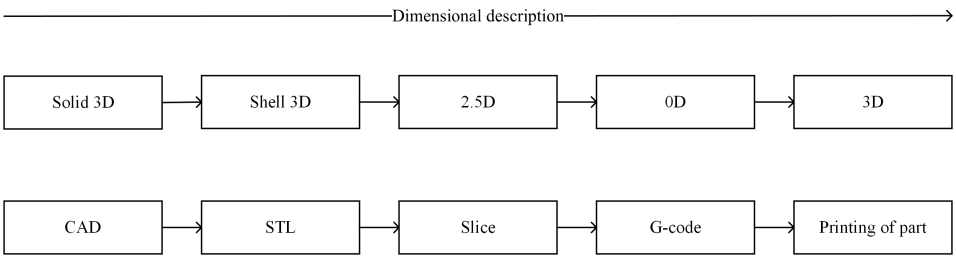

Figure 12: Steps in production of a 3D printed part adapted from Buswell *et al* (2016).

FDM is classified as open-source (*e.g.* Printrbot and Prusa i3) or closed-source (*e.g.* Stratasys and Flashforge). Modifications, emendation and upgrades can be made to the source code of open-source printers. Open-source printers are adaptable with respect to print settings, material of construction and software programs used. The material of construction and software programs are fixed for closed-source printers and cannot be amended by the user. It is important to note that an open-source printer does not entail that the printer has an open chamber and vice versa. An enclosed- or an open chamber affects the adhesion between the deposited layers and print stability. Several materials are sensitive to the fact whether an open- or closed chamber is used. The temperature distribution within a printed part is affected by chamber temperature, bed temperature and nozzle temperature.

The mechanical construction of a printer affects the stability, accuracy and tolerance of a part. A printer (*e.g.* Printrbot) in which the bed can only move sideways and the nozzle upwards and downwards will produce a different print when compared to a printer (*e.g.* Prusa i3) in which the bed moves forward and backwards while the nozzle moves sideways. In addition, different jerk will be experienced in Z-movement bed printers–the bed moves upwards and downwards, while the nozzle moves sideways (*e.g.* Creality Ender-6). The part orientation relates to the axis of most significant jerk. Jerk caused when printing small enclosures is reduced by altering the mechanical motion of both the bed and nozzle. The mechanical construction and whether or not the chamber is enclosed are two parameters seldomly discussed in literature, but have a major effect on the quality and mechanical properties of a printed part. Refer to Section 3.6 for a detailed comparison between the mechanical construction of various printers currently on the market.

This study was performed based on academic literature available and from an academic point of view. The academic and reality are two different worlds that operate independently from one another. Literature focuses primarily on cartesian printers, while those used in industry are predominantly Digital Light Processing (DLP)- Delta-, polar- and continuous fibre FDM printers. In DLP printers, the entire layer is cured by a projected

© University of Pretoria

light source. The technology is similar to Stereolithography (SLA) except for the manner in which the layers are traced (Markforged, 2022). Delta printers have higher stability, temperature conditions and working space. There is also more nozzle flexibility in Delta printers than cartesian printers (Baroiu, F Sovaila & S Sovaila, 2016). The reduced accuracy should be taken into consideration when operating Delta printers. Continuous fibre FDM printers include Mark II produced by Markforged, Fiber™ produced from Desktop Metal, Composer produced by Anisoprint, CFAM Prime produced by CEAD, CF3D produced by Continuous Composited and CBAM-2 produced by Impossible Objects (Aboushama & Beyerlein, 2020; Kuncevich, 2019).

It is difficult to find comparable data as there is no standards for the particular study at hand (Phillips, Kortschot & Azhari, 2022). Articles regarding the effect of parameters on the mechanical strength of a printed part are much less than the information available on open sources (*e.g.* vlogs, blogs, manufactures brochures and YouTube videos). Various search terms were included in Scopus. When the search term read ((fdm OR fff OR mex OR (fused AND deposition AND modelling) OR (fused AND filament AND fabrication) OR (material AND extrusion AND methods)) AND NOT (metal)), 34 227 results were obtained. After "mechanical" was included in the search term, ((mechanical) AND (fdm OR fff OR mex OR (fused AND deposition AND modelling) OR (fused AND filament AND fabrication) OR (material AND extrusion AND methods)) AND NOT (metal)), 7 760 search results were obtained. The search term ((parameter* OR setting*) AND (fdm OR fff OR mex OR (fused AND deposition AND modelling) OR (fused AND filament AND fabrication) OR (material AND extrusion AND methods)) AND NOT (metal)) resulted in 7 662 results. After changing the latter to read as ((parameter* OR setting*) AND (mechanical) AND (fdm OR fff OR mex OR (fused AND deposition AND modelling) OR (fused AND filament AND fabrication) OR (material AND extrusion AND methods)) AND NOT (metal)), 2 270 results are obtained.

The results reduced to 82 when ((standardisation OR standardization) AND (fdm OR fff OR mex OR (fused AND deposition AND modelling) OR (fused AND filament AND fabrication) OR (material AND extrusion AND methods)) AND NOT (metal)) was used. The results obtained reduced even further when the search term was changed to ((standardisation OR standardization) AND (mechanical) AND (fdm OR fff OR mex OR (fused AND deposition AND modelling) OR (fused AND filament AND fabrication) OR (material AND extrusion AND methods)) AND NOT (metal)). The latter resulted in 17 search results. After the search term was changed slightly to ((standardisation OR standardization) AND (parameter* OR setting*) AND (fdm OR fff OR mex OR (fused AND deposition AND modelling) OR (fused AND filament AND fabrication) OR (material AND extrusion AND methods)) AND NOT (metal)),

© University of Pretoria

21 results were obtained. The last search resulted in 28 search results. The search term used was ((standardisation OR standardization) AND (parameter* OR setting* OR mechanical) AND (fdm OR fff OR mex OR (fused AND deposition AND modelling) OR (fused AND filament AND fabrication) OR (material AND extrusion AND methods)) AND NOT (metal)).

From the above discussion it was evident that there were numerous publications available in this field of study. Various publications were obtained in the field of FDM/FFF and MEX when evaluating "mechanical" work done, "parameters*" and "setting*". As soon as the focus field was reduced to "standards" and "standardisation" the number of publications was limited and reduced drastically. In this section, the advantages, disadvantages, parameters, design considerations and printers used in FDM are discussed.

3.1 Advantages

There are several advantages associated with FDM and therefore it is one of the most widely used processes. The advantages of FDM include (Medellín-Castillo & Zaragoza-Siqueiros, 2019):

- The costs associated with maintenance, technology, power and material are low.
- The instrumentation can be used/installed in various work environments (*e.g.* suitable in an office or a workshop).
- Various geometric parts can be fabricated much easier (*e.g.* personal or commercial).
- A wide range of materials can be used as feedstock.
- Materials ranging in different colours can be used.
- Material handling is an uncomplicated process.
- Simple operation of technology (*e.g.* operates at a relatively low temperature).
- Generates minimal dust and noise pollution as well as odours production.

3.2 Disadvantages

All processes have disadvantages associated with them and actions should be taken to compromise for their effect. The disadvantages prohibit designers from developing unlimited parts and several include (Medellín-Castillo & Zaragoza-Siqueiros, 2019):

© University of Pretoria

- The parts are produced at relatively low speeds with accuracy and quality fluctuations.
- Part sizes are directly limited by the size of a printer (*i.e.* the larger the print, the larger the printer required).
- The mechanical properties obtained are not always desired and may vary.
- Warping, distortion, shrinkage and the staircase effect occur.
- The application of support structures and the removal thereof.

3.3 Industrial application

FDM is a relatively new method used for the production of parts, but the advantageous factors associated with it makes it a desirable method to utilise in various fields. The fields in which FDM is used include:

- Biomedical field (*e.g.* dental-, leg- and arm prosthetics) (Thompson *et al*, 2016).
- Medical field (*e.g.* hip replacements and spinal screws) (Thompson *et al*, 2016).
- Construction (*e.g.* concrete deposition on building sites) (Tahmasebinia *et al*, 2018).
- Manufacturing of mechanical parts *(e.g.* aerospace and automobile industry) (Yadav, R Srivastava & Dev, 2020).
- Fashion industry (*e.g.* home furnishing, jewellery and shoes) (Thompson *et al*, 2016).
- Electronics (*e.g.* telephone networks) (Fischer, 2015).
- Sport (*e.g.* printed bike helmets, football masks and mouth guards) (Fischer, 2015).

© University of Pretoria

3.4 Parameters

The parameters selected during the printing process have a considerable effect on the quality and mechanical properties of a print. Mwema & Akinlabi (2020) categorised FDM parameters into two groups, namely machine- and material parameters. Figure 13 illustrates these. The parameters can further be divided into four categories. These categories include printing-, geometric-, material- and printing software (*e.g.* Cura) parameters. Table 2 is a summary of the descriptions of several printing parameters as illustrated in Table 3. Table 3 illustrates various parameters as divided into the four categories.

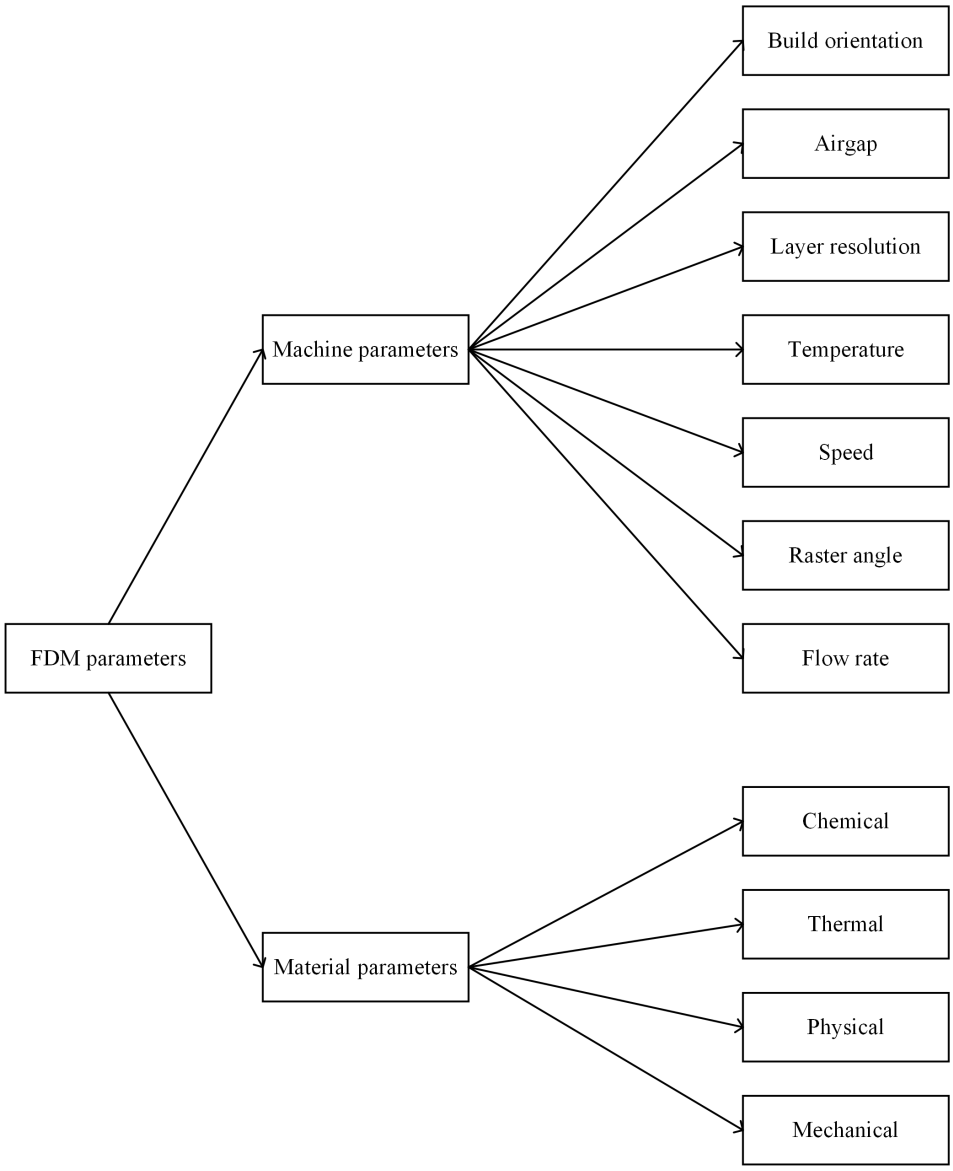

Figure 13: FDM parameters as adapted from Mwema & Akinlabi (2020).

© University of Pretoria

Table 2: A summary of the descriptions of various printing/machine parameters.

Parameter	Description	Reference
Build orientation	The dimensions of a part are specified in three directions, namely the X, Y and Z.	Medellín-Castillo & Zaragoza-Siqueiros (2019)
Location of part on build platform	The location of the part with respect to the build platform.	Mohamed, Masood & Bhowmik (2016)
Layer thickness	Layer thickness is also known as the slice height and is a function of the nozzle diameter and filament diameter used. It is the height of the extruded layer.	Mohamed, Masood & Bhowmik (2016)
Airgap	The distance between two rasters is known as the airgap.	Mohamed, Masood & Bhowmik (2016)
Infill percentage	Also known as the infill density used in a print.	Algarni (2021)
Raster angle	The orientation of the deposited material beads when taking the X-axis of the build platform as reference point.	Mohamed, Masood & Bhowmik (2016)
Extrusion temperature and build plate temperature	The temperature supplied to the printer heating elements from the external source. The temperature of the build platform.	Mwema & Akinlabi (2020)
Extrusion width	The width of the deposited bead of filament.	Dudescu & Racz (2017)
Environmental temperature and humidity	The effect of environmental conditions on printed parts.	Fang *et al* (2020)
Nozzle diameter	The nozzle determines the size and shape of the extruded filament. Most readily used nozzle diameter is 0.4 mm.	Gibson, Rosen & Stucker (2015)
Printing speed	Printing speed vary between 10 mm/s and 250 mm/s.	Algarni (2021)

© University of Pretoria

Table 3: FDM parameter categorisation (Wang *et al*, 2020; Sola *et al*, 2022)

Printing/machine parameters	Geometric parameters	Material parameters	Cura parameters
Build orientation/build direction	Length of overhang	Type of material	Initial layer height
Location of part on build platform	Tangential transitions	Material composition	Line width
Layer thickness	Thin sections/stair-step effect	Material flow rate	Wall speed
Airgap	Fillets	Pre-drying of filament	Top/bottom speed
Infill percentage	Wall thickness	Post treatment	Fan speed
Infill pattern	Sharp edges	Filament diameter	Adhesion type
Raster angle	Sharp angles and/or draft angle	Filler content	Generation of support
Extrusion temperature/nozzle temperature/melt temperature	Columns and pins	Additive content	Retraction
Extrusion width	Threads	Compounding strategy	Adhesion type
Extrusion multiplier	Holes	Extrusion parameters	Number of shells
Build plate/platform temperature	Living hinge		Bottom layers
Build chamber temperature and pressure	Text		Top layers
Build chamber oxygen and humidity	Bosses and ribs		Raster gap
Printing speed	Undercuts		
Nozzle diameter	Combined elements		
Callibration	Mass of specimen		

© University of Pretoria

Parameters have a direct influence on the structural properties of a part and are functions of each other. The interconnectivity between parameters should be considered during the evaluation of the effect of parameter choice on the mechanical properties of a printed part. Some of the functions include:

- Location of part on platform is a function of the number of parts that have to be printed.
- Material feed rate is a function of the melt flow rate through the nozzle.
- Number of contours is a function of the layer thickness.
- Extrusion temperature is a function of the type of material.
- Printing speed is a function of the extrusion speed and the nozzle diameter.
- Melt temperature is a function of the type of material.
- Material flow rate through the nozzle is a function of the extrusion temperature.
- Bed temperature is a function of the type of material.

According to Medellín-Castillo & Zaragoza-Siqueiros (2019), printing parameters including the layer thickness, build orientation, infill pattern and infill percentage are the primary contributors that affect the mechanical properties of a part. The infill pattern and the infill percentage were two of the most influential parameters. It has been observed that the strength of the part increased as the infill percentage increased. Therefore, it was advised by Medellín-Castillo & Zaragoza-Siqueiros (2019) to use high infill percentage values. Parts with satisfactory strength were produced when using an infill percentage ranging from 50% to 100%. As the infill percentage increased the printing time per part also increased. Material cost and production time should be optimised which will result in a lower infill percentage (*e.g.* 60%). There are seven primary infill pattern types as illustrated in Figure 14. Figure 15 is an illustration of the six primary build orientations.

© University of Pretoria

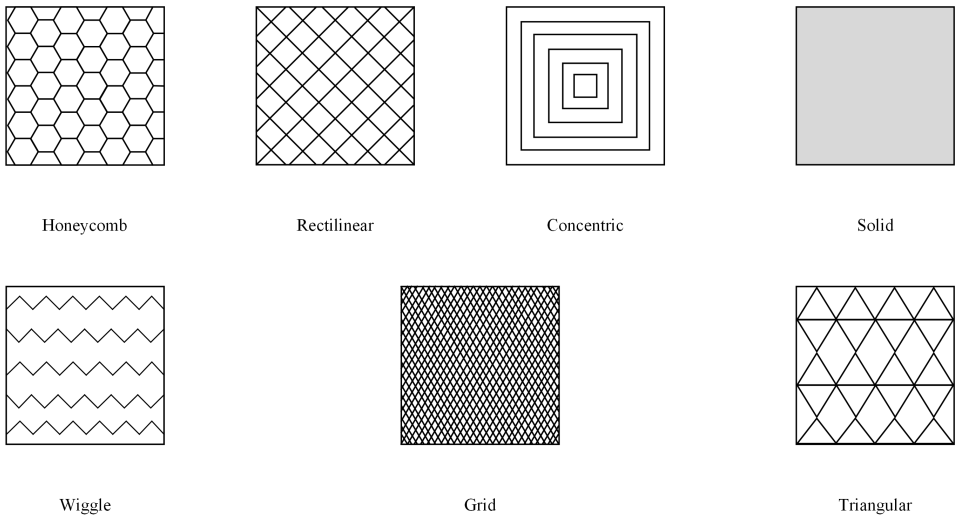

Figure 14: The seven primary infill patterns Dezaki & Ariffin (2020).

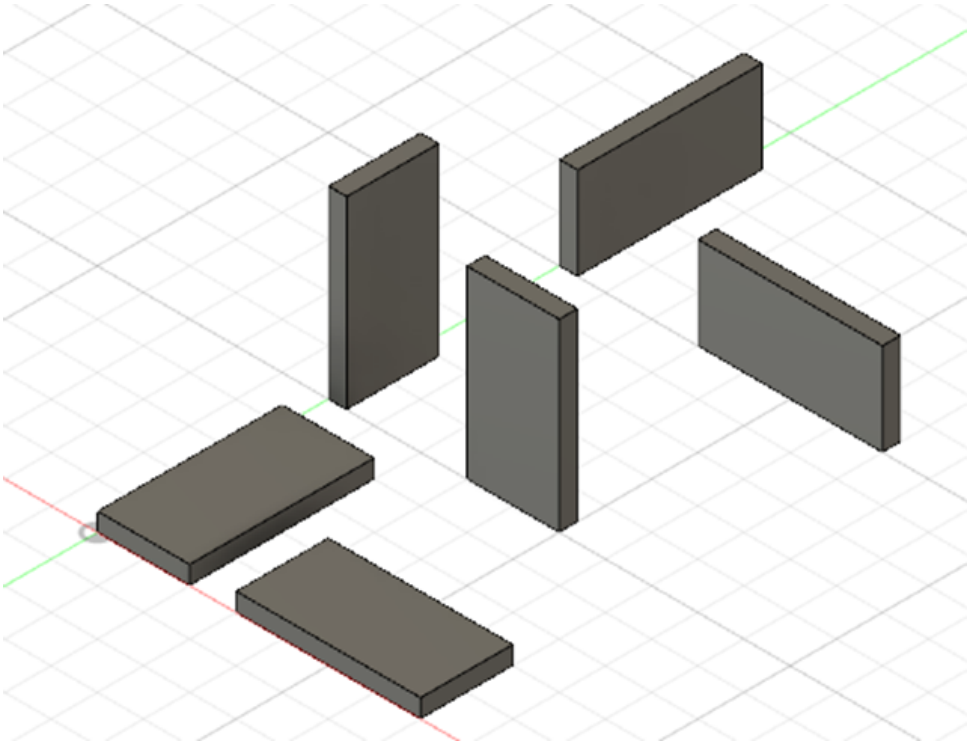

Figure 15: The six primary build orientations adapted from ISO & ASTM (2019).

Medellín-Castillo & Zaragoza-Siqueiros (2019) reported that a smaller layer thickness should be used to ensure that an increase in part strength was obtained. The number of contours should be increased to obtain the desired structural strength. It should be low enough to ensure that the print is completed in a reasonable period and to reduce material consumption (Medellín-Castillo & Zaragoza-Siqueiros, 2019). Figure 16 is an illustration of layer thickness.

© University of Pretoria

Figure 16: An illustration of layer thickness.

In a study performed by Mohamed, Masood & Bhowmik (2016), the layer thickness (A), air gap (B), raster angle (C), build orientation (D), road width (E) and number of contours (F) were studied. Mathematical models were developed to determine their effect on process quality characteristics (*e.g.* dynamic flexural modulus (DFM), build time (BT) and material consumption (MC)). Equation 1 illustrates the mathematical model determined for BT, while Equation 2 illustrates the mathematical model determined for MC. It was suggested that the Q-optimal design was the most efficient design to be used for FDM and was therefore used in their study.

$$\begin{aligned} BT(min) = {} & 21.616 - 129.180A - 3.732B + 0.022C + 0.056D + 4.395E \\ & + 0.777F + 11.039AB - 1.262AF - 0.073DE - 0.627EF \\ & + 224.347A^2 - 2.307 \times 10^{-4}C^2 - 1.721 \times 10^{-4}D^2 \end{aligned} \tag{1}$$

and

$$\begin{aligned} MC(cm^3) = {} & 0.972 - 0.545A - 2.423B + 6.301 \times 10^{-4}D + 3.866E \\ & + 0.025F - 0.332AB - 1.439AE + 1.185BE + 0.113BF \\ & - 0.049EF + 1.888A^2 + 1.088B^2 - 7.410 \times 10^{-6}D^2 - 3.248E^2 \end{aligned} \tag{2}$$

The ranges for the parameters were determined as 0.127 mm $\leq A \leq$ 0.3302 mm, 0 mm $\leq B \leq$ 0.5 mm, 0°$\leq C \leq$ 90°, 0°$\leq D \leq$ 90°, 0.4572 mm $\leq E \leq$ 0.5782 mm and $1 \leq F \leq$ 10. The optimal settings had a minimum bias. Equation 3 illustrates the mathematical model determined for DFM.

$$\begin{aligned} DFM(MPa) = {} & -1992.089 + 2507.582A - 2404.225B - 0.732C + 0.0519D \\ & + 10168.137E + 6.090F - 688.983AB - 1725.895AE \\ & + 1818.298BE + 88.567BF - 7.228E - 0.03CD \\ & - 2924.348A^2 + 1175.176B^2 + 9.988 \times 10^{-3}C^2 - 9910.801E^2 \end{aligned} \tag{3}$$

Analysis of Variance (ANOVA) was used to validate the models. It was observed that certain process parameters (*e.g.* airgap, number of contours, build orientation and layer

© University of Pretoria

thickness) had a greater effect on BT and MC than others. The latter was also observed for DFM. MC and BT decreased as air gap and layer thickness were increased. It was suggested to use no airgap, thick layers and 10 contours to improve DFM. (Mohamed, Masood & Bhowmik, 2016)

In a study performed by Ferrell, Clement & TerMaath (2021), it was noted that the tensile properties of FDM parts were impacted by the print orientation, fabrication technique and sample geometry and size. The latter should be taken into consideration when considering a material qualification. Additional parameters affecting the tensile properties of FDM parts include the CAD file, STL file, G-code, part geometry and size (Sola *et al*, 2022).

The influence of the physical design and geometric parameters on the mechanical properties of a part are seldom discussed in literature. Design considerations (as discussed in Section 3.5) are proposed to improve the visual quality of a print, but not specifically the mechanical properties. In a study performed by Khoshkhoo, Carrano & Blersch (2018) the effect of part thickness on distortion was investigated. The thickness of a printed specimen had an influence on the type of potential distortion observed, especially when evaluating high aspect ratio specimens. It was observed that wavy edge type distortion occurred in thin samples (*e.g.* 1 mm), while reverse coil set distortion occurred in thicker samples (*e.g.* 3 mm and 6 mm). An increase in the wall thickness caused a reduction in the possible distortion. The distortion in the thin samples was also affected by the build orientation. (Khoshkhoo, Carrano & Blersch, 2018)

© University of Pretoria

Figure 17 is an illustration of the cause-and-effect diagram based on parameters used in previous studies as discussed in literature. Sola *et al* (2022) summarised a similar diagram illustrating the various parameters affecting the tensile properties of FDM parts.

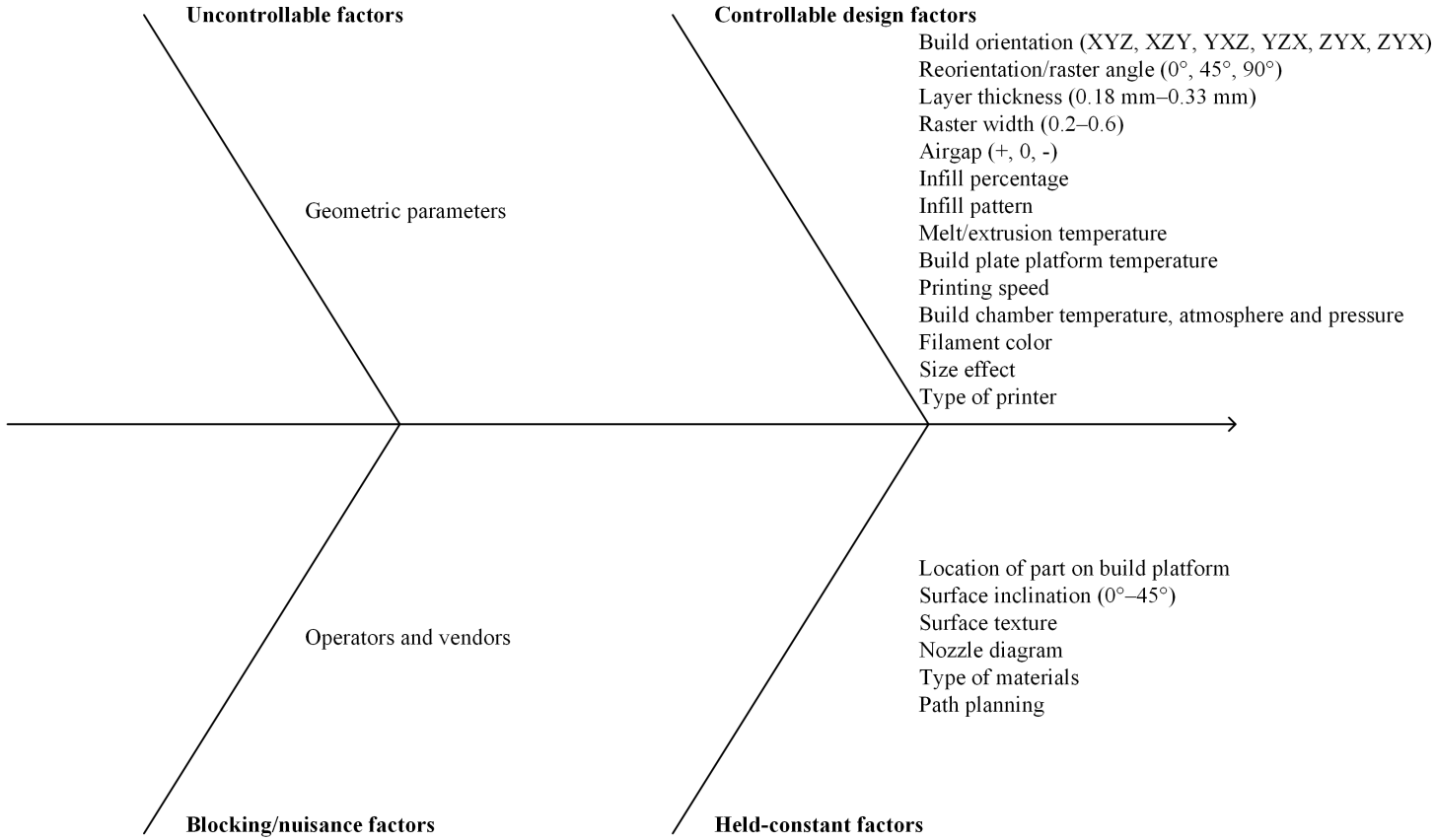

Figure 17: A cause-and-effect diagram for FDM adapted from Villalpando, Eiliat & Urbanic (2015).

© University of Pretoria

3.5 Design considerations and troubleshooting

Design guidelines are used as a starting point during the troubleshooting process. To understand the design and preparation of FDM parts, the build process should first be considered. The design considerations discussed below are compiled in such a manner that they can be applied to conventional plastics and produce high-quality fabricated parts (Stratasys, 2021).

The dimensional accuracy of the parts produced is influenced by several factors. These factors include the nozzle diameter, layer thickness, system resolution, distortion, warping, material properties, shrinkage, build parameters as well as part orientation and geometry. It is important to design parts within the capabilities of the system (Medellín-Castillo & Zaragoza-Siqueiros, 2019). Several defects including bubbles and bulges, incorrect bead deposition position, overfill, scars, stringing, underfill as well as warpage and shrinkage were identified by Oleff *et al* (2021).

3.5.1 Shrinkage and warp

The accuracy and quality of a print are influenced by warping, distortion and shrinkage which occur in a part during printing. These defects are caused by the generation of internal stresses and can be reduced by decreasing the layer thickness (Medellín-Castillo & Zaragoza-Siqueiros, 2019). Another alternative would be to divide large designs into several parts or to design a part in such a way that the length to width ratio is small. Medellín-Castillo & Zaragoza-Siqueiros (2019) advised users to make use of materials with a low glass transition temperature (T_g) and shrinking coefficient. By increasing the build volume, the effect of warping can also be reduced (Medellín-Castillo & Zaragoza-Siqueiros, 2019).

Shrink rates are automatically added by Stratasys Direct Manufacturing. Therefore, it is not required to include shrink factors in the design. Adjustments can be made to the default values when problems occur during large scale production of similar parts. Walls can be added to the thin-walled sections of a fabricated part to eliminate the possible effect of warping. (Stratasys, 2021)

3.5.2 Holes

Narrow holes produced through FDM have the tendency to be undersized or distort. It was recommended by Medellín-Castillo & Zaragoza-Siqueiros (2019) to orientate the axes

© University of Pretoria

of holes to be perpendicular to the build plate. The holes can be drilled or reamed when the print quality was poor or the tolerance should be of a desired value (Stratasys, 2021).

3.5.3 Pins and columns

Tip size, tip length and part orientation influence the minimum size of a pin or column. The slice thickness also contributes when expanding a pin or column to its minimum size. Stratasys (2021) suggested that features up to 0.48 mm can be produced.

3.5.4 Wall thickness and thin sections

The wall thickness and the thin sections of a fabricated part are a function of the layer thickness. Table 4 summarises the minimum wall thicknesses used with the corresponding layer thicknesses. The wall thickness should approximately be four times that of the layer thickness. A part becomes brittle and warping may occur when it contains multiple minimum-thickness vertical walls without the necessary support structures (Stratasys, 2021). Geometric distortion and breakable walls may be a result of an insufficient layer thickness. Medellín-Castillo & Zaragoza-Siqueiros (2019) recommends a wall thickness of 0.1 mm to 1.5 mm.

Table 4: Recommended wall thicknesses as adapted from Stratasys (2021).

Layer thickness (mm)	Wall thickness (mm)
0.18	0.71
0.25	1.02
0.33	1.32

3.5.5 Threads

Stratasys (2021) recommended that sharp edges should be avoided during the design of build-in threads, as it acts as stress concentrators. Threads should not be applied in holes with a diameter less than 1.60 mm. The usage of an American Screw Thread (ACME) design with rounded crests and roots and a "dog point" head have been found to be advantageous. The "dog point" head should preferably not be less than 0.80 mm. A die or a tap can be used as an alternative to producing threads. (Stratasys, 2021)

© University of Pretoria

3.5.6 Undercuts, draft angles and fillets

FDM allows for the fabrication of several features including O-ring grooves. The draft can be neglected during the fabrication of FDM parts. The improvement in part strength and the reduction of stress concentrators are brought about by the introduction of fillets. The radius of a fillet is described as

$$R_0 = R_i + t \tag{4}$$

where R_0 is the outer radius, R_i is the inner radius and t is the wall thickness (Stratasys, 2021).

3.5.7 Size and build orientation

The size of a fabricated part is a function of and primarily determined by the build plate dimensions of a specific printer. According to Medellín-Castillo & Zaragoza-Siqueiros (2019), the largest commercially available build volume is 1000 mm × 800 mm × 500 mm. As the technology is expanding the build chambers being manufactured are also enlarging. If the designed part is too large it should be sectioned and printed as separate parts. The largest surface area of the part should be positioned to face the build surface to improve part quality (Medellín-Castillo & Zaragoza-Siqueiros, 2019).

The mechanical properties (*e.g.* tensile strength) of the printed part are dependent on the build orientation. The strongest strength in the tensile mode is obtained in the X-Y direction while the weakest strength is obtained in the Z direction. The build orientation is chosen in such a manner to either reduce the support required (*i.e.* an increase in support structures result in an increase in material cost), reduce the printing time, improve surface finish, maximise the geometric accuracy or obtain certain desired mechanical properties (Stratasys, 2021). Factors including the minimum number of layers that lead to the shortest build time, a reduction in feedstock consumption, satisfactory mechanical properties and surface roughness are also taken into consideration when determining the final build orientation. The stair-case effect (especially in sloped and curved surfaces) is reduced by changing the build orientation. The latter directly affects the surface finish of a part. Medellín-Castillo & Zaragoza-Siqueiros (2019), discussed various algorithms that were used to determine the optimal build orientation. Two suggestions were made to enhance the build direction, the first was to align the principal load direction and build direction to be perpendicular, while the second was to align the axis of asymmetric parts with the build direction (Medellín-Castillo & Zaragoza-Siqueiros, 2019).

© University of Pretoria

3.5.8 Assemblies and sectioning parts

The assembling of parts refers to the junction of two or more separately fabricated objects. Stratasys (2021) suggested that parts should have an acceptable clearance to prevent fusing of the parts. The tolerance of the FDM machine determines the minimum clearance between parts. A design can be sectioned into multiple parts before printing, as a result, there are several advantages (Stratasys, 2021):

1. The use of support is reduced.
2. Overhanging features can be built separately.
3. All features can be preserved during the production and post-processing phase (especially fragile features).
4. Larger designs (*i.e.* originally too large for build volume) can be fabricated.

3.5.9 Living hinges and text

Living hinges subjected to a small number of cycles can be produced through FDM. Stratasys (2021) recommended that another hinge design should be utilised when more cycles are required.

3.5.10 Text size

The recommended minimum text sizes that should be used in FDM are summarised in Table 5.

Table 5: Recommended text sizes as adapted from Stratasys (2021).

Location on part	Recommended size
Top or bottom build plane	16-point boldface
Vertical walls	10-point boldface

3.5.11 Bosses, ribs and gussets

Hollow designs are supported by bosses. The bosses are supported by ribs and/or gussets. A reduction in the wall thickness of bosses and ribs are not required. The wall thickness

© University of Pretoria

of bosses is either the same as that of the part or it can be 0.5 mm less (Stratasys, 2021). It should be noted that all geometric features produced by FDM will exhibit certain repeatability, resolution and accuracy, which may differ from the desired values (Medellín-Castillo & Zaragoza-Siqueiros, 2019).

It is advised by Medellín-Castillo & Zaragoza-Siqueiros (2019) to reduce the required support structure by adjusting/changing the orientation of the part. To ensure that the filament does not fall from their nominal position, overhangs should be designed to be short in length. The most important aspect of support is the ease of removal of these structures. Holes, internal cavities, enclosed volumes and channels should be either avoided or designed in such a manner to ensure ease of removal of support (Medellín-Castillo & Zaragoza-Siqueiros, 2019). Medellín-Castillo & Zaragoza-Siqueiros (2019) recommended gap heights to be at least 0.4 mm, while no length restrictions were specified.

3.5.12 Finishing of parts

Post-processing alongside the choice of material, build orientation, support structures and environmental conditions are responsible for the stability of a part (Medellín-Castillo & Zaragoza-Siqueiros, 2019). Several post-processing techniques are utilised to improve the quality (*e.g.* obtain desired tolerances and geometric features), strength, integrity and environmental resistance (*e.g.* UV) of a printed part. The most well-known technique is the removal of support, either by breaking- or soaking it off in water (Xometry, 2021). Post-processing techniques include turning, milling, tapping, sawing, sealing, smoothing, plating, burnishing and drilling (Stratasys, 2021). The technique utilised depends on the predetermined requirements for a printed part.

3.6 Printers

There has been an evolution in the mechanical construction and working principles of 3D printers. The elements that determine the quality of a print are jerk during printing, stability of extruder head/nozzle and stability of the bed. The latter is influenced by parameters such as bed levelling (*e.g.* auto level sensor), linear rails and stepper motors. This section summarises the evolution in the operation and mechanical construction of different printer models. There are various professional printers on the market, which are more robust and produce reliable parts with repeatable quality. The latter was not discussed as the manufacturers evaluated in this section were selected due to the availability and usage in South Africa.

© University of Pretoria

3.6.1 Prusa3D

The evolution of the models is the RepRap Mendel, Prusa Mendel, Prusa Mendel (Iteration 2), Prusai3, Prusai3 MK2 and MK2S as well as the Prusai3 MK3 and MK2.5. The latest models are the Prusai3 MK3S and MK3S+. The RepRap Mendel is the base construction for the Prusai3 series with its build platform being cubic. The bed is heated to ensure better adhesion between the bed and print. The print time is reduced when using a Prusa Mendel. Snap-fit is used during the assembly of Prusa Mendel (Iteration 2). The accuracy and printing speed of the Prusa Mendel were improved by changing the frame to a single aluminium vertical frame, as implemented in the Prusai3. The installation of the Prusa Nozzle allows for printing with filament comprising of a 1.75 mm or 2.85 mm diameter. Mesh bed levelling, automatic geometry skew correction and an increase in build volume were introduced in the Prusai3 MK2 and MK2S models. The fans, stepper-motors and extruder were altered in the Prusai3 MK3 and MK2.5 which contributed to the faster print speeds obtained. In the latest models, several filaments can be printed simultaneously. The latter is automated. Prusa3D manufactures open-source printers. The nozzle is fastened to a crossbeam which allows it to move sideways, upwards and downwards. The movable bed advances in a forward and backward manner and is located at the base of the printer. (Minetola *et al*, 2018)

3.6.2 Creality

Creality has three series, namely the Ender-, CR- and CP series. The evolution of the models in the Ender series is the Creality Ender-3, Ender-5, Ender-6 and the latest model is the Creality Ender-7. These models are discussed in this document. The printers in the Ender series are all open-source printers. It is optional to enclose the framework of the Ender-6 with acrylic plates. The nozzle of the Ender-3 is connected to a crossbeam which allows it to move sideways. The crossbeam is connected to two leadscrews which allow the nozzle to move upwards and downwards. The bed moves forward and backwards and is located at the base of the printer. The Ender-3 and the printers produced by Prusa3D are mechanically similar. (SC3 Technology, 2021)

The Ender-5 printers are divided into the Ender-5 Plus 3D Printer and the Ender-5 Pro 3D Printer. The nozzle of the Ender-5 is fastened to a crossbeam which is connected to a conveyer belt that moves along $\frac{3}{4}$ of the circumference of the top frame. This allows the nozzle to move sideways, forward and backwards, but not upward and downward. The latter is advantageous as it ensures nozzle stability and improves print accuracy. The bed of the Ender-5 is secured on all four corners and use leadscrews for upwards and

© University of Pretoria

downwards movement. The Pro model has a double Y-axis control system. The Plus model has a larger build envelope than the Pro model. The Plus model also resumes printing after a power failure. (SC3 Technology, 2021)

An additional filament sensor has been added to the Ender-6, to pause the print after filament breakage or runout. In the Ender-6, the print is also resumed after power outages. The upwards and downwards motion of the bed is controlled by a single leadscrew located at the back of the bed. The crossbeam is connected to a conveyer belt that moves around the whole circumference of the top frame and propel the nozzle in this manner. Printing speeds of 250 mm/s can be achieved by the Ender-7. The coordinate operations and the dual motors run in parallel with each other. The Ender-6 and Ender-7 use a core XY structure. (SC3 Technology, 2021)

3.6.3 Ultimaker BV

Several models have been developed by Ultimaker and include the Ultimaker 2+ Connect, Ultimaker S3, Ultimaker S5 and Ultimaker S5 Pro Bundle. The Ultimaker 2+ Connect has the smallest build volume in comparison to the other Ultimaker models. It has several features which include network connectivity, touchscreen, geared feeder, heated build plate and dedicated support. The model lacks several additional features such as dual extrusion, swappable print core, filament flow sensor and composite material compatibility. The latter has been incorporated in the Ultimaker S3 and Ultimaker S5 models. The Ultimaker S5 Pro Bundle possess all the previously mentioned features. Features including environmental control and automatic material handling have been incorporated in the Ultimaker S5 Pro Bundle, making it a state-of-the-art piece of machinery. (Ultimaker, 2021)

The Ultimaker 2+ Connect has a single extruder and nozzle. The nozzle is fastened to two crossbeams which are perpendicular to each other and situated at the top of the printer frame. This enables the nozzle to move forward and backwards as well as sideways. The bed moves upwards and downwards as the print progresses. Dual extrusion, precision drivers and advanced auto bed levelling were incorporated in the Ultimaker S3. The Ultimaker S3 has two nozzles which allow for alternation between filaments to create complex prints. The Ultimaker S5 also offer dual extrusion and has a larger build volume when compared to the Ultimaker S3. The bed and nozzle movement of the Ultimaker S3 and Ultimaker S5 is similar to that of the Ultimaker 2+ Connect. The Ultimaker S5 Pro Bundle includes a humidity-controlled storage area that keeps up to six filament spools. The latter allows for continuous dual or single extrusion. The model has a lid that creates a fully enclosed chamber for air-flow control. Various materials can be printed on

© University of Pretoria

the Ultimaker S5 Pro Bundle due to this fact. All Ultimaker printers can be operated remotely due to the cloud 3D printing function build in. (Ultimaker, 2021)

3.6.4 Flashforge

Printers manufactured by Flashforge are divided into two categories, namely professional and consumer. The series in the professional category are Creator 4-, Hunter-, WaxJet400-, Creator 3-, Focus- and AD1 series. The series in the consumer category is Guider II- Inventor-, Finder-, Foto-, Creator Pro-, Adventurer- and Dreamer series. The Inventor, Inventor II, Adventurer 3, Guider IIs and Hunter are readily available in South Africa and therefore were discussed in this document. (ZF3 Technology, 2021)

The Inventor has dual extrusion and an enclosed chamber. Belts are used to move the nozzle along the X/Y axis. The print head is installed in a linear rail system. The enclosed chamber makes the model advantageous to use when printing acrylonitrile butadiene styrene (ABS). One of the primary advantages of the Inventor II is its wireless connection. Another feature of this model is the fact that the print stops as soon as the front door is opened, whereafter the print is resumed. The nozzle of the Inventor II is connected to a crossbeam. It is propelled back and forth by two crossbeams that are parallel to one another and is fastened to the sides of the printer's top frame. The bed moves upwards and downwards as a new print is started and a print commences respectively. The latter is true for both Inventor and Inventor II. (ZF3 Technology, 2021)

The mechanics of the Adventurer 3 are similar to that of the Prusai3. The bed moves forward and backwards while the nozzle moves sideways as well as upwards and downwards. The extruder head is installed on two crossbeams (parallel to one another). The latter is connected to crossbeams situated on either side of the chamber (*i.e.* along with the height of the printer). This ensures nozzle stability and minimises oscillation. The Guider IIs is an industrial closed-source printer. Layer adhesion and print quality are improved as the Guider IIs. The bed moves upwards and downwards, while the nozzle moves in a similar fashion as the Inventor II. The Hunter model is unique due to its light intensity control system and Z-axis linear motion guide actuator. (ZF3 Technology, 2021)

3.6.5 Printrbot

There are two predominant Printrbot models on the market. These models are the Printrbot Metal Plus and the Printrbot Simple Metal. The stability of the nozzle on the Printrbot Simple Metal has been improved by the introduction of a metal frame as

© University of Pretoria

installed on the Printrbot Metal Plus. The nozzle of the Printrbot Metal Plus is connected to a crossbeam (*i.e.* linear rail system) which moves upwards and downwards. The nozzle moves sideways along the beam. The bed is located at the base of the printer and moves forward and backwards. An aluminium pulley system and a GT2 belt are responsible for the bed and nozzle movement in a Printrbot Metal Plus. The mechanics of this model are similar to those of the Prusai3. An auto level sensor was introduced to improve bed adhesion and print quality. The Printrbot Metal Plus has an open chamber. The Printrbot Simple Metal is constructed entirely out of metal. An aluminium direct-drive extruder, a Z-axis coupler and a GT2 belt pulley system are utilised in this model. It has been noted that both these models are heavy due to their metal casings and construction. It is evident from the above discussion that nozzle and bed movement have a significant influence on print stability and accuracy. (J, 2020)

© University of Pretoria

4 Materials

The parameter choice and the mechanical properties obtained are dependent on the material properties alongside part fabrication (*e.g.* voids and interfacial regions between the layers) (Gibson, Rosen & Stucker, 2015). There is a vast range of materials used in FDM. Material development for FDM has evolved over the past years, which led to not only polymers but also organics, ceramics and metals being printed (Medellín-Castillo & Zaragoza-Siqueiros, 2019). The polymers should ideally be amorphous and not crystalline (Gibson, Rosen & Stucker, 2015; Mazzanti, Malagutti & Mollica, 2019). Medellín-Castillo & Zaragoza-Siqueiros (2019) summarised the AM materials into various categories as illustrated in Figure 18.

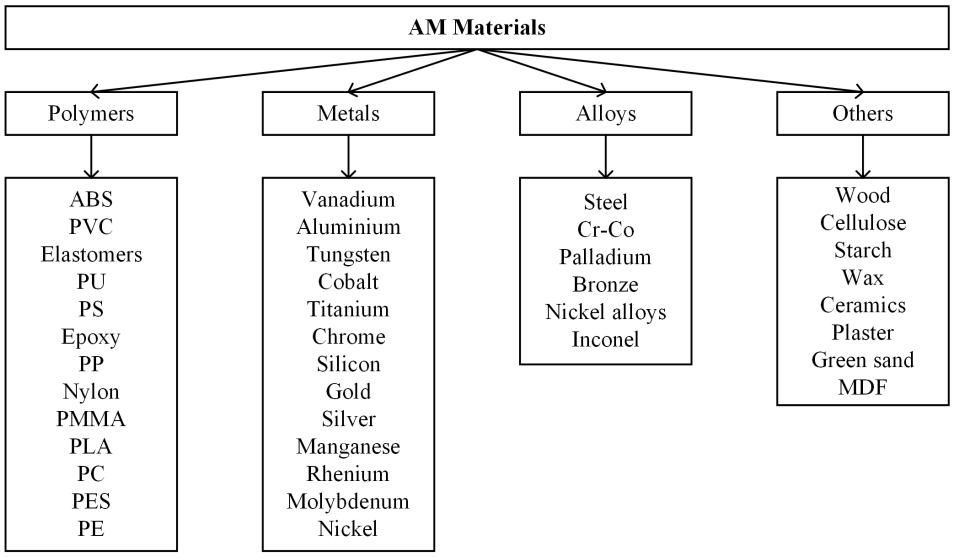

Figure 18: AM materials adapted from Medellín-Castillo & Zaragoza-Siqueiros (2019).

The materials used as feedstock in FDM are primarily in filament form. The filament is produced by using a single screw or twin-screw extruder. The filament diameter should be regulated throughout the extrusion process to ensure that it is uniform to suit the nozzle of the printer. Filament production is dependent on screw speed, temperature and pressure of extrusion. The structural-, mechanical-, physical-, chemical- and rheological properties affect the printability, applicability and post-processing of the filament. (Daminabo *et al*, 2020)

The pre-treatment of filament (*i.e.* in desiccator cabinets or dehumidified chambers) is important (Bates-Green & Howie, 2017). The two primary materials used in FDM are ABS and polylactic acid (PLA). According to Gibson, Rosen & Stucker (2015) the most readily used material is ABSplus. The latter has been derived from neat ABS. ABS is a copolymer comprising of acrylonitrile (heat resistance), styrene (rigidity) and butadiene

© University of Pretoria

(impact strength) (Banjanin *et al*, 2018). The properties (*e.g.* elongation, tensile- and flexural modulus) between materials such as ABS, ABSi, ABSplus and ABS/PC varies (Gibson, Rosen & Stucker, 2015). ABS is a desirable material for FDM as it is resistant to moisture, heat and chemicals (Banjanin *et al*, 2018).

Mwema & Akinlabi (2020) reconned that the most applied material is PLA. The usage of PLA is advantageous because it is environmentally friendly and is harmless to the health of both animals and humans. PLA breaks down into biomass, water, inorganic salts and non-poisonous gases, which makes it composable (Mwema & Akinlabi, 2020). The material is produced from renewable sources and it has a melting point ranging from 180 °C to 220 °C. It exhibits satisfactory flexural strengths and modulus when used in its semi-crystalline form. One of the main advantages is that no heated bed is required when using PLA as sufficient adhesion is obtained between the bed and part during printing (Mwema & Akinlabi, 2020).

Composite filaments are more readily used in FDM. According to Blaj & Oancea (2021), a composite filament is defined as a filament comprising of two or more materials with varying chemical- and physical properties. The properties of the composite filament are superior when compared to the properties of the individual filaments. The length of the fibres may vary and has a notable effect on the mechanical properties of the filament. An example of such a composite filament is carbon fibre filaments (CFF). The strength and rigidity of the filament increase as the carbon fibres are reinforced in the matrix of the thermoplastic materials. CFF PLA, CFF PETG and CFF ABS are examples of reinforced filaments. (Blaj & Oancea, 2021)

According to V Srivastava (2017), a newly developed polymer/metal composite for FDM was ABS filled with metal particles. The presence of filler led to several problems which included filament diameter variation, nozzle clogging and the presence of plasticiser led to layer delamination. Mazzanti, Malagutti & Mollica (2019) summarised biodegradable and non-biodegradable filaments with their corresponding fillers, compatibilisers, plasticisers and toughening agents.

Parts can either be printed from one type of material or multiple materials, depending on the predetermined design specifications and printer mechanics. Other materials used in FDM include nylon, acrylonitrile styrene acrylate (ASA), wax, elastomer, polyphenylsulfone (PPSF), polycarbonate (PC), polycaprolactone (PCL), polypropylene (PP), polybutylene terephthalate (PBT), carbon fibre, graphene-doped PLA and polyethene (PE) (Medellín-Castillo & Zaragoza-Siqueiros, 2019; Mwema & Akinlabi, 2020). Gibson, Rosen & Stucker (2015) mentioned that PC-based materials (*e.g.* PC-ISO), ULTEM 9085 and polyphenylsulfone (PPSF) are alternatives to the standards materials used in FDM.

© University of Pretoria

The temperature- and chemical resistance as well as the loading of filament depends on the type of material used. ULTEM 1010 resin and ULTEM 9085 resin have high-temperature resistances, while Nylon 12 Carbon Fibre (CF) and Nylon 12 have moderate temperature resistances. ABA has a low-temperature resistance while PC has a moderate temperature resistance. Table 6 summarises the polymer materials used in FDM. (Stratasys, 2018)

According to Loh *et al* (2020), materials used in extrusion equipment (*e.g.* Ultimaker BV S5 and Zortrax SA M300 Plus) were Materialise ABSi, Materialise ABS-ESD7, Materialise ULTEM 9085, Materialise PC-ABS, Smartfill PETG MDT, 3DXSTAT™ ESD PEKK-A, FluorX™ PVDF 3D Filament, Sakata 3D HR-PLA 3D870, BlackMagic 3D Conductive and AMIDEX™ Nylon 6/66 Copolymer. Figure 19 is an illustration of the materials used in FDM.

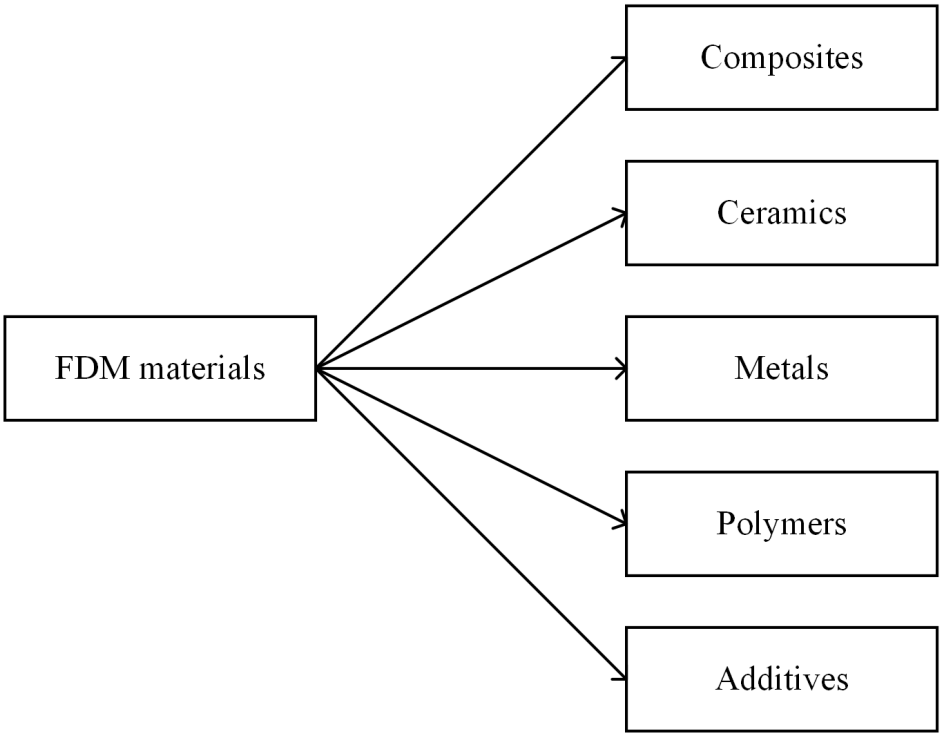

Figure 19: Materials used in FDM.

The thermomechanical properties and the effect of melt rheology on polymer printing were not discussed in particular in this study as it was not a subject investigated during the development of the material evaluation guideline. Osswald (2017) can be referenced for matters relating to viscosity, melt rheology and polymer processing (*e.g.* extrusion). For an extensive discussion on polymer characteristics (*e.g.* melting- and glass transition temperature), Young & Lovell (2011) can be references.

© University of Pretoria

One of the main concerns regarding filament is the inconsistency in chemical composition between manufacturers. The information provided by the suppliers are scarce and in some instances unreliable. X-ray diffraction (XRD) can be used to determine the chemical composition of a filament through phase identification, if such information is required (Mwema & Akinlabi, 2020).

© University of Pretoria

Table 6: A summary of several polymers used in FDM (Daminabo *et al*, 2020).

Material class	Material sub-class
Acrylonitrile styrene acrylate (ASA)	-
Amphora	-
Acrylonitrile butadiene styrene (ABS)	ABS-M30, ABS-ESD7, ABSi, ABSplus-P430
Antero	Antero 800 NA (PEKK), Antero 840 CNO3 (PEKK)
Cellulose and nano-cellulose	-
High-impact polystyrene (HIPS)	-
Lignin	-
Nylon (PA)	PA12, PA12CF, PA6, PA11, PA6,6
Thermoplastic polyurethane (TPU) elastomer	TPU 92A elastomer
Thermoplastic elastomer (TPE)	-
Thermoplastic polyester elastomer (TPC)	-
ULTEM	ULTEM 1010 Resin, ULTEM Resin 9085, CG Resin
Poly butylene succinate (PBS)	PBS/PLA
Polyethylene terephthalate (PET)	PET-G, PET-CF
Poly hydroxo alkanoate (PHA)	-
Polycarbonates (PC)	PC-ABS, PC-ISO
Polyphenylsulfone (PPSF/PPSU)	-
Polypropylene (PP)	PP-Glass, PP-CF10, PP-CF20
Polystyrene (PS)	-
Polyethylene (PE)	-
Polysulfone (PSU)	-
Polyetherimide (PEI)	ULTEM
Polyaryletherketone (PAEK)	Polyetheretherketone (PEEK)
Polyaryletherketone (PAEK)	Polyetherketoneketone (PEKK)
Polyphenylsulfone (PPSU)	-
Polymethyl methacrylate (PMMA)	-
Polylactic acid (PLA)	PLA-3052D, Graphite/PLA, PLA/MWCNT
Polyvinyl acetate (PVA)	-
Polyvinylidene fluoride (PVDF)	-

© University of Pretoria

5 Previous studies

The effect of different parameters on the mechanical properties of a printed part has been investigated and are summarised in Table 7.

Table 7: A summary of various studies performed in the past with respect to FDM.

No	Material	Parameters tested	Tests performed	Discussion	Reference
1	ABS	Orientation of layered rasters	Tensile	The tensile strength was the largest for 0° raster angles. The strength decreased as the angles changed from +45°/-45° to 45° and 90°.	C Ziemian, Sharma & S Ziemian (2012)
2	PLA	Raster angle, moisture content	Tensile	It was observed that the optimum strain and strength were obtained when the material had a 10% moisture content and when a 90° raster angle was used. Increasing the moisture content resulted in an increase in the ultimate tensile strength (UTS).	Algarni (2021)
3	ABS	Part orientation, raster width, layer thickness, raster angle, airgap	Tensile	Mathematical models were constructed and the parameters were optimised. The tensile strength for the specimens were the largest when using a 0 °-part orientation, a minimum layer thickness and raster width, increasing the raster angle and a negative airgap.	Onwubolu & Rayegani (2014)

© University of Pretoria

No	Material	Parameters tested	Tests performed	Discussion	Reference
4	ABS	Infill pattern	Tensile	The tensile strength of printed specimens was compared to that of injection moulded specimens. The latter was stronger than the printed specimens. Tensile strength was greatly affected by the infill pattern used. Concentric infill should be used to obtain the best elongation, while rectilinear infill should be used to obtain the best strength.	Khan *et al* (2017)
5	PLA	Infill patterns, build direction	Tensile	The highest strength was obtained when grid and honeycomb infill patterns were used. The quality of- and the adhesion within the samples improved when printing at 0°. The strength of the print decreased as the build orientation was increased.	Dezaki & Ariffin (2020)
6	PLA	Deposition angle, extruder temperature, printing speed	Tensile	ANOVA was used to determine the relationship between the mechanical properties of a specimen and the printing parameters. It was noted that there were several interactions between the parameters.	Ouhsti & Haddadi (2018)
7	ABS	Infill patterns, infill density, build orientation	Tensile	Maximum tensile strength was obtained when using a wiggle infill pattern, a 0° build orientation and aligning the raster in the same direction as the printing direction.	Dudescu & Racz (2017)

© University of Pretoria

No	Material	Parameters tested	Tests performed	Discussion	Reference
8	PLA	Build orientation, size effect	Tensile	Two observations were noted. The first was that build orientation affected the tensile strength more than the Young's modulus and the second was that both the Young's modulus and tensile strength decreased as the number of layers increased.	Vălean *et al* (2020)
9	ABS	Infill density, infill pattern, shell thickness, extrusion multiplier	Tensile	Deformation decreased and strength increased as the infill density was increased. The infill density correlates to cost and therefore is reduced in the majority of cases. When increasing the shell thickness to relatively high values, the infill of small samples and features appear to be solid. An increase in the extrusion multiplier resulted in a decrease in dimensional accuracy and more densely printed parts. Printing time and material consumption are reduced by varying the infill pattern. It was suggested that the optimum settings are a honeycomb infill pattern, 40%–50% infill density, 2–3 lines shell thickness and an extrusion multiplier that should exceed 0.9.	Ćwikla *et al* (2017)
10	ABS	Layer thickness, infill density, raster angle	Tensile	The optimum parameters were determined as 0.5 mm layer thickness, 80% infill density and 55° raster angle. A tensile strength of 31.57 MPa was obtained. Surface response methodology was used to predict various mathematical equations.	Samykano *et al* (2019)

© University of Pretoria

UNIVERSITEIT VAN PRETORIA
UNIVERSITY OF PRETORIA
YUNIBESITHI YA PRETORIA

No	Material	Parameters tested	Tests performed	Discussion	Reference
		Build orientation, specimen type	Tensile	Weibull moduli ranging from 26 to 69 and from 30 to 41 were obtained for specimens without and with holes respectively.	
		Layer thickness, printing orientation, printing plane	Tensile Compression	Optimum tensile results were obtained when using a YZ-H printing plane and a 0.09 mm layer thickness. Optimum compression results were obtained when using XY-H and XY-D printing planes.	
		Build orientation, printer type	Tensile Flextural	Optimum tensile- and flexural moduli of 2294 MPa and 2247 MPa respectively were obtained when printing on a Fortus 450 at 90°.	
		Raster angle, build orientation	Tensile Compression Water absorption	Optimum tensile- and compression moduli were obtained when the parts were printed with a 45° raster angle. Optimum water absolution was achieved in parts printed in the Z direction and with a 0°/90° raster angle.	
		Print orientation, part structure	Compression	Print orientations (*e.g.* 0°and 45°) in a solid cube resulted in interlayer delamination which led to differences in stress-strain relationships. The previously mentioned print orientations resulted in high yield stresses and initial elastic moduli in 3D braid preforms.	
		Raster angle, build orientation	Torsion	A raster angle of 0° and a build orientation of YXZ resulted in high strength and fracture strain.	

© University of Pretoria

No	Material	Parameters tested	Tests performed	Discussion	Reference
11	ABS	Vacuum system	Tensile	When using vacuum assisted systems, better tensile properties were obtained when compared to atmospheric systems. Adhesion between the layers improved when using a vacuum system because the heat was maintained for longer periods. Scanning Electron Microscopy (SEM) was used to study the microstructure of the printed samples.	Maidin *et al* (2017)
12	ABS	Extrusion temperature	Tensile	A mathematical model was developed to investigate the effect of temperature on printed parts. Interface growth and temperature at the interface of two strands/roads decreased as time progressed. SEM was used to investigate the bonding effect.	Bhalodi, Zalavadiya & Gurrala (2019)
13	PLA ABS	Repeatability/ consistency of mechanical properties	Tensile Compression	Inconsistency in tensile testing results were obtained for the PLA samples, while consistency was noted for the ABS samples. The latter was due to a better-controlled environment for ABS printing–adhesion between layers improved. The opposite was observed for the two materials after analysing the compression testing results.	Banjanin *et al* (2018)
14	ABS	Layer thickness	Compression	The compression strength of ABS parts decreased as layer thickness increased. ABSplus specimens have larger compression strength when compared to ABS specimens. The printed specimens had a lower compression strength than nominal stock material.	Vidakis *et al* (2015)

© University of Pretoria

No	Material	Parameters tested	Tests performed	Discussion	Reference
15	PC	Environmental humidity and temperature	Infrared thermography	A 5.4 °C/mm temperature gradient within printed specimens were observed. Reduction in warping and an increase in mechanical properties were achieved by increasing the environmental temperature. It was recommended to use dry filament (low moisture content).	Fang *et al* (2020)
16	PLA	Pigmentation and environmental humidity	Tensile	Dimensional values similar to those of the nominal ones were obtained for filament without pigmentation. Dimensional deviations were observed as the extrusion temperature was increased. Improved mechanical strength was observed with an increase in extrusion temperature. Reduction/lack of pigmentation resulted in improved surface quality. Parts became more fragile when a drier storage environment was utilised.	Valerga *et al* (2018)
17	CF-ABS	Print orientation, specimen geometry, specimen preparation and extrusion effects	Tensile	The strength and repeatability of the samples were impacted by the part size and geometry. Fabrication techniques and naming conventions should be standardised. Test results should be reported in conjunction with extrusion control setting data. Printer variability should be taken into consideration in the qualification process.	Ferrell, Clement & TerMaath (2021)

© University of Pretoria

No	Material	Parameters tested	Tests performed	Discussion	Reference
18	CF-ABS and ABS	Conditioning moisture and heat	Tensile	As the conditioning temperatures approached the glass transition temperature, the ultimate tensile strength reduced. The tensile strength decreased and variability increased as the printed samples were exposed to moisture.	Ferrell, Arndt & TerMaath (2021)
19	PLA	Specimen geometry	Tensile	Elastic moduli was determined to be similar for both the ASTM D638 Type I sample and Type IV.	Sacco, Chua & Moon (2018)
20	PLA (Cu, Fe and steel)	Specimen orientation and infill	Tensile	Samples where the upper surface layer and orbital transition were parallel to the infill exhibited the lowest tensile strength. Additives to the virgin polymer resulted in a decrease in tensile strength. The latter was improved by adjusting the production parameters.	Török *et al* (2021)
21	PEKK-A	Printing methods	Tensile	The mean tensile strength were observed to be the highest for individually printed vertical specimens. The latter can be attributed to the short layer time resulting in high levels of diffusion. The rate of cooling was lower for the other three specimens. Different local temperatures near the interface were observed for the different methods due to the variation in layer times.	Davies *et al* (2021)

© University of Pretoria

No	Material	Parameters tested	Tests performed	Discussion	Reference
22	ABS, PLA, PET-G and TPU	Printing temperature, extruder nozzle and filament material	Fine particle emissions	The least emissions were observed by printing at lower temperatures. A nozzle diameter of 0.4 mm was determined to be optimal for PLA, PET-G and ABS. A nozzle diameter of 0.6 mm was determined to be optimal for TPU as the emissions were the lowest. The most critical period was observed to be at the start of the printing process.	Chýlek *et al* (2021)
23	PLA	Print orientation, raster angle	Tensile	Existing standards should be utilised for tensile testing. Printing and set-up parameters should be reported. Specimen size had an influence on the samples printed with a 0 °C raster angle.	Sola *et al* (2022)
24	ABS	Layer thickness and build orientation	Tensile	An increase in layer thickness resulted in an increase in the tensile strength. An increase in build orientation resulted in a decrease in tensile strength. The tensile strength was increased as the build time was decreased.	Nayak, Sahu & Mahapatra (2020)

© University of Pretoria

Gaps in the previous studies include the optimisation of more than four parameters simultaneously, recommending optimal slicing parameters, describing which of these parameters have an influence during the mechanical testing of the samples, the lack of creating a broad overview.

© University of Pretoria

6 Experimental

The gap identified in the development of standards for FDM was the primary factor of interest in this study. The development of a material evaluation guideline will not only provide a basis for operation, but also ensure that reliable and repeatable prints are produced with little to no variance. It will also promote progress in the research field through the generation of scientific information, data and observations. Quality control was incorporated in the material evaluation guideline. This ensured that the produced parts adhered to predetermined customer specifications. The material evaluation guideline can be used during the material development (*i.e.* filament) phase, to test whether or not a certain material is printable.

The inter-connectivity of mechanical-, geometric-, printing- and material parameters were evaluated. The effect of the slicing software (*e.g.* Cura®) on the geometric features of a print was not evaluated due to a steep escalation in the number of experiments caused when included in the Design of Experiments (DOE). The effect of printing parameters on the mechanical properties of a printed part was evaluated. As illustrated previously, certain parameters have a greater effect on the mechanical properties of a part when compared to others. It was determined that build orientation, infill percentage/density, infill pattern, raster angle, layer thickness, extrusion/printing speed, nozzle temperature and build plate/bed temperature had a prominent effect on the mechanical properties of a printed part. In the majority of studies, two or three parameters were evaluated while only one test was conducted.

Based on the information presented in the previous sections, it was noted that an infill percentage/density ranging between 50% and 100% resulted in parts with satisfactory strength. FDM promotes the production of parts in the shortest time frame with a decrease in material cost. Taking the latter into consideration an infill percentage of 50% was used.

Infill patterns can be divided into 2D and 3D patterns. Part geometry and the design of a print depend on this parameter. This was not one of the main factors investigated and therefore a 2D line infill pattern was used. Material development and the printability of a filament are not functions of build orientation, therefore a 0° (flat) build orientation was used. Incorporating the raster angle into the DOE resulted in an exponential increase in experiments, therefore this parameter was excluded from the DOE and a constant -45°/45° raster angle was used.

© University of Pretoria

Two primary default layer thicknesses are 0.15 mm and 0.2 mm. A layer thickness of 0.15 mm was used to ensure an increase in part strength. The extrusion speed/printing speed, nozzle temperature and build plate/bed temperature are functions of the type of material used during printing. These were determined through screening to be the most important parameters affecting the tensile strength of a printed part and were used as the variables in the DOE.

The slicing software limits the parameters that can be altered, as it varies between printer brands and manufacturers (*e.g.* New Cura Slicer 4.8.0 for the Creality Ender-6). Open-sourc printers were used. The path planning/slicing software (Cura) were kept constant throughout the execution of the experiments. This ensured that the material evaluation guideline developed can be used for any open-source printer that uses Cura as its slicing software. Parameters including the geometry of the print were kept constant by using a standard ASTM D638 Type 1 tensile bar. All the printers used in this study had a nozzle diameter of 0.4 mm, while the filament had a diameter of 1.75 mm.

It was evident that several tests were conducted on printed specimens to evaluate their mechanical properties. These tests included Dynamic Mechanical Analysis (DMA) (*i.e.* determination of the glass transition temperature and stiffness), tensile testing, bending/flexural testing, compression testing, impact testing and fractography (Scanning Electron Microscopy (SEM)). As illustrated in the previous sections, tensile strength is the dominant mechanical property evaluated for printed parts and therefore it was also the test conducted during the development of the material evaluation guideline.

A two-level fractional factorial design was used to develop the DOE. Screening was used to determine the variables to vary. Each of the three variables had three levels (*i.e.* low, medium and high). The procedure followed to obtain the final DOE are summarised in this Section 6.2. The statistical DOE was developed to be generic. The latter was done to enable various filament brand and printer model combinations to be evaluated. The DOE consisted of six experiments. Ten repeats of each experiment were printed. Tensile tests were performed on all printed specimens.

6.1 Overview

The aim was to develop a material evaluation guideline. It was required to determine one method that could have been used for multiple types of filaments and printers, given the printers operate with the same slicing software. Figure 20 is an illustration of the cause-and-effect diagram obtained after parameter elimination. Several of the important factors in the study included:

© University of Pretoria

- One type of filament was used during printing. The DOE was executed with various filaments from different suppliers (*e.g.* Wanhao PLA, Ultimaker PLA, Build volume PLA).
- Multiple printers were used (*e.g.* Creality Ender-6 and Wanhao Duplicator 9 I3).
- Each parameter had a low-, medium- and high level as indicated in Table 8.
- The material evaluation guideline can be adjusted for different types of filament (*e.g.* ABS and/or PET).
- A generic method with set printing parameters was determined.
- The behaviour of each type of filament was validated by printing various brands of filament on multiple printers.
- Testing for repeatability. It was evaluated whether more expensive filament had a better print quality or whether the same trends were observed irrespective of filament cost.
- Tensile strength was tested according to ASTM D638.

Table 8: Low, medium and high levels of the parameters used in the DOE.

Levels (-)	Printing temperature (°C)	Bed temperature (°C)	Printing speed (mm/s)
Low	190	30	30
Medium	200	40	40
High	210	50	50

© University of Pretoria

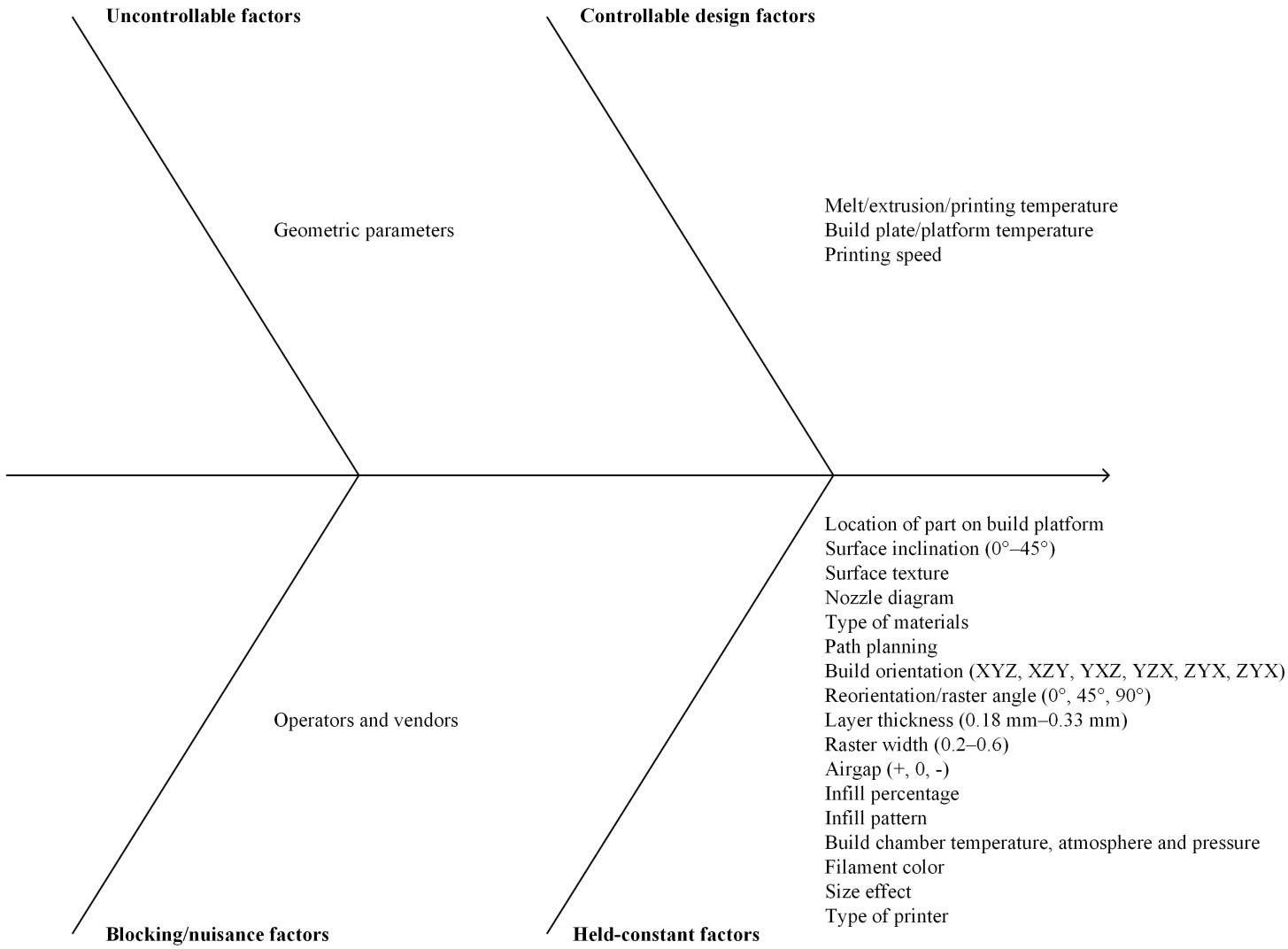

Figure 20: The cause-and-effect diagram developed after parameter elimination.

© University of Pretoria

6.2 Design of Experiments (DOE)

The operation and working principles of a system are determined by observing and studying the process. The interactions between parameters and their cause-and-effect relationships are determined by varying the input variables (x) to the system. The change in the output variables (y) is observed and analysed. Hypotheses and theories are formulated as experiments are performed. Montgomery (2013) defined an experiment as a set of runs performed to determine the cause for the changes in the output variables as the input variables are varied. Mathematical models and relationships are determined after an experimental analysis is performed. It is important to construct the process in such a manner that external factors have little to no effect on the experiments performed. A DOE makes such a process possible. (Montgomery, 2013)

DOE involves experimental strategy and planning. The planning is performed to ensure that sufficient data is collected, data is analysed appropriately and that feasible results and conclusions are obtained (Montgomery, 2013). A statistical approach is used to obtain conclusions, while an objective approach is used when the data is subjected to experimental error. An experimental problem can be divided into two branches. The first is the DOE and the second is the statistical data analysis (Montgomery, 2013). There are three primary reasons to construct a DOE. These are to obtain better optimisation and understanding (*e.g.* modelling), to minimise the usage of resources and time as well as to generate reliable data by minimising the impact of variance (Viljoen, 2020).

In the current study, a two-level fractional factorial design was used, *i.e.* 2^{k-p} design where k is the number of variables and p is the fraction. Note in this case, $k = 3$ and $p = 1$, yielding a half fraction of the full design. One additional lack-of-fit point and a centre point were added to the design. Therefore, six distinct experimental conditions were tested. Fractional factorial designs are very efficient for screening and for quantifying the effect of the main effects on the response. However, in many fractional factorial designs, such as the 2^{3-1} design in this case, the two-order interaction between the variables cannot be estimated since they are confounded with the main effects. The addition of the one lack-of-fit point allowed the estimation of the interaction between the printing temperature and bed temperature only. The centre point allows for the estimation of curvature and estimation of experimental error. The points used in the two-level fractional factorial design are illustrated in Figure 21.

© University of Pretoria

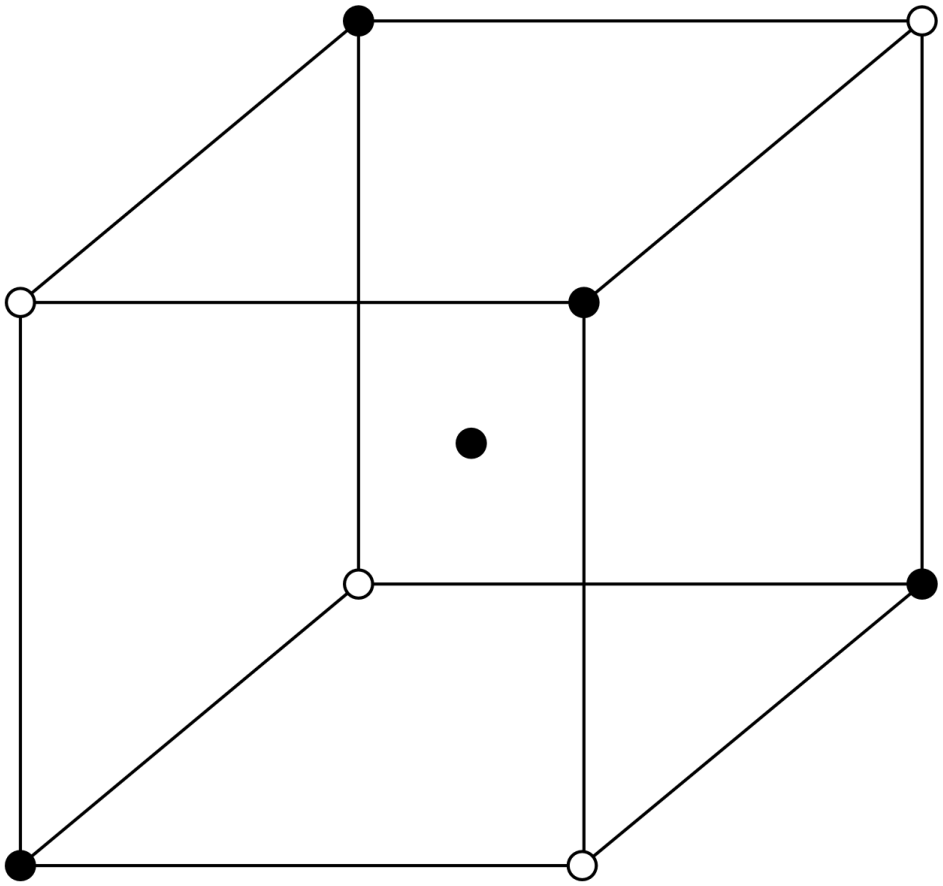

Figure 21: The fractional factorial method excluding the lack-of-fit point (Montgomery, 2013).

Ten replications were performed per experimental condition, which increases the degrees of freedom for error and consequently also improves estimation of experimental error. Table 9 summarises the coordinates of the points used in the two-level fractional factorial design. The low level was assigned a -1, the medium level was assigned a 0 and the high level was assigned a 1.

Table 9: The coordinates of the points used in the three-level fractional factorial design.

No	Coordinate
1	$< 0, 0, 0 >$
2	$< -1, -1, -1 >$
3	$< 1, 1, -1 >$
4	$< 1, -1, 1 >$
5	$< -1, 1, 1 >$
6	$< 1, 1, 1 >$

© University of Pretoria

6.2.1 Printing parameters

Variables analysed in DOEs can be divided into four categories namely continuous-, discrete numeric-, categorical- and blocking variables (Viljoen, 2020). The build plate/platform temperature, printing speed and melt temperature were the three variables included in the DOE due to their reported significant influence on the mechanical properties of a printed part. As previously mentioned, the variables each had three levels namely a low-, medium- and high level as summarised in Table 8.

The build plate temperatures were chosen to ensure a decrease in printing time, a decrease in power consumption, optimise production and to ensure adhesion between bed and print. The printing speed was chosen to decrease printing speed and increase print stability. This machine parameter is limited by the printer model used and its predetermined range suggested by the manufacturer. Printing speed was not regularly used as a variable in previous studies. The printing temperature range was determined by evaluating the suggested ranges by several filament manufactures and suppliers. Several printing parameters were kept constant. A negative airgap was used. These parameters are summarised in Table 10.

Table 10: The parameters that were kept constant during the execution of the experiments.

No	Parameter	Description	Units
1	Material type	Polylactic acid (PLA)	-
2	Printing orientation	Flat (0 °C)	-
3	Layer height	0.15	mm
4	Infill density	50	%
5	Infill pattern	Lines (2D)	-
6	Cooling (fan speed)	100	%
7	Shells	3	-
8	Print acceleration	1500	mm/s^2
9	Travel acceleration	1500	mm/s^2
10	Support pattern (generate support)	Lines	-
11	Retraction	Enabled	-
12	Support X/Y Distance	0.5	mm
13	Flow	100	%
14	Raster angle	-45/45	°

© University of Pretoria

As previously discussed, the three variables that were used in the DOE were printing temperature (*i.e.* melt or extrusion temperature), bed/build plate temperature and printing speed. The coordinates, as summarised in Table 9, was used to construct the DOE. Table 11 summarises the six experiments consisting of different combinations of low, medium and high levels of the parameters. The DOE as illustrated below was the bases used for each filament printed on a specific model printer. Parameter A, -B and -C were the printing temperature, bed temperature and printing speed respectively.

Table 11: The DOE constructed based on the two-level fractional factorial design.

Experiment (-)	Coordinate (-)	Printing temperature (°C)	Bed temperature (°C)	Printing speed (mm/s)
1	<0, 0, 0>	200	40	40
2	<-1, -1, -1>	190	30	30
3	<1, 1, -1>	210	50	30
4	<1, -1, 1>	210	30	50
5	<-1, 1, 1>	190	50	50
6	<1, 1, 1>	210	50	50

6.2.2 Materials

PLA was the primary material type used in all the experiments. Different brands of PLA were used and printed on various model printers. Pigment was kept constant by using only black filament. Table 12 summarise the various PLA filament brands and its corresponding suppliers in South Africa that were used during experimentation.

Table 12: Filament brands and its corresponding manufacturer.

Number	Brand	Supplier
1	Zortrax PLA	Build volume
2	FlashForged PLA	Build volume and Additive Manufacturing Solutions 3D
3	CRON PLA	3D Printing Store
4	Build volume PLA	Build volume
5	Wanhao PLA	3D Printing Store

© University of Pretoria

Buildvolume and CRON are South African fabricated filament, where Flashforge, Zortrax and Wanhao filament can be obtained overseas. The CRON filament purchased in South Africa is equivalent to HAIO 3D manufactured in China and the Buildvolume filament purchased in South Africa is equivalent to Formfatura RPLA. All filament that were used and are discussed in this document were purchased in South Africa.

6.2.3 Apparatus

The printers used in the study were open-source printers. Table 13 summarises the various printer models with their corresponding manufacturers that were used during the execution of the DOE. Several modifications were made to Ender-5, Ender-5 Plus and Duplicator 9 300. The other models were standard and they were used as purchased. A PVA glue stick (*e.g.* Pritt) was used in the cases where it was observed that the desired bed adhesion was not achieved. Figure 22 illustrates the six different printer models as summarised in Table 13.

Table 13: The printer models used to produce the various prints.

No	Manufacturer	Model	Modifications
1	Creality	Ender-3 Max	Standard
2	Creality	Ender-5	Bed support structure and no printability mods
3	Creality	Ender-5 Plus	Metal extruder and X sync indicator
4	Creality	Ender-6	Standard
5	Wanhao	Duplicator 9 I3	Standard
6	Wanhao	Duplicator 9 300	Metal extruder and Capricorn tubing

© University of Pretoria

(a)

(b)

(c)

(d)

(e)

(f)

Figure 22: (a) Ender-3 Max, (b), Ender-5, (c), Ender-5 Plus, (d) Ender-6, (e) Duplicator 9 I3 and (f) Duplicator 9 300 (Wanhao, 2021; Creality, 2021).

© University of Pretoria

6.2.4 Samples printed and printer settings

Six experiments (*i.e.* sixty prints) were printed for each filament on a printer to complete a set. Table 14 summarises the sets of prints completed on various printers and by using different brands of PLA. The settings that were changed in Cura are indicated in Table 15. The default settings were used for the other printing parameters.

Table 14: Printing sets completed based on the DOE.

No	Printer model	Material brand	Total number of prints
1	Creality Ender-3 Max	Wanhao PLA	60
2	Creality Ender-5	Wanhao PLA	60
3	Creality Ender-5 Plus	Wanhao PLA	60
4	Creality Ender-6	Build volume PLA	60
5	Creality Ender-6	Wanhao PLA	60
6	Creality Ender-6	FlashForge PLA	60
7	Creality Ender-6	Zortrax PLA	60
8	Creality Ender-6	CRON PLA	60
9	Wanhao Duplicator 9 300	Wanhao PLA	60
10	Wanhao Duplicator 9 I3	CRON PLA	60

© University of Pretoria

Table 15: The printing parameters that were set in Cura for each experiment.

Experiment		
Parameter	Description	Units
Ambient temperature	17–21	°C
Material	X PLA (*i.e.* generic PLA in Cura)	-
Printing orientation	Flat (0°)	-
Print location	Middle of build plate/bed	-
Printer type	X	-
Build surface	X	-
Specimen type	ASTM D638 Type I	-
Number of specimens	10	specimens
Test performed	Tensile testing	-
Nozzle diameter	0.4	mm
Filament diameter	1.75	mm
Layer height	0.15	mm
Number of bottom layers	3	-
Number of top layers	3	-
Number of shells/wall line count	3	-
Raster angle	-45/45	°
Infill density	50	%
Infill pattern	Lines (2D)	-
Support pattern (generate support)	Lines (2D)	-
Printing temperature	190, 200 and 210	°C
Build plate temperature	30, 40 and 50	°C
Cooling (fan speed)	100	%
Printing speed	30, 40 and 50	mm/s
Print acceleration	1500	mm/s^2
Travel acceleration	1500	mm/s^2
Build plate adhesion type	Brim	-
Retraction	Enabled	-
Support X/Y distance	0.5	mm
Flow	100	%

© University of Pretoria

6.3 Tensile testing

6.3.1 ASTM D638

Tensile property data was obtained by using ASTM (2015). Standard ASTM D638 Type I test specimens were printed because it was suggested to use the sample if reinforced composites were tested. The dimensions for the specimen included an overall width of 19 mm, a narrow section width of 13 mm, an overall length of 165 mm and a thickness of 3.2 $\pm$ 0.4 mm. Figure 23 shows the specimen printed on the various printers. (ASTM, 2015)

New rolls of filament were purchased and used. The bed and nozzle were preheated to the predetermined temperatures as stipulated in the DOE. It was important to ensure that the mechanical components (*e.g.* extruder) were fastened after the heating stage was complete. The next stage involved the feeding of the filament to the print head. The SD card was inserted into the control panel where after the STL file was selected from the list as displayed on the interface of the control panel. Bed levelling can either be set in the firmware or performed manually. On the majority of printers, it was performed automatically after the STL file was selected. A brim was printed before the specimen. Ten specimens of each experiment were printed. The print sequence was set to be one at a time. The specimen was removed after the print was completed. In the cases where the print clung to the bed, a bed scraper was used to remove the print.

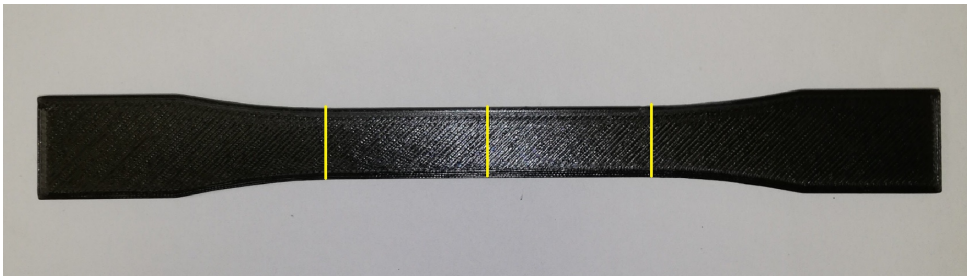

Figure 23: A standard ASTM D638 Type I tensile bar (ASTM, 2015).

A visual inspection was performed on all printed samples. Quality control was incorporated in the material evaluation guideline by doing a visual inspection as stipulated in Section 6.4 of ASTM D638 (ASTM, 2015). Factors evaluated during the visual inspection included the adhesion between layers, the adhesion between infill and shell, the quality of the infill density and whether or not stressors were visible on the edge of the sample.

© University of Pretoria

The preconditioning included storing the samples in a dark chamber to reduce the effect of UV light. The chamber had an average temperature and humidity of 22.4 °C and 36% respectively. The preconditioning was executed for 48 hours before commencing with the tensile testing in an ambient temperature which varied between 17 °C and 21 °C. The thickness and width of each sample were measured by using a Mitutoyo micrometer and a vernier calliper respectively. The equipment is illustrated in Figure 24. Three readings were taken and an average of the values was used during the determination of the tensile strength. The locations of the readings are indicated in Figure 23.

(a)

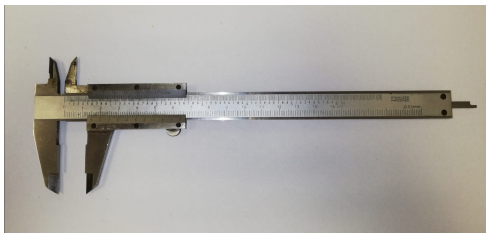

(b)

Figure 24: (a) A Mitutoyo micrometer and (b) a vernier calliper.

6.3.2 Tensile machine

The mechanical properties of the specimens were determined by using tensile testing. The tensile machine had a fixed- and movable member. The pneumatic clamps/grips were controlled by means of hydraulic foot pedals. The tensile bars were placed between the open clamps and fastened by using the foot pedals. The latter was done in such a manner to ensure that slippage relative to the clamps was reduced.

The tensile testing was performed on a Lloyd Instruments LRX Plus tensile machine (trademark of Ametek Incorporated). Figure 25 is an illustration of the tensile machine. The machine had a 5 kN load cell. A testing speed of 5 mm/min, a load rate of 15 N/min and a nominal strain rate of 0.1 mm/(mm.min) were selected as machine settings according to ASTM D638. A $\frac{Preload}{Stress}$ of 5.6 N and a $\frac{Preload}{Stress}$ speed of 21 mm/min were used. The tensile strength, percentage elongation, elongation at break, elongation at yield, nominal strain, nominal strain at break, modulus of elasticity, secant modulus and ultimate tensile strength are variables that can be determined. (ASTM, 2015)

© University of Pretoria

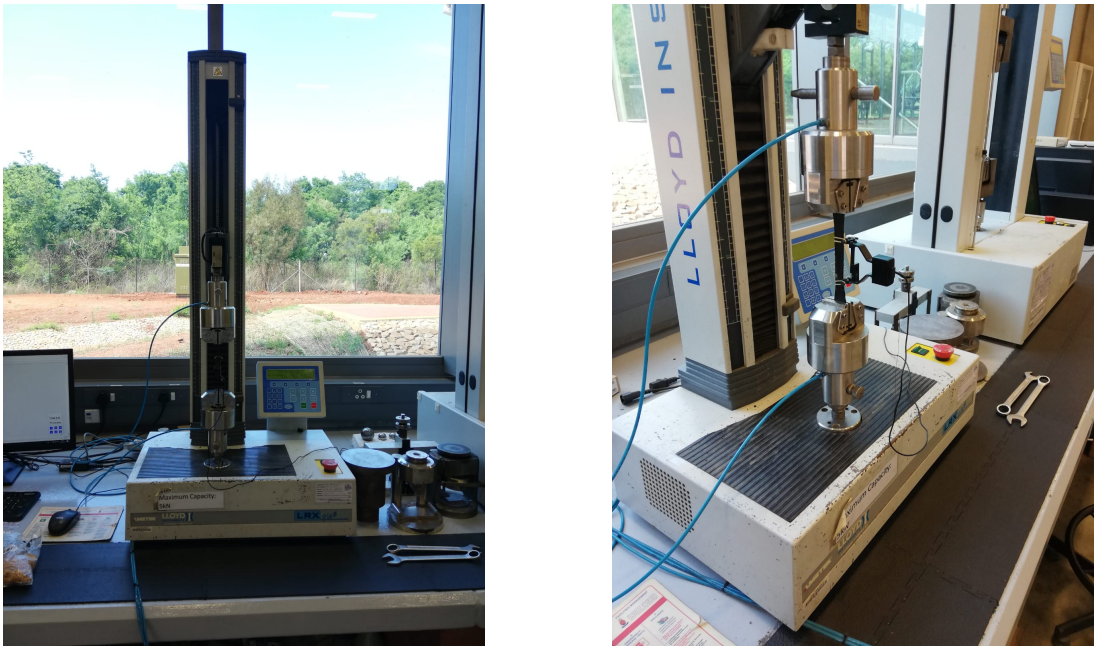

(a) (b)

Figure 25: The tensile machine used during testing.

The elongation of each specimen was measured by placing an extensometer on the vertical edge of each sample. The placement of the extensometer on a specimen and the extensometer are illustrated in Figure 26. The distance (Δl) between the two metal plates of the extensometer is 50 mm. The ambient temperature and humidity were recorded during the testing of each sample. Ten specimens of each experiment were tested and the results were recorded.

(a) (b)

Figure 26: (a) The placement of the extensometer on a specimen and (b) the extensometer.

© University of Pretoria

7 Results and Discussion

7.1 Visual inspection on printed samples

The samples were printed during the winter months. The ambient temperature only affected prints that were printed with cooler bed temperatures. Warping was observed when the combination between these two temperatures were too low. Adhesive (*e.g.* Pritt®) was used to resolve this problem. The latter could affect the properties of a printed sample. During the printing process, it was observed that the samples that were printed with a bed temperature of 30 °C in combination with the cooler ambient temperatures exhibited poor bed adhesion. It was noted that bed adhesion was not a problem with higher bed temperatures. A visual inspection was performed on the samples as discussed in Section 6.4 of the standard ASTM D638 (ASTM, 2015). Stressors were recorded to determine whether they had an impact on the fracture obtained during the tensile testing. Table 16 summarises the visual inspection performed on the samples printed from different material brands and on various printer models.

* No maintenance had to be done and no print difficulty were experienced on the printers.

© University of Pretoria

Table 16: A summary of the visual inspection performed on the printed samples.

No	Material brand	Printer model	Description
1	Build volume PLA	Creality Ender-6*	The samples had a smooth glossy surface finish. No visible flaws were observed at the conjunction between the shell and infill. Distinctive grooves illustrating the -45°/45° raster angle was observed on the top layer of the samples. The samples of the various experiments had a similar visual appearance. None of the samples were under-extruded. The layer adhesion obtained was satisfactory from a visual analysis perspective.
2	CRON PLA	Creality Ender-6	The samples had a similar appearance as those printed with the Build volume PLA. Some of the Experiment 5 samples had scraper marks in the grip region of the print. None of the samples was under-extruded and there was no difficulty removing the brim.
3	Flashforge PLA	Creality Ender-6	The samples had a similar appearance as those printed with the Build volume PLA. There was difficulty removing the brim from the Experiment 1 and Experiment 3 samples. Two spools of filament were used to complete the set. The second spool was used to print an additional Experiment 4 set as well as an Experiment 5 and Experiment 6 set. Little to no variance was noticed between the prints from the different spools, except for one Experiment 4 sample. The sample was printed with the second spool and exhibited scraper marks on the surface of the print. The layer adhesion was satisfactory from a visual analysis perspective.

© University of Pretoria

No	Material brand	Printer model	Description
4	Wanhao PLA	Creality Ender-6	The samples were not as glossy in appearance as the Build volume samples. The samples of the various experiments had a similar visual appearance. None of the samples was under-extruded. The brim was easily removed from the prints.
5	Zortrax PLA	Creality Ender-6	The Experiment 3 samples had holes in the shell (*i.e.* under-extruded). The latter could be possible stressors that lead to undesirable fractures during the break. There was difficulty removing the brim from the samples. The samples were matt. It was harder in comparison with the other material brands printed on the Creality Ender-6. The distinctive grooves were not as visible on the top layer–the prints had a uniform top layer. Two spools of filament were used to complete the set. No visible difference in part appearance were observed between the sets printed with the different spools. Problems were encountered with the feeding of the second spool.
6	CRON PLA	Wanhao Duplicator 9 I3	The samples had a matt appearance in comparison to the CRON PLA samples printed on the Creality Ender-6. The samples in the set had a uniform top layer. Under-extrusion was noted in the layers between the top and bottom layers giving the print a hollower appearance. There was difficulty removing the brim from the Experiment 4, Experiment 5 and Experiment 6 samples.
7	Wanhao PLA	Creality Ender-3 Max	The Experiment 1 samples were under-extruded as it had a hollow appearance in comparison to those printed on the Creality Ender-6. The Experiment 2 and Experiment 3 samples had a hybrid appearance–parts of the sample were under-extruded while other parts were printed with the correct infill percentage/density. There was difficulty removing the brim from the Experiment 5 and Experiment 6 samples.

© University of Pretoria

No	Material brand	Printer model	Description
8	Wanhao PLA	Creality Ender-5*	The samples had a similar hybrid appearance as those printed on the Creality Ender-3 Max. The top layer of the Experiment 1, Experiment 2 and Experiment 4 samples were under-extruded and exhibited a hollow appearance. There was no difficulty removing the brim from the samples in the set.
9	Wanhao PLA	Creality Ender 5-Plus	Irregularity with the layer deposition of the top layers of the Experiment 1 samples were noted. It was not a solid deposition which resulted in open grooves between the shell. Small holes were visible between the shell and the infill. The Experiment 5 and Experiment 6 samples had a mark on the bottom layer caused by the building platform. There was difficulty removing the brim from the Experiment 3, Experiment 4, Experiment 5 and Experiment 6 samples.
10	Wanhao PLA	Wanhao Duplicator 9 300	The print quality was poor in comparison to the other sets of prints. The Experiment 1 samples were under-extruded and the top layer formed folds. The Experiment 4 samples had a similar appearance as the samples printed on the Creality Ender-3 Max. There was difficulty removing the brim from the Experiment 4, Experiment 5 and Experiment 6 samples.

© University of Pretoria

7.2 Visual inspection on broken samples

It was interesting to note that the tensile tests were not affected by the stressors or small flaws in a sample. The testing was therefore robust. Problems encountered during the tensile tests included fractures occurring above or below the metal blades of the extensometer resulting in no reading being recorded. The extension of the samples is limited to the type of extensometer used. In some instances (*e.g.* with the samples printed on the Wanhao Duplicator 9 300) the extension was more and therefore the results obtained were not a true resemblance of the elongation of the sample. Table 17 summarises the visual inspection performed on the broken samples.

© University of Pretoria

Table 17: A summary of the visual inspection performed on the broken samples.

No	Material brand	Printer model	Description
1	Build volume PLA	Creality Ender-6	Brittle failure was observed. The majority of the samples fractured in the transition area between the grip region and the plastic deformation region. The samples that fractured in the plastic deformation region tended to craze in the transition area. One of the Experiment 3 samples had two brittle fractures in the plastic deformation region that occurred simultaneously.
2	CRON PLA	Creality Ender-6	Brittle failure was observed. The majority of the samples fractured in the transition area between the grip region and the plastic deformation region. Fracture occurring in the plastic deformation region was scarce.
3	Flashforge PLA	Creality Ender-6	Brittle failure was observed. All samples, except for one Experiment 6 sample, fractured in the transition area between the grip region and the plastic deformation region.
4	Wanhao PLA	Creality Ender-6	All the samples in the set fractured similarly. The fracture was not completely brittle. The top and bottom layers shifted in opposite directions. This resulted in the infill to be visible. The fracture occurred in the transition area between the grip region and the plastic deformation region of the samples. The deformation of individual deposited strands between the top and bottom layer were visible. The strands had a frayed appearance.

© University of Pretoria

UNIVERSITEIT VAN PRETORIA
UNIVERSITY OF PRETORIA
YUNIBESITHI YA PRETORIA

No	Material brand	Printer model	Description
5	Zortrax PLA	Creality Ender-6	Brittle fracture was observed. One of the Experiment 1 samples fractured in the plastic deformation region. The rest of the samples fractured in the transition region. The majority of the Experiment 2 samples fractured in the plastic deformation region. Necking was observed in these samples causing white scars alongside the shell. The latter was also observed with several Experiment 5 samples (these samples were printed with the second filament spool). It was noted that some of the Experiment 5 samples both fractured and crazed.
6	CRON PLA	Duplicator 9 I3	Brittle fracture was observed. The majority of Experiment 1 samples broke in the plastic deformation region, while the samples in the other experiments fractured in the transition area. One Experiments 3 sample, one Experiment 4 sample and two Experiment 5 samples had two brittle fractures that occurred simultaneously.
7	Wanhao PLA	Creality Ender-3 Max	The samples in the set broke in a similar brittle manner. All the samples fractured in the plastic deformation region. One of the Experiment 2 samples had an interesting appearance upon fracture–some of the deposited strands in the shell remained unbroken. The latter elongated, while the rest of the sample fractured.
8	Wanhao PLA	Creality Ender-5	The samples had a similar appearance as the fractured samples printed on the Creality Ender-3 Max. One of the Experiment 5 samples had a similar appearance as the Experiment 2 sample printed on the Creality Ender-3 Max.

© University of Pretoria

No	Material brand	Printer model	Description
9	Wanhao PLA	Creality Ender-5 Plus	No brittle failure was observed. All the samples in the set fractured in a similar manner. The fracture occurred in the plastic deformation region. As the test commenced the one side of the shell fractured. Strand deformation, alignment and breakage were observed. The samples did not fracture altogether by the time the extensometer reached its maximum. The strands in the opposing shell were aligned and straightened but did not fracture by the time the latter occurred.
10	Wanhao PLA	Duplicator 9 300	The fibre deformation and elongation were visible in the samples of Experiment 1 and Experiment 2. Several strands did not break by the time the extensometer had reached its maximum. Necking was observed in these samples. The samples of Experiment 3 and Experiment 4 fractured in a brittle sense but less when compared to the CRON PLA samples printed on the Duplicator 9 I3. The strands aligned in both the shell and infill during the tensile testing of the Experiment 5 and Experiment 6 samples. Not all strands broke, leaving the tested sample conjoined and not in two pieces.

© University of Pretoria

7.3 Tensile data

Tensile tests were performed on the samples to improve the understanding of the mechanical properties of the printed specimens. Brittle failure was the expected failure mechanism. According to McCrum, Buckley & Bucknall (1999) it is common to observe localised yielding over a specified region while brittle crack propagation occurs.

The force, specimen elongation and machine elongation were measured during the tensile tests. The cross-sectional area of all specimens were measured before commencing with the tests. The latter together with the force were used to calculate the stress. The specimen elongation and Δl were used to determine the strain. Young's modulus was calculated as it is the slope of the graph in the linear region. The maximum load was obtained as well as the elongation at break was measured when the samples fractured. (McCrum, Buckley & Bucknall, 1999)

It was expected to observe specimens fracture in the narrow region. It was also expected that the more expensive filament would exhibit a greater UTS. Little variance in UTS was expected between sets printed with the same brand of filament (*e.g.* Wanhao PLA) on various printer models. After the tensile tests were conducted it was noted that the samples exhibited different stress-strain behaviour irrespective of the fact that several were printed with the same brand of filament or on the same printer model. The phenomena was summarised in four groups where each group represented a different stress-strain behaviour.

Figure 27 is an illustration of samples where the fibres started aligning as the force and the specimen extension both reached a maximum. It was difficult to tell the material and part behaviour apart from one another as there was no distinctive necking and/or crazing region. At elongation at break the specimen did not fracture into two segments. Discolouration of the black Wanhao PLA filament was visible and it was evident that several fibres were still aligned in the direction of the raster angle.

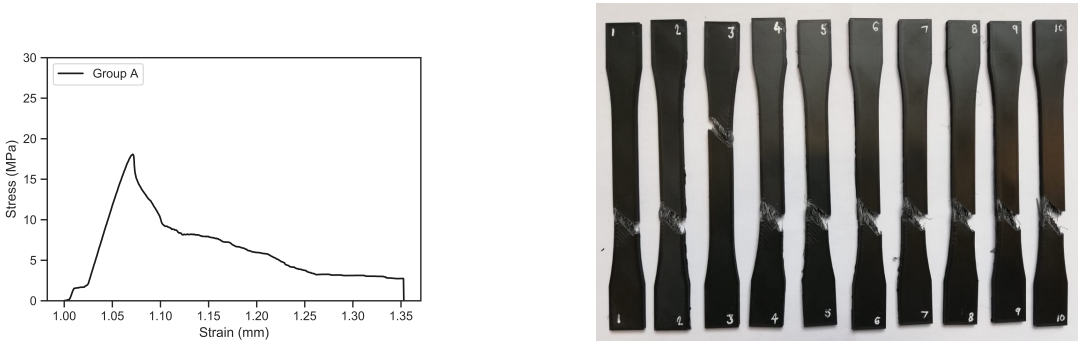

(a) (b)

Figure 27: Stress-strain behaviour of Group A.

© University of Pretoria

Figure 28 is an illustration of samples in which the fibres aligned in a vertical direction before reaching elongation at break. Several fibres were still intact and no brittle fracture were observed. A neck formed resulting in a more prominent necking region when compared to Figure 27.

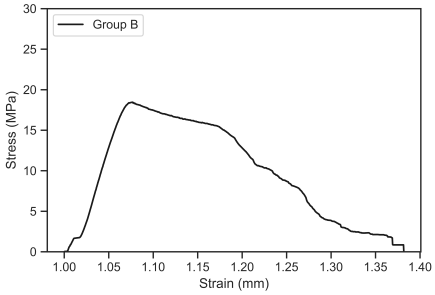

(a)

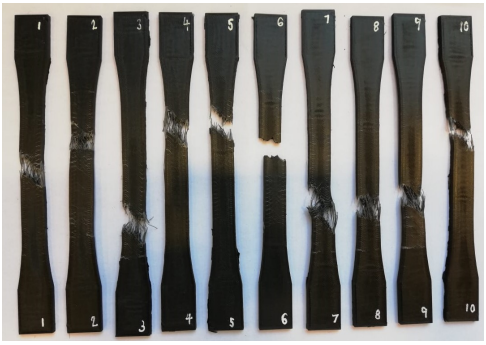

(b)

Figure 28: Stress-strain behaviour of Group B.

In Figure 29 the first necking region was followed by a steep decrease in the gradient of the curve, resembling similar behavior to fracture. The sample entered a second necking phase before final fracture. It exhibited two fractures in the shell–the first resulted from vertical fibre elongation resulting in complete fracture in the width of the specimen and the second was only in a portion of the shell. No brittle failure were observed.

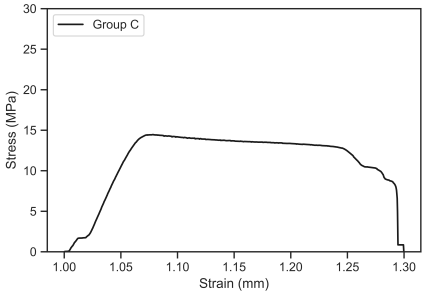

(a)

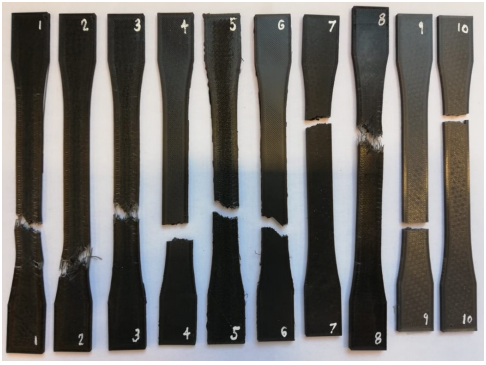

(b)

Figure 29: Stress-strain behaviour of Group C.

Group D represents samples that exhibited brittle failure. It was interesting to note that the majority of samples fractured in the transition area between the grip region and the plastic deformation region. After investigation, it was noted that the infill start and z-seam alignment were not randomised in Cura, which resulted in a groove being printed in that location. This stressor may have been the reason for the observed fractures. None of the previous academic studies pointed this out as important. Figure 30 is an illustration of the stress-strain behavior of Group D.

© University of Pretoria

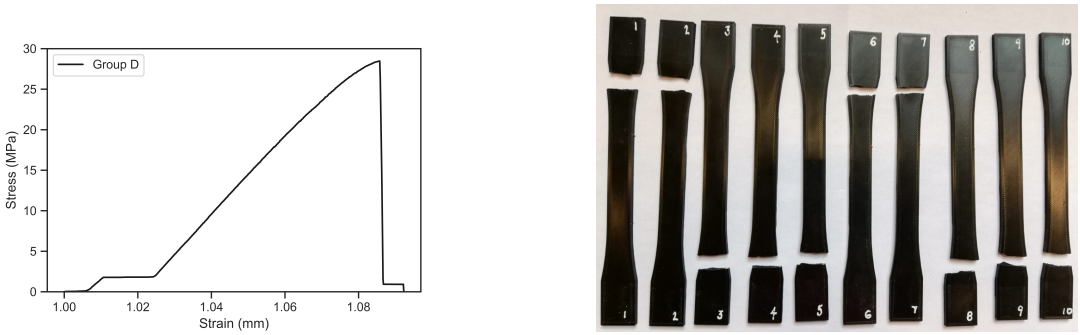

(a) **(b)**

Figure 30: Stress-strain behaviour of Group D.

The average UTS, standard deviation (SD) of the UTS, elongation (ε) at UTS, SD of the elongation at UTS, Young's modulus (E), SD of Young's modulus, elongation at break and the SD of elongation at break were calculated for each experiment printed with one type of filament on a specific printer. The latter for various filament on different types of printers are summarised in Table 18.

© University of Pretoria

Table 18: Mechanical properties for various filament on different types of printers.

Filament (-)	Printer (-)	Experiment (-)	Average UTS (MPa)	Average UTS SD (-)	ε at UTS (mm/mm)	ε at UTS SD (-)	E (N/mm)	E SD (-)	ε at break (mm/mm)	ε at break SD (-)
Wanhao	Ender-6	1A	17.75	0.87	1.06	0.003	435.98	8.01	1.07	0.002
		2A	17.11	0.52	1.06	0.003	429.76	12.99	1.08	0.017
		3A	19.59	1.25	1.07	0.004	437.65	9.98	1.07	0.003
		4A	17.93	1.12	1.07	0.003	435.50	12.75	1.07	0.002
		5A	17.95	1.21	1.06	0.004	446.14	15.19	1.08	0.011
		6A	19.25	1.47	1.07	0.004	440.25	9.80	1.07	0.002
Build -volume	Ender-6	1A	28.77	1.79	1.09	0.004	524.65	13.65	1.10	0.024
		2A	27.31	2.03	1.09	0.005	499.93	8.47	1.09	0.010
		3A	28.87	1.27	1.09	0.005	485.96	7.09	1.10	0.009
		4A	28.69	1.48	1.08	0.004	495.46	40.23	1.08	0.004
		5A	27.82	2.13	1.09	0.006	464.46	14.52	1.09	0.011
		6A	28.81	1.23	1.09	0.006	485.93	5.79	1.10	0.029
Flashforge	Ender-6	1A	27.69	1.74	1.09	0.008	466.25	4.83	1.08	0.029
		2A	25.89	1.56	1.08	0.006	456.07	7.56	1.08	0.006
		3A	27.41	1.69	1.09	0.006	458.13	8.77	1.09	0.006
		4A	27.43	1.35	1.09	0.005	465.27	3.97	1.09	0.005
		5A	31.31	1.16	1.09	0.005	482.82	7.96	1.10	0.006
		6A	30.80	1.80	1.10	0.005	479.35	7.52	1.10	0.007
Zortrax	Ender-6	1A	24.45	0.40	1.08	0.004	566.69	15.77	1.09	0.012

© University of Pretoria

Filament (-)	Printer (-)	Experiment (-)	Average UTS (MPa)	Average UTS SD (-)	ε at UTS (mm/mm)	ε at UTS SD (-)	E (N/mm)	E SD (-)	ε at break (mm/mm)	ε at break SD (-)
		2A	24.41	0.46	1.08	0.003	559.51	16.27	1.12	0.008
		3A	23.84	0.74	1.07	0.006	569.88	7.82	1.08	0.012
		4A	24.18	0.75	1.07	0.004	573.11	6.04	1.07	0.004
		5A	25.57	0.32	1.08	0.008	536.73	11.64	1.10	0.018
		6A	24.63	0.43	1.08	0.003	563.55	11.68	1.08	0.006
CRON	Ender-6	1A	30.12	1.22	1.10	0.006	469.83	9.58	1.11	0.020
		2A	32.50	2.62	1.10	0.005	500.66	28.31	1.11	0.015
		3A	32.60	6.39	1.10	0.015	527.34	14.56	1.11	0.020
		4A	33.63	1.64	1.10	0.008	509.86	16.09	1.11	0.017
		5A	33.84	1.75	1.10	0.008	505.21	9.09	1.11	0.015
		6A	35.34	0.78	1.10	0.006	514.11	8.20	1.11	0.015
Wanhao	Ender-3 Max	1A	16.92	0.51	1.06	0.002	405.81	16.70	1.06	0.002
		2A	16.61	1.11	1.07	0.003	397.25	9.05	1.07	0.003
		3A	14.15	0.81	1.06	0.005	392.62	9.50	1.06	0.005
		4A	18.46	1.22	1.07	0.005	410.11	8.13	1.07	0.005
		5A	17.69	0.72	1.07	0.003	403.57	9.39	1.07	0.003
		6A	18.80	1.17	1.07	0.004	408.10	10.96	1.07	0.017

© University of Pretoria

UNIVERSITEIT VAN PRETORIA
UNIVERSITY OF PRETORIA
YUNIBESITHI YA PRETORIA

Filament (-)	Printer (-)	Experiment (-)	Average UTS (MPa)	Average UTS SD (-)	ε at UTS (mm/mm)	ε at UTS SD (-)	E (N/mm)	E SD (-)	ε at break (mm/mm)	ε at break SD (-)
Wanhao	Ender-5	1A	16.00	0.77	1.06	0.002	379.64	6.88	1.06	0.002
		2A	15.00	0.75	1.06	0.002	369.67	10.31	1.07	0.003
		3A	13.66	0.68	1.07	0.003	334.55	7.71	1.07	0.003
		4A	12.98	1.35	1.07	0.008	318.04	16.36	1.07	0.006
		5A	12.89	1.18	1.06	0.006	342.91	25.18	1.07	0.005
		6A	13.97	1.92	1.07	0.005	339.96	18.35	1.07	0.005
Wanhao	Ender-5 Plus	1A	16.58	0.75	1.06	0.001	383.33	15.51	1.31	0.068
		2A	17.63	0.98	1.07	0.002	381.79	7.67	1.17	0.066
		3A	18.30	2.85	1.07	0.002	399.35	85.76	1.25	0.028
		4A	18.10	0.75	1.07	0.004	401.08	18.73	1.24	0.105
		5A	17.35	0.75	1.07	0.002	374.40	7.67	1.26	0.055
		6A	17.50	0.72	1.07	0.003	372.28	4.45	1.25	0.103
CRON	D9 I3	1A	26.22	1.29	1.09	0.004	377.59	127.84	1.11	0.012
		2A	19.33	1.70	1.08	0.004	351.71	24.02	1.09	0.012
		3A	22.68	1.73	1.09	0.003	403.55	21.89	1.09	0.005
		4A	23.57	1.57	1.09	0.003	409.18	20.48	1.10	0.008
		5A	25.93	2.65	1.09	0.003	440.12	39.79	1.09	0.006
		6A	29.48	0.90	1.09	0.002	471.84	17.28	1.10	0.005

© University of Pretoria

Filament	Printer	Experiment	Average UTS	Average UTS SD	ε at UTS	ε at UTS SD	E	E SD	ε at break	ε at break SD
(-)	(-)	(-)	(MPa)	(-)	(mm/mm)	(-)	(N/mm)	(-)	(mm/mm)	(-)
Wanhao	D9 300	1A	17.91	1.11	1.07	0.002	343.48	25.06	1.35	0.067
		2A	18.32	0.80	1.08	0.003	351.54	13.44	1.38	0.054
		3A	18.06	0.62	1.08	0.002	352.19	22.70	1.25	0.042
		4A	17.72	4.59	1.07	0.007	372.08	89.96	1.17	0.115
		5A	16.59	0.78	1.08	0.002	314.00	13.42	1.38	0.038
		6A	17.23	0.78	1.08	0.003	319.71	13.88	1.33	0.047

© University of Pretoria

7.3.1 Wanhao PLA on the Creality Ender-6

The weighted least squares method was used to statistically quantify the effect of the parameters tested according to the DOE. To ensure that the ANOVA model assumptions were satisfied, the residuals had to be normally distributed. To address this, the standard deviation of the average UTS for the ten samples, in each experiment, was used as the weight. The linear model was fitted by using a p-value of 0.05.

Tools such as jitter plots and box plots were used to visually exhibit the UTS values in MPa. A jitter plot was used to visualise the average UTS of each experiment. The distribution within a population was illustrated by means of a box plot. The mean for each set of samples is illustrated by means of a red dot. One sample of Experiment 5 was discarded and excluded from all analysis due to engineering judgement (UTS out of range). Figure 31 is a combined jitter and box plot which illustrates the UTS obtained for each sample in each experiment. The standard deviation for the average UTS for Experiment 2 was 0.52, which was the least when compared to the other experiments.

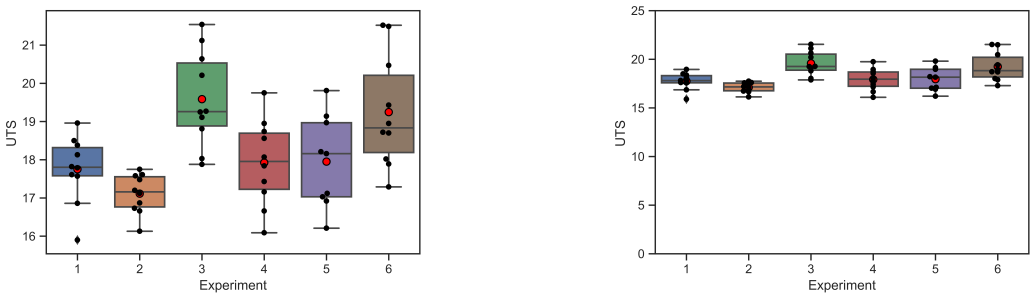

Figure 31: Sample comparison for Wanhao PLA on the Creality Ender-6.

The F ratio was evaluated to determine whether sufficient variation is explained by the model. Table 19 also summarises the regression model results. The Estimate column provides the regression coefficients for the variables. Note printing- and bed temperature have different units than printing speed, which affects the regression coefficients. Statistical significance of the coefficients was determined by evaluating the p-values. The percentage error in the model was determined by dividing the root mean square error (RMSE) by the average UTS. The smaller the RMSE, the better the model performance relative to the UTS. The significance of the interaction A*B was tested after it was determined that parameter C was statistically insignificant. After evaluating the p-value, both variables had a significant effect on the UTS and, from the regression model, UTS increases significantly for an increase in both printing- and bed temperatures. The model error was calculated as 1.11%.

© University of Pretoria

Table 19: The ANOVA obtained for Wanhao PLA/Creality Ender-6.

Term	Estimate	Standard Error	t Ratio	Prob >[t]
Intercept	2.4529	3.6767	0.67	0.5074
A	0.0646	0.0179	3.62	0.0006
B	0.0661	0.0178	3.72	0.0005
	Value			Probability
F ratio	14.2564	-	-	<0.0001
R^2	0.3374	-	-	-
R^2 adjusted	0.3137	-	-	-
Root mean square error (RMSE)	1.2162	-	-	-
Percentage error in model	1.11	-	-	-

7.3.2 Buildvolume PLA on the Creality Ender-6

Figure 32 is a combined jitter and box plot for Buildvolume PLA printed on the Creality Ender-6. Less variance was observed between the different experiments after scaling when compared to the Wanhao PLA. The latter was noted for Experiment 3, Experiment 4, Experiment 5 and Experiment 6. Despite the fact that all experiments had outliers, Experiment 4 still exhibited the best repeatability. The standard deviation for the average UTS for Experiment 6 was 1.23, which was the least when compared to the other experiments.

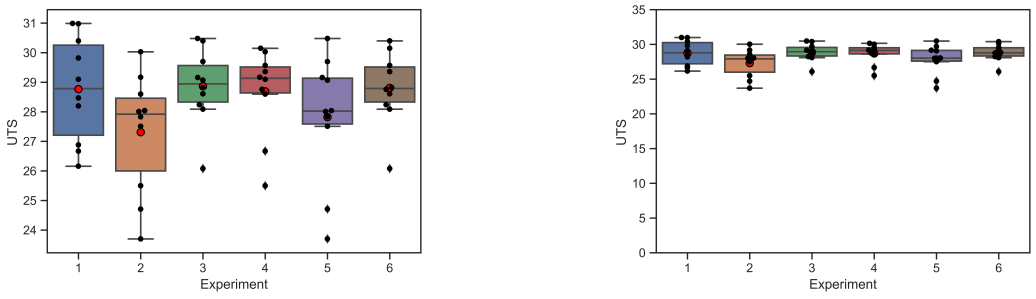

Figure 32: Sample comparison for Buildvolume PLA on the Creality Ender-6.

© University of Pretoria

The same procedure was followed, as explained in Section 7.3.1, to determine which parameters as well as interactions were statistically significant. Table 20 summarises the regression model results and interaction equation obtained. Only printing temperature was statistically significant with a p-value of 0.02. The latter resulted in a 0.06 MPa increase in UTS for one unit increase in temperature. The model error was calculated as 1.30%.

Table 20: The ANOVA obtained for Buildvolume PLA/Creality Ender-6.

Term	Estimate	Standard Error	t Ratio	Prob >[t]
Intercept	16.1332	4.9234	3.28	0.0018
A	0.0608	0.0246	2.47	0.0165
	Value			Probability
F ratio	6.0925	-	-	0.0165
R^2	0.0951	-	-	-
R^2 adjusted	0.0795	-	-	-
Root mean square error (RMSE)	2.2201	-	-	-
Percentage error in model	1.30	-	-	-

7.3.3 Flashforge PLA on the Creality Ender-6

One sample of Experiment 6 was discarded and excluded from all analysis due to engineering judgement (UTS out of range). The average UTS of the six experiments ranged between 25.89 MPa and 31.31 MPa. It was noted that the repeatability of Experiment 3, Experiment 4 and Experiment 5 were less, after comparing the Flashforge PLA to the Buildvolume PLA. The standard deviation for the average UTS for Experiment 5 was 1.16, which was the least when compared to the other experiments. Figure 33 illustrates the jitter and box plots for Flashforge PLA printed on the Creality Ender-6.

© University of Pretoria

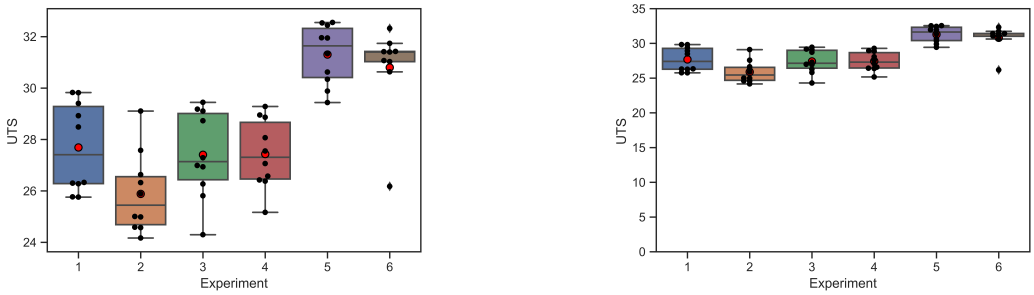

Figure 33: Sample comparison for Flashforge PLA on the Creality Ender-6.

Table 21 summarises the regression model results and interaction equation obtained. After evaluating the p-value, bed temperature, printing speed and the interaction between these two parameters were statistically significant. The model error was calculated as 1.15%.

Table 21: The ANOVA obtained for Flashforge PLA/Creality Ender-6.

Term	Estimate	Standard Error	t Ratio	Prob >[t]
Intercept	17.0187	1.2702	13.40	<0.0001
B	0.1334	0.0235	5.67	<0.0001
C	0.1381	0.0232	5.95	<0.0001
B*C	0.0052	0.0024	2.21	0.0313
	Value			Probability
F ratio	28.2279	-	-	<0.0001
R^2	0.6063	-	-	-
R^2 adjusted	0.5848	-	-	-
Root mean square error (RMSE)	1.9578	-	-	-
Percentage error in model	1.15	-	-	-

7.3.4 Zortrax PLA on the Creality Ender-6

Two rolls of filament were used to complete the whole set of 60 Zortrax samples on the Creality Ender-6. Experiment 1 up and until Experiment 4 were printed with the first roll and Experiment 5 and Experiment 6 were printed with the second roll. The Zortrax PLA

© University of Pretoria

did not exhibit the highest average UTS when compared to the other types of filament, but the best repeatability was observed between the different samples and experiments. Figure 34 illustrates the latter. Experiment 5 had the smallest standard deviation of 0.32 despite the outlier detected.

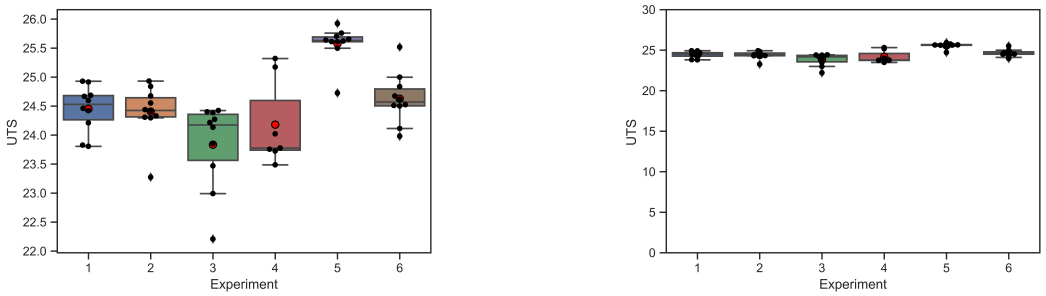

(a) (b)

Figure 34: Sample comparison for Zortrax PLA on the Creality Ender-6.

Various samples of Experiment 4 were printed on two different printers and rolls of filament. This was done to determine whether variance occurred due to small differences between extruded filament batches or manufactured printers. Both the printers and rolls were newly purchased goods. Table 22 summarises the printer and roll combination used.

Table 22: A summary of similar experiments printed on different printers and filament rolls.

No	Experiment	Printer 1	Printer 2	Roll 1	Roll 2
1	4A	X		X	
2	4A		X	X	
3	4A		X		X

Figure 35 illustrates that the average UTS for the different rolls printed on various printers ranged between 19.81 MPa and 25.32 MPa. Repeatability between the samples was noted after a visual inspection was performed. It was evident that the effect of different printers and filament rolls from the same manufacturer had a negligible effect on the average UTS obtained between the samples.

© University of Pretoria

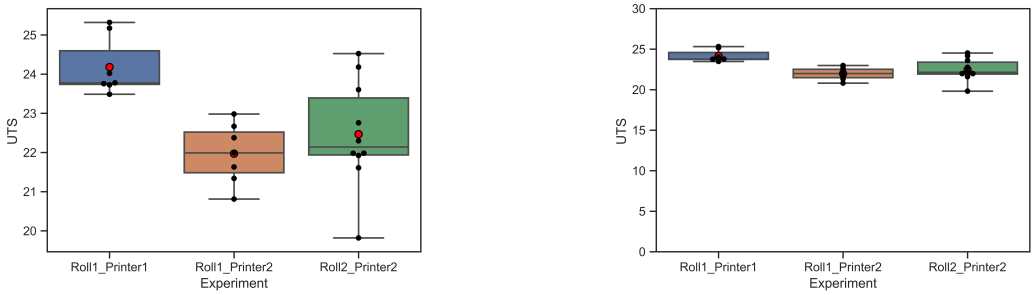

Figure 35: Comparison of Experiment 4 samples for Zortrax PLA on the Creality Ender-6.

Table 23 summarises the regression model results and interaction equation obtained. The model error was the least between all filament/printer combinations and was calculated as 0.27%. UTS decreases for an increase in printing temperature, while it increases for an increase in bed temperature and printing speed.

Table 23: The ANOVA obtained for Zortrax PLA/Creality Ender-6.

Term	Estimate	Standard Error	t Ratio	Prob >[t]
Intercept	31.8335	1.7605	18.08	<0.0001
A	-0.0486	0.0091	-5.36	<0.0001
B	0.0212	0.0086	2.46	0.0171
C	0.0384	0.0082	4.69	<0.0001
	Value			Probability
F ratio	14.8971	-	-	<0.0001
R^2	0.4575	-	-	-
R^2 adjusted	0.4268	-	-	-
Root mean square error (RMSE)	0.4019	-	-	-
Percentage error in model	0.27	-	-	-

7.3.5 CRON PLA on the Creality Ender-6

CRON PLA was not the most expensive filament, but it exhibited the highest average UTS. The UTS for the six experiments ranged between 30.12 MPa and 35.34 MPa, with Experiment 6 having the lowest standard deviation of 0.78. In Figure 36 it is evident that only Experiment 3 had outliers.

© University of Pretoria

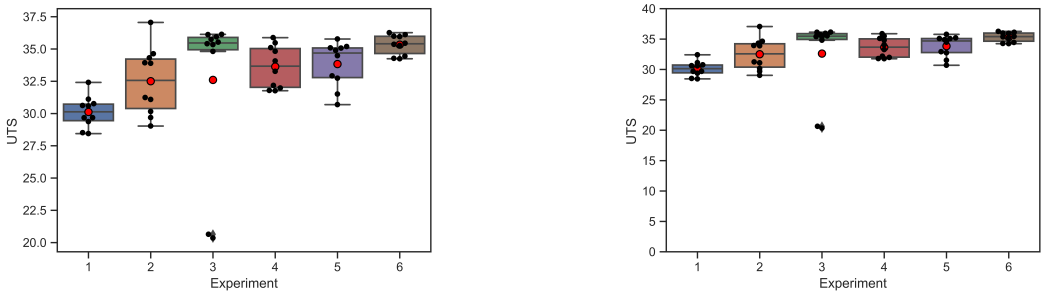

(a) (b)

Figure 36: Sample comparison for CRON PLA on the Creality Ender-6.

After determining the linear interaction model, it was observed that none of the parameters had statistical significance as the p-values were greater than 0.05. The model error was calculated as 3.53%. Table 24 summarises the regression model results and interaction equation obtained.

Table 24: The ANOVA obtained for CRON PLA/Creality Ender-6.

Term	Estimate	Standard Error	t Ratio	Prob >[t]
Intercept	27.5496	14.0354	1.96	0.0546
A	0.0097	0.0714	0.14	0.8927
B	0.0203	0.0716	0.28	0.7775
C	0.0654	0.0659	0.99	0.3253
	Value			Probability
F ratio	0.3518	-	-	0.7880
R^2	0.0185	-	-	-
R^2 adjusted	-0.0341	-	-	-
Root mean square error (RMSE)	6.9969	-	-	-
Percentage error in model	3.53	-	-	-

7.3.6 Wanhao PLA on the Creality Ender-3 Max

Outliers were observed after analysing the tensile data of Experiment 2, Experiment 3 and Experiment 4. It is evident from Figure 37 that Experiment 1 had the smallest standard deviation when evaluating the average UTS. The average UTS of Experiment 6 was 18.80 MPa, which was the highest when compared to the other experiments.

© University of Pretoria

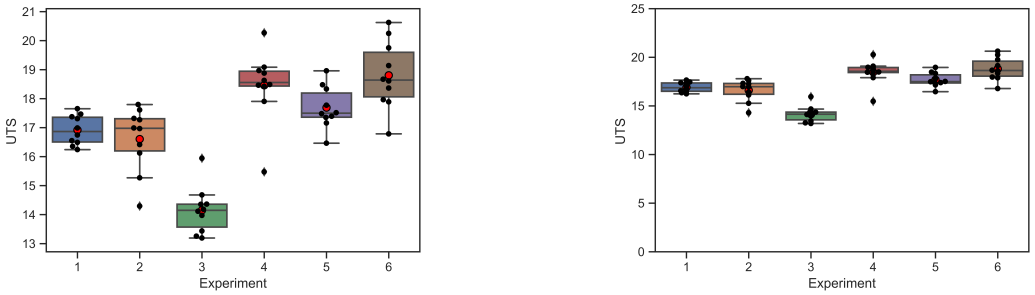

Figure 37: Sample comparison for Wanhao PLA on the Creality Ender-3 Max.

Table 25 summarises the regression model results and interaction equation obtained. Bed temperature, printing speed and the interaction between these two parameters had an effect on UTS, where bed-temperature caused a decrease in UTS. The model error was calculated as 1.00%.

Table 25: The ANOVA obtained for Wanhao PLA/Creality Ender-3 Max.

Term	Estimate	Standard Error	t Ratio	Prob >[t]
Intercept	12.6736	0.7976	15.89	<0.0001
B	-0.0506	0.0146	-3.46	0.0010
C	0.1560	0.0150	10.40	<0.0001
B*C	0.0059	0.0015	3.96	0.0002
	Value			Probability
F ratio	40.2375	-	-	<0.0001
R^2	0.6831	-	-	-
R^2 adjusted	0.6661	-	-	-
Root mean square error (RMSE)	1.0152	-	-	-
Percentage error in model	1.00	-	-	-

7.3.7 Wanhao PLA on the Creality Ender-5

Figure 38 illustrates no distinctive correlation between the UTS of the various experiments. The average UTS for Experiment 1 was the highest at 16.00 MPa, while the standard deviation for the average UTS for Experiment 3 was the smallest at 0.68.

© University of Pretoria

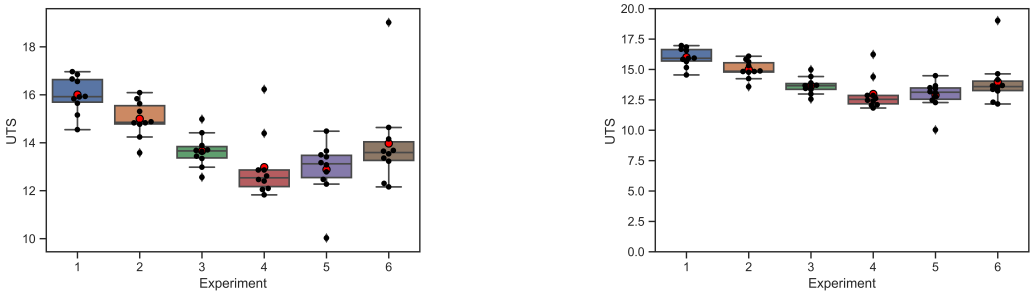

(a) (b)

Figure 38: Sample comparison for Wanhao PLA on the Creality Ender 5.

Table 26 summarises the regression model results and interaction equation obtained. After evaluating the p-value, printing speed had a significant effect on the UTS and, from the regression model, UTS decreases significantly for an increase in this parameter. The model error was calculated as 1.96%.

Table 26: The ANOVA obtained for Wanhao PLA/Creality Ender-5.

Term	Estimate	Standard Error	t Ratio	Prob >[t]
Intercept	16.8150	1.1180	15.04	<0.0001
C	-0.0655	0.0247	-2.65	0.0103
	Value			Probability
F ratio	7.0371	-	-	0.0103
R^2	0.1082	-	-	-
R^2 adjusted	0.0928	-	-	-
Root mean square error (RMSE)	1.6596	-	-	-
Percentage error in model	1.96	-	-	-

7.3.8 Wanhao PLA on the Creality Ender-5 Plus

Wanhao PLA printed on the Creality Ender-5 Plus exhibited no outliers within the data for Experiment 4 and Experiment 6. The average UTS for the six experiments ranged between 16.58 MPa and 18.30 MPa, with Experiment 1, Experiment 5 and Experiment 6 having a standard deviation of 0.75. Figure 39 illustrates the jitter and box plots for the various experiments.

© University of Pretoria

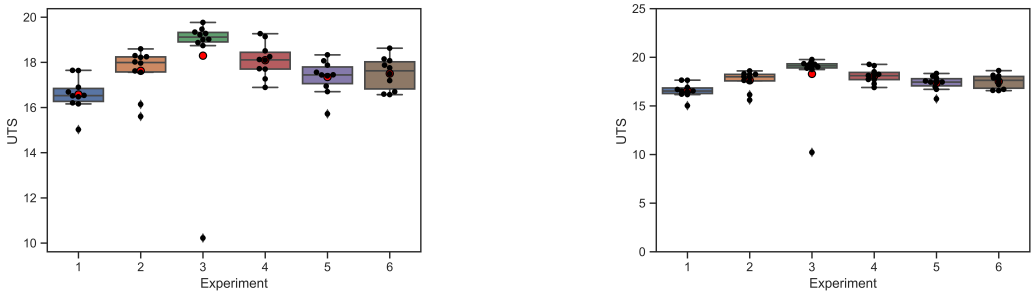

Figure 39: Sample comparison for Wanhao PLA on the Creality Ender-5 Plus.

After determining the linear interaction model, it was observed that none of the parameters had statistical significance as the p-values were greater than 0.05. The model error was calculated as 1.97%. Table 27 summarises the regression model results and interaction equation obtained.

Table 27: The ANOVA obtained for Wanhao PLA/Creality Ender-5 Plus.

Term	Estimate	Standard Error	t Ratio	Prob >[t]
Intercept	11.4284	6.2924	1.82	0.0747
A	0.0361	0.0321	1.12	0.2658
B	-0.0014	0.0321	-0.04	0.9662
C	-0.0244	0.0278	-0.88	0.3844
	Value			Probability
F ratio	0.8214	-	-	0.4876
R^2	0.0421	-	-	-
R^2 adjusted	-0.0092	-	-	-
Root mean square error (RMSE)	2.0825	-	-	-
Percentage error in model	1.97	-	-	-

7.3.9 CRON PLA on the Wanhao Duplicator 9 I3

The average UTS varied between 19.33 MPa and 29.48 MPa, where Experiment 6 had the highest average UTS and Experiment 2 had the lowest average UTS. Experiment 6 had the smallest standard deviation of 0.90 and was also the only experiment to exhibit

© University of Pretoria

outliers. Figure 40 illustrates the jitter and box plots for the various experiments printed with CRON PLA on the Wanhao Duplicator 9 I3.

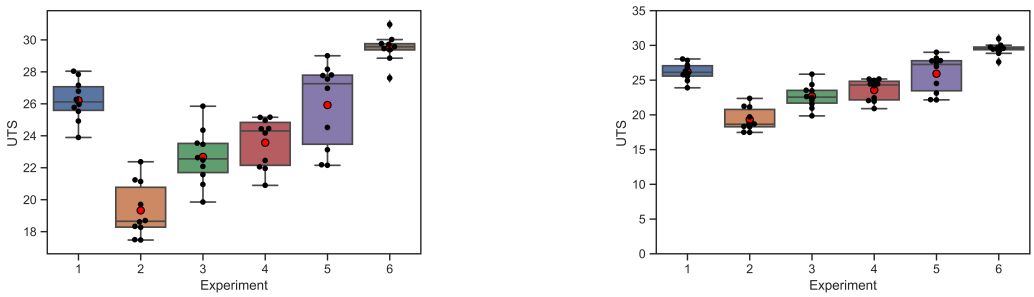

(a) **(b)**

Figure 40: Sample comparison for CRON PLA on the Wanhao Duplicator 9 I3.

Table 28 summarises the regression model results and interaction equation obtained. After evaluating the p-value, both variables had a significant effect on the UTS and, from the regression model, UTS increases for an increase in both bed temperature and printing speed. The model error was calculated as 2.04%.

Table 28: The ANOVA obtained for CRON PLA/Wanhao Duplicator 9 I3.

Term	Estimate	Standard Error	t Ratio	Prob >[t]
Intercept	9.3166	1.8311	5.09	<0.0001
B	0.1543	0.0341	4.53	<0.0001
C	0.2008	0.0338	5.93	<0.0001
	Value			Probability
F ratio	34.2575	-	-	<0.0001
R^2	0.5503	-	-	-
R^2 adjusted	0.5342	-	-	-
Root mean square error (RMSE)	3.0076	-	-	-
Percentage error in model	2.04	-	-	-

The CRON PLA samples printed on the Wanhao Duplicator 9 I3 exhibited different behaviour than those printed on the Creality Ender-6, in the sense that repeatability varied between the various experiments more substantially. The latter is illustrated in Figure 41. The Creality Ender-6 was a new printer without services and/or modifications

© University of Pretoria

being done on the machine. It was noted that the UTS for all experiments printed on the Creality Ender-6 were higher than those printed on the Wanhao Duplicator 9 I3.

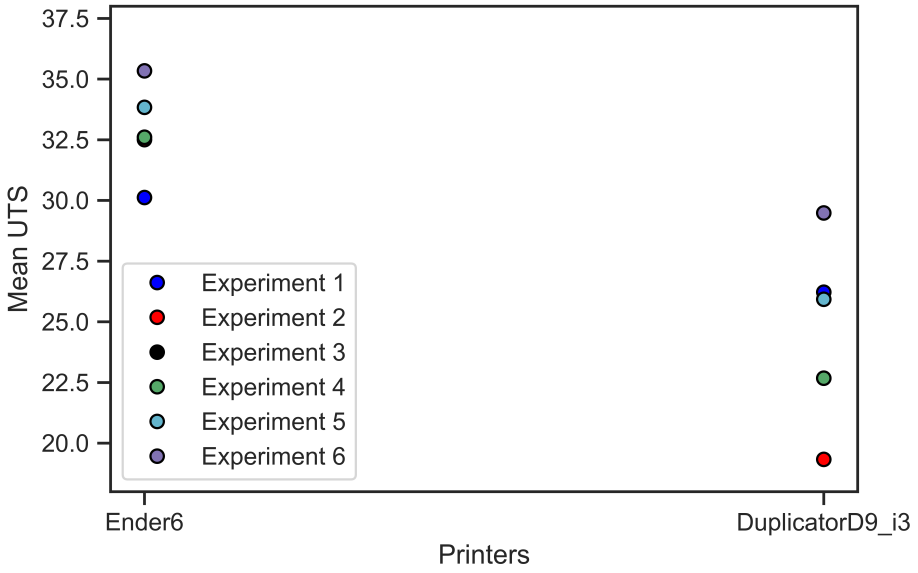

Figure 41: CRON PLA comparison between different printers.

7.3.10 Wanhao PLA on the Wanhao Duplicator 9 300

In Figure 42 it is shown that Experiment 3, Experiment 4 and Experiment 5 had outliers. Experiment 2 had the highest average UTS of 18.32 MPa and Experiment 3 had the smallest standard deviation of 0.62.

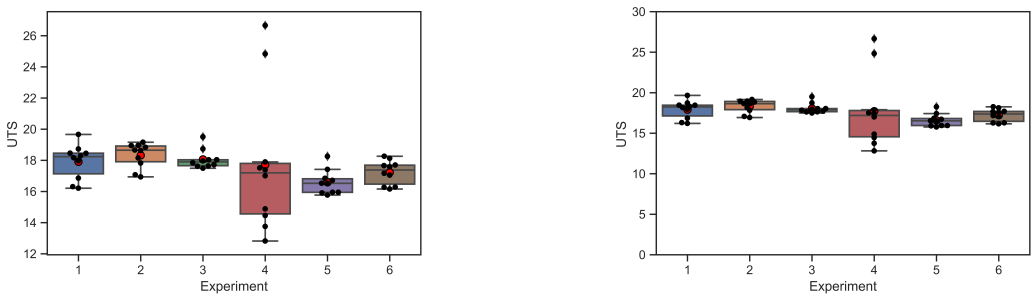

Figure 42: Sample comparison for Wanhao PLA on the Wanhao Duplicator 9 300.

All three parameters had a p-value greater than 0.05 making the effect on UTS statistical insignificant. The model error was calculated as 3.79%. Table 29 summarises the regression model results and interaction equation obtained.

© University of Pretoria

Table 29: The ANOVA obtained for Wanhao PLA/Wanhao Duplicator 9 300.

Term	Estimate	Standard Error	t Ratio	Prob >[t]
Intercept	16.5223	12.5722	1.31	0.1941
A	0.0226	0.0631	0.36	0.7217
B	-0.0299	0.0523	-0.57	0.5693
C	-0.0525	0.0641	-0.82	0.4163
	Value			Probability
F ratio	0.3157	-	-	0.8140
R^2	0.0166	-	-	-
R^2 adjusted	-0.0361	-	-	-
Root mean square error (RMSE)	4.0074	-	-	-
Percentage error in model	3.79	-	-	-

The effect of the printing temperature, bed temperature and printing speed varied between the various printer/filament combinations. In some cases causing an increase in the UTS and in other a decrease. All cases yielded printable parts. Printing temperature caused an increase in the UTS, in the minority of cases. No blockages or problems were experienced with material flow from the nozzle, irrespective of the printing temperature used. Bed adhesion improved as the bed temperature was increased. The latter also improved warping. Printing speed either had no or a positive effect on the UTS. The overall print quality from a visual inspection point of view for all samples was similar with no notable outlier.

Ouhsti & Haddadi (2018) mentioned that there were several interactions between the deposition angle, printing temperature and printing speed. In this study, the regression models illustrating interaction between the various parameters, were in the minority. Consistency in tensile testing results were observed, which differed from that reported by Banjanin *et al* (2018).

The availability of a printer model and filament brand, in conjunction with the funding available, were the primary reasons for the asymmetric filament/printer combinations used in this study. After performing the statistical analysis, it was noted that the utilised method yielded adequate model results, where the model errors were lower than 4.00%. The latter was used as justification that the method can be deployed irrespective from filament/printer combination used.

© University of Pretoria

Wanhao PLA, Buildvolume PLA, Flashforge PLA, Zortrax PLA and CRON PLA were printed on the Creality Ender-6. The results obtained for the various experiments are summarised in Figure 43. All experiments exhibited a similar trend–CRON PLA had the highest average UTS, while Wanhao PLA had the lowest average UTS. It was interesting to note that the lowest UTS was observed for Experiment 2 (lowest printing- and bed temperature), while Experiment 6 (highest printing- and bed temperature) exhibited the highest UTS. The latter may be a result of improved inter-layer adhesion due to elevated temperatures.

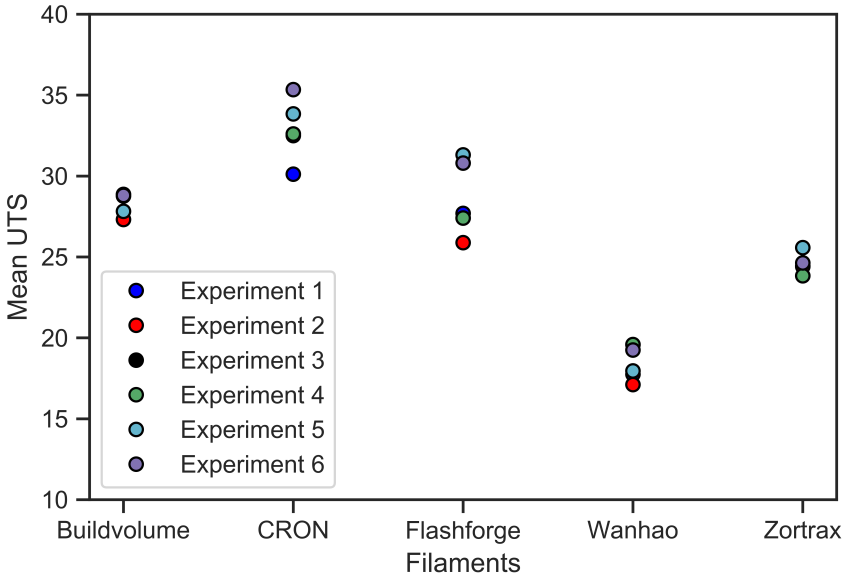

Figure 43: Creality Ender-6 comparison between different filaments.

Wanhao PLA was printed on the Creality Ender-3 Max, Creality Ender-5, Creality Ender-5 Plus, Creality Ender-6 and Wanhao Duplicator 9 300. The various experimental results were compared with one another and is shown in Figure 44. A different trend between experiments were noted for Experiment 1 and Experiment 2. For the majority of experiments the Creality Ender-6 and Creality Ender-5 yielded the highest and lowest average UTS's respectively. All experiments yielded similar average UTS values for the various samples in the different experiments. It was interesting to note that the regression models obtained for the various filament/printer combinations differed. The latter can be associated with the variation observed in the stress-strain behaviour, as depicted by Group A, Group B, Group C and Group D.

© University of Pretoria

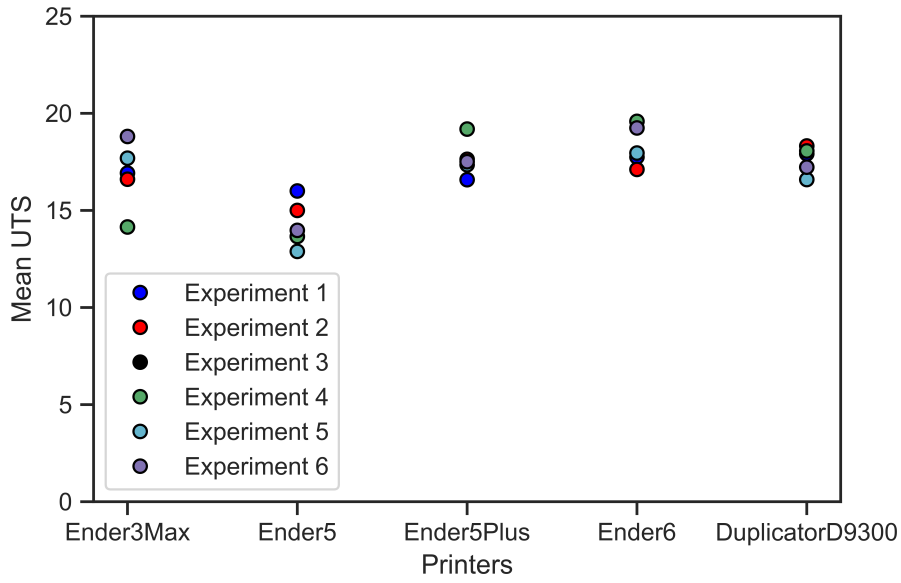

Figure 44: Wanhao PLA comparison between different printers.

It was interesting to note that the cost of filament was not directly proportional to the average UTS obtained. CRON PLA exhibited the highest average UTS, while Wanhao PLA exhibited the lowest average UTS. The filament printed on the Creality Ender-6 were compared to one another and is illustrated in Figure 45. Zortrax PLA exhibited the best repeatability between samples of a specific experiment as well as between various experiments. It was evident that repeatability was proportional to the cost per filament.

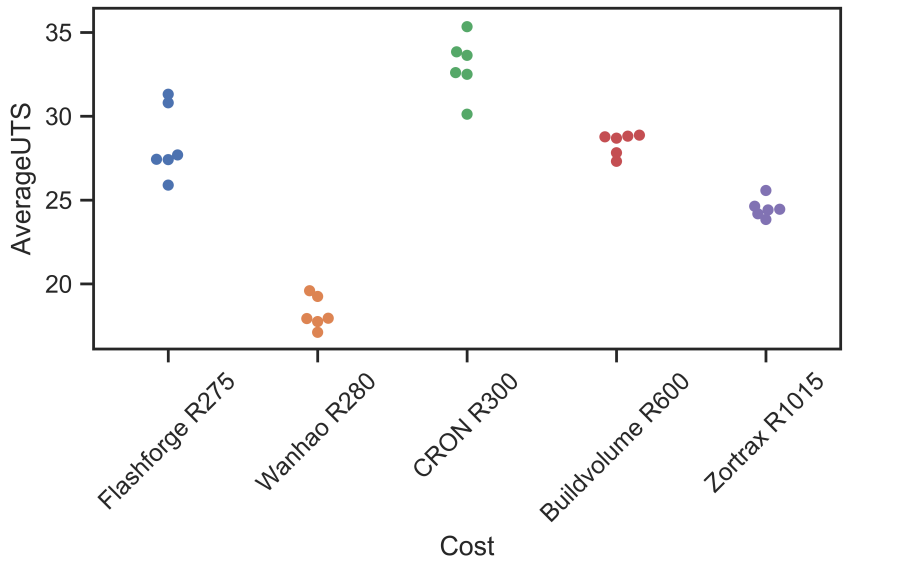

Figure 45: Cost comparison between filaments printed on the Creality Ender-6.

© University of Pretoria

7.4 Material evaluation guideline

The generic DOE and the parameters specified in the Cura® slicing software will result in a printable part irrespective of the printer model and/or filament brand. The procedure does not guarantee the repeatability of the prints within an experiment as it is dependent on filament quality. Table 30 summarises the material evaluation guideline for PLA parts printed by using FDM.

Table 30: The material evaluation guideline for PLA filament.

Description	Specification
DOE	Summarised in Table 11
Pinter type	Open-source
Periodic preventative maintenance	As specified by printer manufacturer
Type of material/feedstock	PLA
Structural characteristics	Tensile bar Type I
Mechanical properties	Tensile strength
Procedure for tensile testing	ASTM D638
Slicing software	Cura®
Slicing parameters	Refer to Table 15
Structural support required	None
Past production finish	None
Characteristics of manufacturing process	Cost associated with purchasing filament(s) and printer(s)
Data quality, resolution and representation	Comparable data obtained giving a true representation of part failure

© University of Pretoria

8 Conclusion and Recommendations

FDM is used for the production of various parts including those with complex geometries. It is a developing field with various opportunities for expansion, especially on the research and publication front. The mechanical properties (*e.g.* tensile, compression and torsion) of a printed part are of utmost importance. These outcomes and specifications are predominantly associated with the mechanical properties of a part. Parts are fabricated for specific applications and should meet certain predetermined design outcomes and specifications. The available studies for FDM are limited and in the majority of studies, tensile tests were conducted. No guidelines, specifications and procedures are available for FDM that can be used during the printing process to ensure repeatable parts.

Layer thickness, build orientation, infill pattern and infill percentage were identified as the main parameters affecting the mechanical properties of a print. Literature suggests that the understanding of the interaction between the primary parameters of a printed part is in the developing stage. Extrusion/printing speed, nozzle temperature and build plate/bed temperature were recognised as the parameters with the greatest effect on a parts mechanical properties. The latter was evident from academic literature and the literature study. It was observed that not only these parameters had an influence on the observed properties. Parameters such as a random z-start also had a noticeable effect. The analytical analyses performed on printed specimens are primarily tensile-, compression- and torsion tests.

A generic statistical two-level fractional factorial DOE were developed in which different filament brands were used to print on multiple printer models. Tensile tests were performed to verify both the repeatability between samples within a specific experiment and those between diverse experiments. It was evident from the linear interaction models that the statistical significance of the parameters varied for the different types of filaments and printers. The effect of the three parameters due to the DOE were statistically quantified but it was not possible to illustrate the effect of the DOE in this manner. The highest average UTS was obtained with CRON PLA, while the best repeatability between samples was obtained with Zortrax PLA. Consistent results were obtained on the Creality Ender 6. The lack of standards for FDM contribute to the gap in the development and generation of scientific information, data and observations. A material evaluation guideline have been developed for PLA and can be used in future for material development purposes. The effect of the slicing software should also be evaluated as there is a direct correlation between the geometric features of the print and this parameter.

© University of Pretoria

References

Aboushama, M and Beyerlein, S (2020), *Evaluation of Continuous Fiber Reinforcement Desktop 3D Printers*, Technische Hochschule Ingolstadt Faculty of Engineering and Management, Germany.

Algarni, M (2021), "The influence of raster angle and moisture content on the mechanical properties of PLA parts produced by Fused Deposition Modelling", *Polymers*, 13: 1–12.

Aliakbari, M (2012), *Additive Manufacturing: State-of-the-Art, Capabilities and Sample Applications with Cost Analysis, Department of Industrial Production KTH*, Department of Industrial Production KTH, Stockholm.

ASTM (2015), *Designation: D638-14 Standard Test Method for Tensile Properties of Plastics*, ASTM International, United States.

ASTM (2017), *Standardization roadmap for additive manufacturing*, ASTM International, United States.

Banjanin, B, Vladić, G, Pál, M, Baloš, S, Dramićanin, M, Rackov, M and Knežević, I (2018), "Consistency analysis of mechanical properties of elements produced by FDM additive manufacturing technology", *RevistaMateria*, 23 (4): 1–16.

Baroiu, N, Sovaila, F and Sovaila, S (2016), "Delta 3D printers", *Journal of Industrial Design and Engineering Graphics*, 11 (1): 29–34.

Bates-Green, K and Howie, T (2017), "Materials for 3D printing by fused deposition", *Technical Education in Additive Manufacturing & Materials*, 1–21.

Bhalodi, D, Zalavadiya, K and Gurrala, P (2019), "Influence of temperature on polymer parts manufactured by fused deposition modelling", *The Brazilian Society of Mechanical Science and Engineering*, 41 (113): 1–11.

Bikas, H, Stavropoulos, P and Chryssolouris, G (2016), "Additive manufacturing methods and modelling approaches: a critical review", *The International Journal of Advanced Manufacturing Technology*, 83: 389–405.

Blaj, M and Oancea, G (2021), "Fused deposition modelling process: a literature review", *Materials Science and Engineering*, 1–19.

© University of Pretoria

Buswell, R, Thorpe, A, Soar, R and Gibb, A (2016), "Design, data and process issues for mega-scale rapid manufacturing machines used for construction", *Automation in Construction*, 17: 923–929.

Chýlek, R, Kudela, L, Pospíšil, J and Šnajdárek, L (2021), "Parameters influencing the emission of ultrafine particles during 3D printing", *International Journal of Environmental Research and Public Health*, 18 (11670): 1–12.

Creality (2021), *Ender-5 3D Printer*, `https://www.creality.com/goods-detail/ender-5-3d-printer`, Accessed: 2021-10-26.

Ćwikla, G, Grabowik, C, Kalinowski, K, Paprocka, I and Ociepka, P (2017), "The influence of printing parameters on selected mechanical properties of FDM/FFF 3D-printed parts", *Materials Science and Engineering*, 227: 1–11.

Daminabo, S, Goel, S, Grammatikos, S, Nezhad, H and Thakur, V (2020), "FDM-based additive manufacturing (3D printing): techniques for polymer material systems", *Materials*, 1–57.

Davies, R, Yi, N, McCutchion, P and Ghita, O (2021), "Mechanical property variance amongst vertical fused filament fabricated specimens via four different printing methods", *Polymer International*, 70: 1073–1079.

Dezaki, M and Ariffin, M (2020), "The effect of combined infill patterns on mechanical properties in FDM process", *Polymers*, 12: 1–20.

Dudescu, C and Racz, L (2017), "Effect of raster orientation, infill rate and infill pattern on the mechanical properties of 3D printed materials", *Acta Universitatis Cibiniensis*, 69 (1): 23–30.

Fang, L, Yan, Y, Agarwal, O, Yao, S, Seppala, J and Kang, S (2020), "Effect of environmental temperature and humidity on the geometry and strength of polycarbonate specimens prepared by fused deposition modelling", *Materials*, 13: 1–16.

Ferrell, W, Arndt, C and TerMaath, S (2021), "Tensile strength dependence of FFF fiber reinforced ABS on environmental conditioning", *Mechanics of Advanced Materials and Structures*, 28 (20): 2163–2176.

© University of Pretoria

Ferrell, W, Clement, J and TerMaath, S (2021), "Uniaxial tensile testing standardization for the qualification of fiber reinforced plastics for fused filament fabrication", *Mechanics of Advanced Materials and Structures*, 28 (12): 1254–1273.

Fischer, F (2015), *Thermoplastics: The Strongest Choice For 3D Printing*, Stratasys, Israel.

Fuchs, S, Praegla, P, Cyron, C, Wall, W and Meier, C (2022), "A versatile SPH modeling framework for coupled microfuid-powder dynamics in additive manufacturing: binder jetting, material jetting, directed energy deposition and powder bed fusion", *Engineering with Computers*, 38: 4853–4877.

Gardan, J (2015), "Additive manufacturing technologies: state of the art and trends", *International Journal of Production Research*, 54 (10): 3118–3132.

Gibson, I, Rosen, D and Stucker, B (2015), *Additive Manufacturing Technologies Rapid Prototyping to Direct Digital Manufacturing*, Springer, New York.

ISO and ASTM (2018), *ISO/ASTM 52910:2018–AM–Design–Requirements, guidelines and recommendations*, ISO/ASTM International.

ISO and ASTM (2019), *ISO/ASTM 52902:2019–AM–Test artifacts*, ISO/ASTM International.

ISO and ASTM (2021), *ISO/ASTM 52900 Additive Manufacturing–General principles–Fundamentals and Vocabulary*, ISO/ASTM International.

J, C (2020), *Adafruit desktop 3D printer buyers guide*, `https://learn.adafruit.com/adafruit-desktop-3d-printer-selection-guide/printrbot-models`, Accessed: 2022-07-13.

Khan, S, Siddiqui, B, Fahad, M and Khan, M (2017), "Evaluation of the effect of infill pattern on mechanical strength of additively manufactured specimens", *Material Science Forum*, 887: 128–132.

Khoshkhoo, A, Carrano, A and Blersch, D (2018), "Effect of build orientation and part thickness on dimensional distortion in material jetting processes", *Rapid Prototyping Journal*, 1–11.

© University of Pretoria

Kuncevich, L (2019-09), *Carbon fiber 3D printers: 2022 guide to continuous fiber printing*, https://www.aniwaa.com/buyers-guide/3d-printers/carbon-fiber-3d-printers/, Accessed: 2022-07-18.

Lim, C (2016), *Fabrication of Elastomer Microfluidic Devices Using Additive Manufacturing Methods*, University of California, Irvine.

Loh, G, Pei, E, Gonzalez-Gutierrez, J and Monzón, M (2020), "An overview of material extrusion troubleshooting", *Applied Science*, 10: 1–28.

Maidin, S, Wong, J, Mohamed, A and Mohamed, S (2017), "Effect of vacuum assisted Fused Deposition Modelling on 3D printed ABS microstructure", *International Journal of Applied Engineering Research*, 12 (15): 4877–4881.

Manjaiah, M, Raghavendra, K, Balashanmugam, N and Davim, J (2019), *Additive Manufacturing: A Tool for Industrial Revolution 4.0*, Springer, New York City.

Markforged (2022), *What is Digital Light Processing (DLP)?*, https://markforged.com/resources/learn/3d-printing-basics/3d-printing-processes/what-is-digital-light-processing-dlp, Accessed: 2021-02-27.

Mazzanti, V, Malagutti, L and Mollica, F (2019), "FDM 3D printing of polymers containing natural fillers: a review of their mechanical properties", *Polymers*, 11: 1–22.

McCrum, N, Buckley, C and Bucknall, C (1999), *Principles of Polymer Engineering*, Oxford Csience Publications, New York, United States.

Medellín-Castillo, H and Torres, J (2009), *Rapid Prototyping and Manufacturing: A Review of Current Technologies*, Universidad Autónoma de San Luis Potosi, Mexico.

Medellín-Castillo, H and Zaragoza-Siqueiros, J (2019), "Design and manufacturing strategies for fused deposition modelling in additive manufacturing: a review", *Chinese journal of Mechanical Engineering*, 32 (53): 1–16.

Minetola, P, Galati, M, Iuliano, L, Atzeni, E and Salmi, A (2018), "The use of self-replicated parts for imporving the design and the accuracy of a low-cost 3D printer", *ScienceDirect*, 67: 203–208.

© University of Pretoria

Mirzababaei, S and Pasebani, S (2019), "A review on binder jet additive manufacturing of 316L stainless steel", *Journal of Manufacturing and Material Processing*, 3 (82): 1–36.

Mohamed, O, Masood, S and Bhowmik, J (2016), "Mathematical modelling and FDM process parameters optimisation using response surface methodology based on Q-optimal design", *Applied Mathematical Modelling*, 10: 10052–10073.

Montgomery, D (2013), *Design and Analysis of Experiments*, 8th edition, John Wiley and Sons, Unites States.

Mwema, F and Akinlabi, E (2020), *Fused Deposition Modelling Strategies for Quality Enhancement*, Springer, New York City.

Nayak, P, Sahu, A and Mahapatra, S (2020), "Effect of process parameters on the mechanical behavior of FDM and DMLS build parts", *Materials Today: Proceedings*, 22: 1443–1451.

Oleff, A, Küster, B, Stonis, M and Overmeyer, L (2021), "Process monitoring for material extrusion additive manufacturing: a state-of-the-art review", *Progress in Additive Manufacturing*, 6: 705–730.

Onwubolu, G and Rayegani, F (2014), "Characterisation and optimisation of mechanical properties of ABS parts manufactured by Fused Deposition Modelling", *Hindawi*, 1–14.

Osswald, T (2017), *Understanding Polymer Processing: Processes and Governing Equations*, Hanser Publications, Germany.

Ouhsti, M and Haddadi, B (2018), "Effect of printing parameters on the mechanical properties of parts fabricated with open-source 3D printers in PLA by Fused Deposition Modelling", *Mechanics and Mechanical Engineering*, 11 (4): 895–907.

Pham, D and Dimov, S (2001), *Rapid Manufacturing: The Technologies and Applications of Rapid Prototyping and Tooling*, Springer, New York City.

Phillips, C, Kortschot, M and Azhari, F (2022), "Towards standardizing the preparation of test specimens made with material extrusion: Review of current techniques for tensile testing", *Additive Manufacturing*, 58 (103050): 1–22.

© University of Pretoria

Sacco, E, Chua, Z and Moon, S (2018), "Comparison of elastic properties for different sample types fabricated with additive manufacturing", *Proceedings of the 3rd International Conference on Progress in Additive Manufacturing*, 577–582.

Samykano, M, Selvamani, S, Kadirgama, K, Ngui, W, Kanagaraj, G and Sudhakar, K (2019), "Mechanical property of FDM printed ABS: influence of printing parameters", *Springer*, 102: 2779–2796.

Schmidleithner, C and Kalaskar, D (2018), *IntechOpen*, `http://dx.doi.org/10.5772/intechopen.78147`, Accessed: 2021-02-27.

Segura, L, Li, Z, Zhou, C and Sun, H (2023), "Droplet evolution prediction in material jetting via tensor time series analysis", *Additive Manufacturing*, 26 (103461): 1–11.

Sola, A, Chong, W, Simunec, D, Li, Y, Trinchi, A, Kyratzis, I and Wen, C (2022), "Open challenges in tensile testing of additively manufactured polymers: A literature survey and a case study in fused filament fabrication", *Polymer Testing*, 117 (107859): 1–28.

Srivastava, V (2017), "A review on advances in rapid prototype 3D printing of multi-functional applications", *Science and Technology*, 7 (1): 4–24.

Stratasys (2018), *Design Guide, Stratasys*, Stratasys Ltd, United States.

Stratasys (2021), *Fused Deposition Modelling (FDM)*, Stratasys Ltd, United States.

Tahmasebinia, F, Niemelä, M, Sepasgozar, S, Lai, T, Su, W, Reddy, K, Shirowzhan, S, Sepasgozar, S and Marroquin, F (2018), "Three-dimensional printing using recycled high-density polyethylene: technological challenges and future directions for construction", *Buildings*, 8 (165): 1–22.

Technology, SC3 (2021), *FDM 3D Printers*, `https://www.creality.com/product/ender-series-3d-printer`, Accessed: 2021-15-08.

Technology, ZF3 (2021), *Consumer grade 3D printer*, `https://www.flashforge.com/product-category/5`, Accessed: 2021-15-08.

Thompson, M, Moroni, G, Vaneker, T, Fadel, G, Campbell, R, Gibson, I, Bernard, A, Schultz, J, Graf, P, Ahuja, B and Martina, F (2016), "Design for additive manufacturing:

© University of Pretoria

trends, opportunities, considerations and constraints", *Manufacturing Technology*, 65 (2): 737–760.

Tilton, B, Dobner, E and Holdownsky, J (2017), *3D Opportunity for Standards: Additive Manufacturing Measures Up*, Deloitte Insights, South Africa.

Török, J, Törökova, M, Duplakova, D, Murcinkova, Z, Duplak, J, Kascak, J and Karkova, M (2021), "Advanced configuration parameters of post processor influencing tensile testing PLA and add-mixtures in polymer matrix in the process of FDM technology", *Applied Sciences*, 11: 2–19.

Ultimaker (2021), *Reliable 3D printers that simply work for you*, `https://ultimaker.com/3d-printers`, Accessed: 2021-08-16.

Vălean, C, Marşavina, L, Mărghitaş, M, Linul, E, Razavi, J and F., B (2020), "Effect of manufacturing parameters on tensile properties of FDM printed specimens", *ScienceDirect*, 26: 313–320.

Valerga, A, Batista, M, Salguero, J and Girot, F (2018), "Influence of PLA filament conditions on characteristics of FDM parts", *Materials*, 11 (1322): 1–13.

Vidakis, N, Petousis, M, Konstantinos, S, Vairis, A, Maniadi, A and Manolis, A (2015), "Experimetal determination of fused deposition modelling parts compressive strength", *9th International Conference: New Horizons in Industry, Business and Education*, 93–98.

Viljoen, D (2020), *Design of Experiments*, Presented at University of Pretoria, South Africa.

Villalpando, L, Eiliat, H and Urbanic, R (2015), "An optimisation approach for components built by fused deposition modelling with parametric internal structures", *Science Direct*, 17: 800–805.

Wang, L, Majstorovic, V, Mourtzis, D, Carpanzano, E, Moroni, G and Galantucci, L (2020), *Proceeding of 5th International Conference on The Industry 4.0 Model of Advanced Manufacturing*, Springer, New York.

Wanhao (2021), *Wanhao 3D Printers*, `https://wanhao.store/collections/wanhao-3d-printers`, Accessed: 2021-10-26.

© University of Pretoria

Wu, X, Teng, J, Ji, X, Xu, C, Ma, D and Sui, S (2023), "Research progress of the defects and innovations of ceramic vat photopolymerization", *Additive Manufacturing*, 65 (103441): 1–23.

Xometry (2021), *Design Guide: Fused Deposition Modelling (FDM)–Version 1.2*, Xometry, Unites States.

Yadav, D, Srivastava, R and Dev, S (2020), "Design and fabrication of ABS part by FDM for automobile application", *Materials Today: Proceeding*, 26: 2089–2093.

Young, R and Lovell, P (2011), *Introduction to Polymers*, CRC Press, United States.

Zhang, J and Jung, Y (2018), *Additive Manufacturing Materials, Processes, Quantifications and Applications*, Elsevier, United Kingdom.

Ziemian, C, Sharma, M and Ziemian, S (2012), *Mechanical Engineering*, InTech, Croatia.

© University of Pretoria